THE STATISTICAL BEHAVIOR OF ELECTROMAGNETIC FIELDS WITHIN APERTURE-COUPLED NESTED REVERBERANT CAVITIES

By

MARSHALL DANIEL SOWELL

Bachelor of Science in Electrical Engineering

Florida State University

Panama City, Florida

2020

Submitted to the Faculty of the
Graduate College of the
Oklahoma State University
in partial fulfillment of
the requirements for
the Degree of
MASTER OF SCIENCE
July, 2022

THE STATISTICAL BEHAVIOR OF

ELECTROMAGNETIC FIELDS WITHIN APERTURE-

COUPLED NESTED REVERBERANT CAVITIES

Thesis Approved:

Dr. James West

Thesis Adviser

Dr. Charles Bunting

Dr. John O'Hara

ACKNOWLEDGEMENTS

I give thanks to my lord and savior, Jesus Christ, and the almighty Father for creating an interesting world and for creating me with a passion to study it. My experience here at Oklahoma State has been priceless on my journey to become an electrical engineer specialized in applied electromagnetics. My deepest thanks to my family, friends, and colleagues back in my home state of Florida, and those here in Stillwater, Oklahoma for being my greatest supporters. Words cannot express my gratitude and love for all of you.

My journey would not be complete without my professors, especially Dr. West for being the greatest source of wisdom and knowledge that I had the privilege of tapping into while studying under his guidance. Along with Dr. West, Dr. Bunting's experience in the world of reverberation chambers has been priceless, especially as another pool of information for me to seek. I pray to be the EMC engineer they have molded me to be and not anything less.

To Dr. O'Hara, my greatest thanks for accepting my request to be on my thesis committee; your time and energy put into answering questions and providing feedback is deeply appreciated. Thank you.

I would not be here at Oklahoma State without the SMART Scholarship and support from Carl Hager at the Naval Surface Warfare Center Dahlgren Division for his encouragement and wisdom– I cannot wait for what he and I will accomplish as I prepare to work underneath his mentorship.

Name: MARSHALL SOWELL

Date of Degree: JULY, 2022

Title of Study: THE STATISITCAL BEHAVIOR OF ELECTROMAGNETIC FIELDS WITHIN APERTURE-COUPLED NESTED REVERBERANT CAVITIES

Major Field: ELECTRICAL ENGINEERING

Abstract: Reverberation chamber (RC) theory shows that the square-magnitude of a single spatial component of a received electric field within an ideally operating chamber follows an exponential distribution. Historical experimentation has shown this ideal distribution is closely approached in well-designed chambers. It has been hypothesized that by nesting another, smaller, reverberant cavity within a larger RC, a multiplicative effect will occur creating double-Rayleigh distributed fields withing the small cavity. A study to measure the nested cavity statistics of the fields when a small chamber is weakly coupled to a large chamber has been performed. Both the external and internal cavities were mechanically stirred during measurements and frequency stirring was applied in post-processing. Three distributions were fit to the measured fields, the double-Rayleigh, exponential, and 2-parameter Weibull distributions. The goodness-of-fit of each distribution was evaluated using rigorous statistical tests. The shielding effectiveness of the smaller chamber was also found.

The double-Rayleigh distribution gave a poor fit to the measured field statistics under all conditions considered. The exponential distribution gave a good fit at higher frequencies and with large coupling, the two chambers are acting as one resonant cavity. Overall, the Weibull distribution gave the best overall fits under all conditions tested. However, the statistical tests still rejected the fits at a higher rate than expected from chance alone. These results suggest that the Weibull distribution can be used to describe the nested-cavity field statistics under general conditions for low precision work but a more accurate statistical description is needed when high-precision results are required.

TABLE OF CONTENTS

Chapter Page

Chapter Page

LIST OF TABLES

Table Page

LIST OF FIGURES

Figure Page

Figure Page

Figure Page

CHAPTER I

INTRODUCTION

Environments such as bunkers, cargo planes, cargo ships, submarines, navy vessels, or lab spaces can, under the right conditions, create an environment that establish large electromagnetic (EM) fields. In the event the power of these fields become large enough, sensitive equipment (test instruments, computers, ordinances) inside these spaces can potentially become damaged or explode. With these environments having similar characteristics - large spaces and typically constructed of metal - it is possible to build a controllable test environment that mimics these spaces.

Reverberation chambers (RCs) were first proposed in 1968 as a new approach for determining the EM field strength inside enclosures [1]. This term *reverberation* has inspiration from room acoustics, when sound lingered in large spaces [2, 3]. The basic forms of acoustic and EM waves are very similar (a detailed comparison between the two forms can be found in [2]), so like sound, EM fields can also dwell in such spaces for a long time. With a long reverberation time, the EM fields are able to diffuse throughout the space [4] creating a testing environment that has become very well adopted for electromagnetic compatibility (EMC) testing. EMC testing allows for the study for the EM environmental effects of systems and how they interact with themselves and in their environment [5]. By understanding the way in which the EM fields interact with test equipment in a RC, it is possible to help prevent equipment malfunction in the event it is exposed

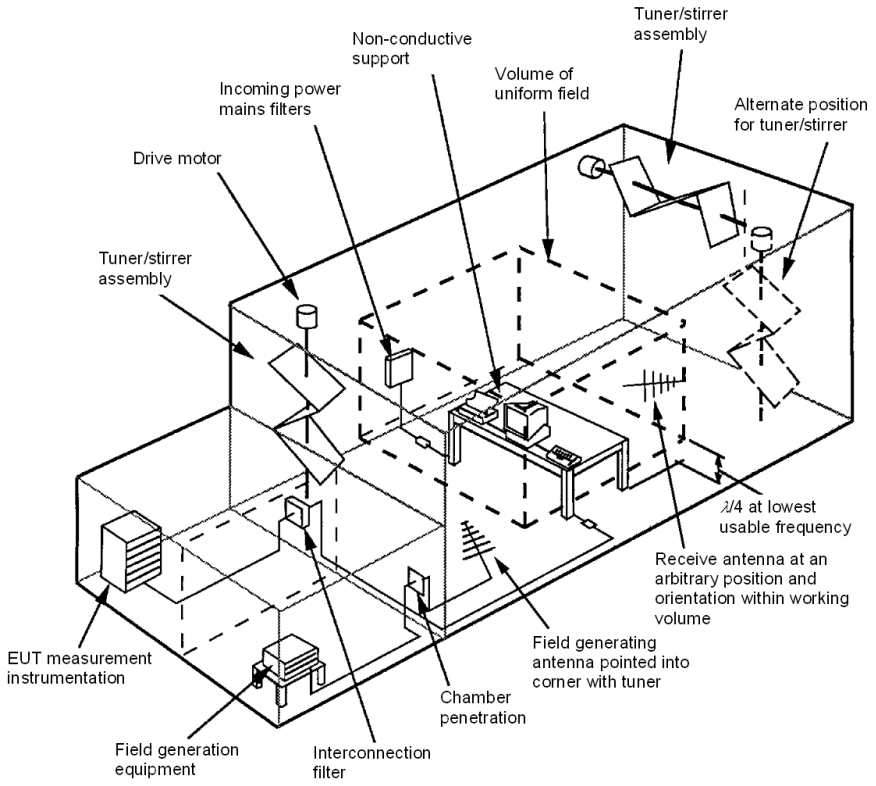

Figure 1.1: Example construction of a reverberation chamber facility [4]

to intentional or unintentional EM fields, making RCs a well accepted for this kind of testing.

The study of EMC, or EM interference (EMI) also insures that not only devices are safe, but people and fuel as well. Several military programs exist to make sure all environments (bunkers, ships, below deck spaces, aircraft) with risk to high EMFs are safe. Radiation Hazard (RADHAZ) procedures were created to mitigate radiofrequency hazards in scenarios when people, ordinances, and/or fuel are exposed to EM radiation.

1.1: REVERBERATION CHAMBER DESIGN

An RC is an electrically large (compared to wavelength), high quality (Q) solid enclosure constructed of metals like copper, aluminum, or steel [6, 7]. The addition of tuners (also known as paddles or stirrers) allows for EM boundary conditions to be discretely or continuously stirred, changing the structure of the EM fields within the chamber [4, 6, 7]. A well-designed RC is shielded

to the point where spillage or leakage of EM radiation is of no concern and is therefore isolated from any external effects. One of the benefits of this isolation of the reverberant environment is its ability to provide repeatability when taking measurements for EM experiments. Figure 1.1 provides an example of a RC facility.

A properly built RC will be well shielded and constructed of metal; for example, the large reverberation chamber at Oklahoma State University is constructed of galvanized steel. Additionally, the incorporation of mechanical tuners creates a changing boundary condition which provides a different (independent), and unique, electrical field every time the tuners move to a new position. Over a large number of tuner positions, any location in the cavity will show the measured field's magnitude and directionality will statistically average out to be the same for all points within a chamber, indicating it as a statistically uniform environment [4]. The physical structure of the tuners themselves will be similar in nature to the walls of the RC because they are large, (in terms of wavelength) highly conductive surfaces able to scatter energy so they do not impact the loading of the chamber [4]. This ability to create a unique and statistical uniform environment are two other key benefits of a RC for EM testing.

It has been speculated about the benefit of multiple tuners inside a chamber as opposed to a single tuner [8]. However it appears as long as the design of the tuner is electrically large, it will be able to redistribute the fields and change the modal structure [6]. It appears that literature does not suggest the minimum requirement of tuners in a RC, it does, however appear that a single tuner [6, 9, 10] or two tuners [11, 12] inside a chamber is most common. In the literature, RCs are sometimes called mode-stirred chambers because of the tuners [6, 7] changing the resonant modes that are established within the cavity.

For statistical calculations using RCs, two mode-stirring techniques are used: mechanical mode stirring and frequency mode stirring [4, 9]. Pure mechanical mode stirring relies on the use of injecting energy into a RC at a single frequency, and then rotating a tuner to change the boundary

conditions and collect new, independent samples needed for analysis. There are two variations when choosing to use the mechanical mode stirring technique: utilizing discrete steps or a continuous stir [4, 6]. The discrete steps allows for the ability to collect N samples based on the N steps the tuner rotates from the degree change, $360°/N$, and is referred to as the *mode-tuned* technique. The *mode-stirred* technique is when the tuner is continuously stirred at a fixed rate and allows for a large amount of samples to be collected. Both have their trade-offs which are described in [6].

For frequency mode stirring, a frequency range is selected and by evenly stepping through a P number of frequencies, the modal environment changes at each frequency. First proposed by Loughry in [13], frequency stirring was indicated as an alternative to mechanical stirring. Unlike using a tuner to change the modal structures, changing the injected energy's frequency in small steps creates new modal structures with each step, creating new independent samples. Choosing a center frequency and selecting a small bandwidth encompassing it with P frequencies to be sampled, the frequency stirring technique allows for a single sample to be collected at each frequency making a total of P samples. The underlying assumption is that each sample will have approximately the same estimated parameter because the change in frequency is relatively small, indicating very similar distributions in a tight bandwidth. Experience shows that frequency stirring is faster because collecting the samples in the bandwidth depends on how fast the test equipment needs to sweep to collect all the samples (waiting on the order of seconds). The mode-tuned technique takes much longer because the tuner must step, wait for the chamber to settle, test equipment collects the sample, and repeat N-1 more times before all the samples are collected (waiting on the order of minutes).

The amplitude of a single spatial component of the electric field captured by a receiving antenna within an ideally operating RC follows a Rayleigh distribution [7, 10]. The Rayleigh distribution is also known as the chi-distribution with two degrees of freedom [7], χ_2, or as a special

case of the Weibull cumulative distribution function where the shape parameter is 2 and the scale parameter is $\sqrt{2}\sigma$, where σ is the Rayleigh parameter [14]. The square magnitude of a single received component of the electric field follows the chi-squared distribution with two degrees of freedom, χ_2^2, also known as the exponential distribution [7]. The Rayleigh statistics and the distribution chosen for experimental analysis will be discussed in later chapters.

1.2: LITERATURE REVIEW

The field intensity within an ideal RC follows a Rayleigh distribution. In [10], the statistical behavior of electric fields within nested reverberation chambers was explored by nesting a small RC within a large RC and using different apertures to couple the two together. Environments like aircraft and ships have sensitive equipment like avionic boxes, computers, test instruments, and ordinances. In the event a large electric field builds-up inside one of these environment, understanding the behavior of the field statistics coupled into these small enclosures becomes crucial to help minimize risks. By accurately describing the internal field statistics inside these enclosures, the ability to mitigate equipment failure becomes achievable because the internal statistical field exposure has been predicted by a statistical description. The hypothesis in [10] was that the field intensity within the nested RC under frequency mode stirring would follow a double-Rayleigh distribution. A single RC has shown to create field statistics that are Rayleigh (exponential for power) distributed, and by nesting a RC within a RC, each able to create their own independent environment, and coupling them together, a multiplicative effect resulting in a double-Rayleigh distribution is hypothesized to occur. The proof is given in a later chapter, but has been experimentally shown in [15], in which two cascaded independent Rayleigh distributions will create a double-Rayleigh distribution. Because the field intensity within a well-operating RC (isolated, statistically uniform electric field) follows a Rayleigh distribution, then the intensity of the field coupled between two nested chambers will theoretically follow the double-Rayleigh distribution. The authors of [10] nest a smaller chamber within a larger chamber, but their

experimental approach is drawn into concern. In order to collect independent samples, they elect to use pure frequency stirring by sampling 401 frequencies within a bandwidth. They observed the statistical behavior of six different 100MHz bandwidths, each centered at $3, 4, 5, \dots, 8$ GHz. By taking advantage of their external chamber containing a tuner, and stepping it 100 times, they collected the frequency stirred data at each step (the small chamber does not have a tuner). For each bandwidth, they have 100 populations with 401 samples in each that they will analyze. The first concern is, by not changing the boundary conditions within the small cavity, they have not created a new environment for new independent data to be observed.

The double-Rayleigh distribution depends on the multiplicative effect of two independent environments coupling together; if x represents the independent sample in the large chamber, and y represents the independent sample in the small chamber, then $w = xy$ is the resulting double-Rayleigh distribution. The authors here have effectively performed the following

$$\begin{bmatrix} w_1 \\ w_2 \\ \vdots \\ w_{100} \end{bmatrix} = \begin{bmatrix} x_1 y_1 \\ x_2 y_1 \\ \vdots \\ x_{100} y_1 \end{bmatrix}, \tag{1.1}$$

where the changing subscript on x indicates the external boundary conditions have been changed, while the subscript on y remains the same because of the unchanged internal boundary conditions. The product of the two is what they have claimed to theoretically be a double-Rayleigh distribution. The theory depends on both samples being unique and independent, and because the internal cavity's boundary conditions have not changed, it will create the same modal characteristics as was in the previous step in the external cavity.

The other concern in the methodology used in [10] regards the statistical test used to establish that a double-Rayleigh distribution was formed. Statistical tests provide a confidence level that a set of data was obtained from a population that does not follow a prescribed distribution. The

null hypothesis, that the data was collected from the given distribution, is rejected when the confidence level exceeds a given value, typically 0.95 (95% confidence) or 0.99 (99% confidence). Statistical tests lose their power to reject the null hypothesis when used under conditions other than for which they were formulated. [10] applied the Kolmogorov-Smirnov (KS) test to the measured field intensities with the moments in the reference double-Rayleigh distribution estimated from the data itself. The KS test, however, was formulated under the assumption that the underlying distribution, including the moments, is fully specified prior to testing [16]. Lilliefors [16] showed that the KS test is much more conservative in rejecting the null hypothesis when the first moment

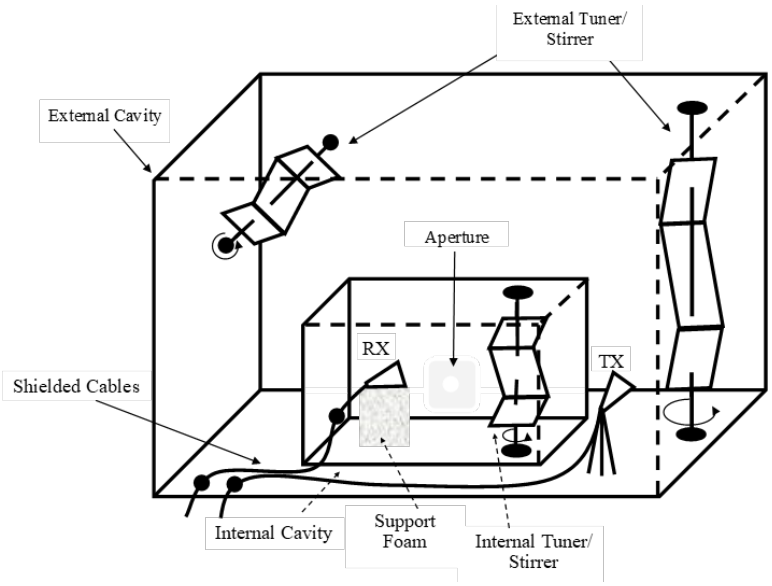

Figure 1.2: Nested Cavity Representation

(mean) and standard deviation are estimated from the collected sample. [17] provides additional study and recommends caution in the use of the KS test when the parameters (including moments) of the test distribution were estimated.

1.3: MOTIVATION OF PROJECT

This project examined the behavior of statistical fields within aperture-coupled nested cavities. By incorporating an internal tuner in a small cavity, as well as, keeping two external and internal tuners synchronized – it was hypothesized that the internal cavity field would follow the double-Rayleigh distribution (Figure 1.2 provides a visual). Like [10], a variety of different shaped apertures were used to determine the conditions under which double-Rayleigh field statistics were obtained. The environments were changed by combination of simultaneous inner and outer mechanical stirring (analogous to the mode tuning technique). Once the tuners settled to their new position, a vector network analyzer swept a defined frequency range. The mechanical mode tuning technique was the primary way in which data was collected so the statistics of each frequency can be analyzed. A hybrid combination of frequency and mechanical stirring was added later to see the overall statistical behavior of a given bandwidth. Additionally, an alternate distribution for the nested cavity was also proposed and tested.

The Anderson-Darling statistical test [18] was used to test the statistics of the field within an RC operating while un-nested (uncoupled or in isolation) against the exponential distribution. The Anderson-Darling test was formulated with estimated parameters so is appropriate for this application.

No rigorous statistical test against the double-Rayleigh distribution when the distribution parameters are estimated was known to the author. However, the use of Pearson's chi-square goodness-of-fit test can be used because of its ability to analyze the behavior of expected versus observed outcomes [19], however it is not a rigorous test [20, 21]. Realizing its lack in rigor, the chi-square test can still be used to have a general sense in how well the theorized double-Rayleigh distribution fits the collected samples.

Along with the statistical tests, the cumulative distribution function (CDF) is useful to describe the distribution of a random variable [22, 23]. Taking advantage of the CDF, it can be calculated to model the behavior of the empirical data, and then used to compare the empirical CDF (ECDF) to the theorized CDFs estimated from the data collected. Plotting the CDFs on top of each other will provide a visual to see which distribution best fits the collected data.

The Anderson-Darling test will be used to test the collected samples against an exponential distribution and a Weibull distribution. The chi-square test will be compare how well the CDFs of each distribution (double-Rayleigh, exponential, Weibull) fit to the empirical CDF.

1.4: OUTLINE OF REMAINING CHAPTERS

The remaining chapters present the following information. Chapter 2 will show where the Rayleigh and exponential statistics are derived, the derivation of the hypothesized double-Rayleigh distribution, and how their respective parameters were estimated. This chapter will also discuss the selected goodness-of-fit tests that were used to confirm or reject each hypothesized distribution and if it accurately describes the measured field statistics at a certain confidence level. Chapter 3 provides information of the experimental setup and how the chambers were validated to work for this study. Chapter 4 shows the validation of acceptable performance of the chambers when operating in isolation. Chapter 5 first presents the shielding effectiveness (SE) of the inner chamber operating both with no aperture and with a coupling aperture in place. The empirical CDF of the samples for the same two cases at $2, 5,$ and 8 GHz are then shown comparing the behavior of the double-Rayleigh and exponential distributions. The appropriate GOF test results will also be presented alongside the CDF results to give a sense of confidence in how well the distributions 'fit' the empirical model. Chapter 6 will show the statistical behavior of the Weibull distribution while also comparing it to the double-Rayleigh's fit at the same three frequencies from chapter 5. The appropriate GOF tests and their results will also be shown here. Chapter 7 will give the conclusions and suggest further work.

CHAPTER II

UNDERSTANDING THE APPLIED STATISTICS

2.1: MOTIVATION FOR STATISTICS

The behavior of EM fields within various geometries like rectangular prisms, cylinders, and spheres have been well studied and Part One of [9] provides a quick review of the fundamentals, while [24, 25] provide a more in-depth analysis. The statistical nature of the fields are assumed to be random because of their interactions with the walls, tuners, and antennas randomly changing their position or polarization [6, 9, 26]. By changing the position of the tuner or sweeping in a frequency range, independent random samples are able to be measured. This randomness forces the need to step away from deterministic solutions and embrace statistical solutions. Specifically, as Hill describes in [9], what is typically known about electrically large cavities is its geometry: length, width, and height; the introduction of cables (necessary for EM measurements), a test device, or an absorbing/scattering material and how it interacts with the fields are typically not known. With a mixture of knowns and unknowns, and the random effect it can create within a cavity, all analysis incorporates the need for statistics to understand the random behavior of the measured fields.

Following [27], a transmitted signal can be represented as

$$s(t) = Re\{u(t)e^{j\pi f_c t}\} = s_I(t)\cos(2\pi f_c t) - s_Q(t)\sin(2\pi f_c t), \tag{2.1}$$

where $u(t) = s_I(t) + js_Q(t)$ is the complex baseband with in-phase, $s_I(t)$, and quadrature, $s_Q(t)$, components. $u(t)$ is also known as the complex envelope of $s(t)$. The structure of an RC allows it to become a multipath environment as a signal bounces around, creating a uniform scattering environment. Additionally, because the number of bounces will be large, the central limit theorem can be invoked on the received signal showing the in-phase and quadrature components as independent, identically distributed Gaussian processes. Taking advantage of this, and by not facing the transmitting (TX) and receiving (RX) antennas at each other, the statistics of the chamber field will follow the Rayleigh distribution [27]. Hill in [9] takes a different approach by focusing on the modal theory of the electric fields, but arrives at the Rayleigh statistical description of the magnitude of a single spectral component of the electric field. The magnitude-squared field follows the exponential distribution [9].

A rigorous understanding of the RC statistics permits a prediction of the mean or peak field to which a device under test within the chamber will be exposed. This property has led to reverberation chambers being well accepted for EMC testing

2.2: CAVITY STATISTICAL BEHAVIOR

2.2.1: Known Distributions

As mentioned in chapter 1, the magnitude of a single component of a well-stirred RC's electric field, $|E_R|$, follows a chi-distribution with two degrees of freedom, otherwise known as a Rayleigh distribution, whose probability density function (PDF) is [7, 28]

$$f(|E_R|) = \frac{|E_R|}{\sigma^2} \exp\left(-\frac{|E_R|^2}{2\sigma^2}\right), \tag{2.2}$$

where $|E_R|$ represents the magnitude of the single spatial component of the received electric field and σ is the scale parameter.

The magnitude-squared component of the individual electric field follows a chi-squared distribution with two degrees of freedom, also known as the exponential distribution [7, 9], with PDF

$$f(z) = \frac{1}{2\sigma^2}\exp\left(-\frac{z}{2\sigma^2}\right), \qquad z \geq 0, \tag{2.3}$$

and cumulative distribution function (CDF)

$$F(z) = 1 - \exp\left(-\frac{z}{2\sigma^2}\right), \tag{2.4}$$

where $z = |E_R|^2$.

2.2.2: Double-Rayleigh Distribution

The double-Rayleigh distribution will appear when the independent random variables of two Rayleigh distributions are multiplied together. Here, the *power* double-Rayleigh (DR) distribution is derived from the product of two independent random variables from two Rayleigh distributions, and then taking their square. Using

$$Z = W^2 = (XY)^2 \tag{2.5.1}$$

and

$$z = w^2, \tag{2.5.2}$$

where W is the amplitude DR random variable (RV) from the product of X and Y Rayleigh RVs, Z is the power form of the DR RV, w is the amplitude DR specific value taken on from W, and z is the power DR specific value from Z. The PDF of the power DR can be found to be [15]

$$f_Z(z) = \frac{2}{\sigma}K_0\left(2\sqrt{\frac{z}{\sigma}}\right), \qquad z \geq 0, \tag{2.6}$$

where $K_0(\sim)$ is the modified Bessel function of the second kind of the zero order. Then by finding $P_Z(Z \leq z)$, the cumulative distribution function (CDF) of the power DR can be found to be

$$P_Z(Z \leq z) = F_Z(z) = \int_0^z \frac{2}{\sigma} K_0\left(2\sqrt{\frac{z'}{\sigma}}\right) dz' = 1 - 2\sqrt{\frac{z}{\sigma}} K_1\left(2\sqrt{\frac{z}{\sigma}}\right), \tag{2.7}$$

where $K_1(\sim)$ is the modified Bessel function of the second kind of the first order. The power form can also be derived from the product of two exponential distributions.

The power DR is a special case of the K-distribution's PDF derived by Redding in [29] with $L = \nu = 1$. In [30], the authors also derive the power DR and it becomes equivalent to equation (2.6 – 2.7) when their $\Omega_{\mathrm{iE}} = \sqrt{\sigma}$.

The nesting of an ideal small RC within an ideal large RC is expected to create a multiplicative effect when the two chambers are weakly coupled. The large chamber randomness creates a Rayleigh-distributed field within its interior, including at the coupling aperture. The aperture weakly couples energy into the inner chamber, whose random environment also yields Rayleigh fields. The effects are multiplicative when the chambers are simultaneously stirred, leading to expected DR field statistics. This behavior is only expected when the shielding effectiveness of the nested cavity is high, giving weakly coupled environments. If the coupling is strong enough, the two chambers will act as one because they are not strongly shielded from each other.

2.3: VALIDATING DISTRIBUTIONS

2.3.1: Simulated CDF Plots

Theoretical CDF plots plotted against an empirical CDF provide a visual aid in describing how well a hypothesized distribution fits the empirical. Figure 2.1 shows the empirical CDF from the square product of two sets of independent, identically distributed ideal Rayleigh distributions.

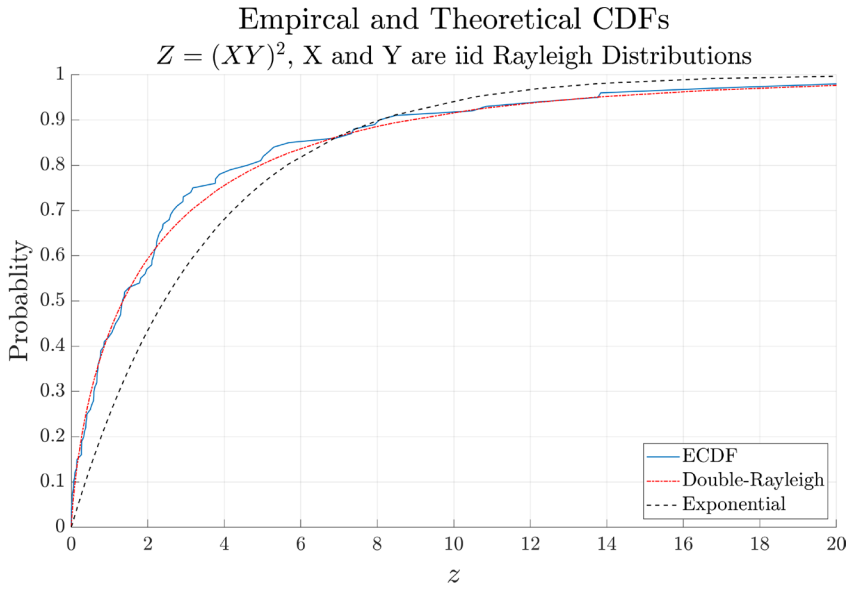

Figure 2.1: Simulated CDF Plots from independent, identically distributed (iid) Rayleigh Distributions: Empirical, Double-Rayleigh, and Exponential

Each Rayleigh distribution set contained 100 samples. The square product of two iid Rayleigh distributions yield a hypothesized double-Rayleigh distribution which is seen by the double-Rayleigh's CDF closely aligning to the empirical CDF. Both the double-Rayleigh and exponential CDFs were estimated from the square product of the two distributions.

2.3.2: Goodness-of-Fit Tests

Goodness of fit (GOF) tests are used to validate or reject the hypothesis that data collected follows a certain distribution. The Anderson-Darling (AD) test, for example, was constructed to test against distributions with an estimated parameter to a well-defined confidence level. It is well suited to testing for exponential or Rayleigh distributed samples. However, the AD test cannot be used to test for DR distributed data. An alternative is plotting a theoretical CDF onto a ECDF, providing a visual GOF test (Figure 2.1). The draw back is this comparison does not provide rigorous confidence levels. Pearson's chi-square GOF, however, will be able to fill-in the visual comparison's shortcomings.

The Pearson's chi-square GOF was introduced in [31] to determine how well observed data fits an arbitrary hypothesized distribution with a defined confidence. This is done by showing the relationship between an observed and expected set of counts by calculating the chi – square test statistic [19, 32]

$$\chi^2 = \sum_{i=1}^{k} \left(\frac{(O_i - E_i)^2}{E_i} \right), \tag{2.7}$$

where O_i is the observed number data in bin i, E_i is the expected number of data in bin i, i is the bin number, and k is the total number of bins. This test can be used when one or more parameters in the distribution were estimated from the data. It may thus be used to test for double-Rayleigh distributed data with an estimated parameter. Since its inception, some inaccuracies with small expected cell counts have been observed [20]. Additionally the chi-square test is less powerful than the AD test in rejecting the null hypothesis with the same data samples [21, 33]. However, [32] has shown that with proper selection of bins, the chi-squared GOF can have performance comparable to a more rigorous test like the AD. Considering that this is a test with foundational statistics, and accepting that there is potential bias associated with it, it can still be used to give a general idea of how well a hypothesized distribution fits to observed data, though not as rigorously as other GOF tests like the AD. Therefore, measured data will be tested against the DR distribution both by applying the chi-squared test and comparing the ECDF with the theoretical distribution CDF.

As alluded to previously, the AD will be the most trusted GOF test when testing the empirical data against the exponential and Weibull distributions. The AD test can assess a handful of distributions – including the exponential distribution [18, 34]. Therefore, all statistical tests will be applied to the magnitude-squared field samples.

The Kolmogorov-Smirnov test is not appropriate for this study since the distribution parameters must be estimated from the collected data [16, 17].

2.4: ESTIMATING THE SCALE PARAMETER

The scale parameter σ in equations (2.1) through (2.6) must be estimated from the data collected. Following [35], the maximum-likelihood estimator (MLE) is used for estimation of the parameters of any distribution considered.

The MLE is implemented by maximizing the likelihood function, or, equivalently, maximizing the log of the likelihood function. Considering the estimation of the exponential distribution parameter, let $\mu = \sigma^2$ and $E_R = x_i$ for the individual samples in equation (2.2):

$$f(x_i|\mu) \quad = \frac{1}{2\mu}\exp\left(-\frac{x_i}{2\mu}\right).$$

The associated likelihood function to be maximized is

$$L(x_i, \mu) \quad = \prod_{i=1}^{n} f(x_i|\mu).$$

The logarithm of the likelihood function is therefore

$$\ln\big(L(x_i, \mu)\big) \quad = \sum_{i=1}^{n}\left(\ln(1) - \ln(2) - \ln(\mu) - \frac{x_i}{2\mu}\right).$$

The log-likelihood function is maximized by setting the partial derivative of all free parameters equal to zero. The free parameter in the exponential distribution is μ, so the likelihood function is maximized using

$$\frac{\partial \ln\big(L(x_i, \mu)\big)}{\partial \mu} \quad = \sum_{i=1}^{n}\left(-\frac{1}{\mu} + \frac{x_i}{\mu^2}\right) = 0.$$

Solving gives the maximum likelihood estimate

$$\mu = \sigma^2 = \frac{\sum_{i=1}^{n} x_i}{n}, \tag{2.9}$$

■

where n is the number of samples used in the estimate [36, 37]. The MLE estimate of the exponential distribution parameter is therefore equivalent to the moment-method estimator using the first moment, otherwise known as the arithmetic mean [36-39].

The MLE of the DR parameter is somewhat more involved. Following the same steps, but instead using the PDF in (2.5) leads to

$$\ln\big(L(z_i,\sigma)\big) = \sum_{i=1}^{n}\left\{\ln(2) - \ln(\sigma^2) + \ln\left(K_o\left(2\sqrt{\frac{z_i}{\sigma^2}}\right)\right)\right\}. \tag{2.10}$$

The estimated σ can be found by evaluating

$$\hat{\sigma}_{mle} = \max_{\sigma}\big\{\ln\big(L(z_i,\sigma)\big)\big\}. \tag{2.11}$$

Equation (2.11) must be evaluated numerically.

CHAPTER III

EXPERIMENTAL SETUP

3.1: CHAMBER DESIGN AND CONSTRUCTION

The reverberation chambers (RCs) being used for the nested cavity study include Oklahoma State University's ETS-Lindgren SMART-80 Reverberation Chamber, and a custom-made RC that will be referred to as the "small chamber". The dimensions are provided in Table 3.1.

SMART-80		Small Chamber	
Dimension	Length (m)	Dimension	Length (m)
L	13.4	L	2.13
W	6.1	W	0.762
H	4.8	H	1.2

Table 3.1: Dimensions of Chambers

The SMART-80 is constructed of galvanized steel while the small chamber was constructed of carbon steel $\left(\sigma = 5.99 \times 10^6 \frac{S}{m}\right)$. The small chamber contains a single Z-fold type tuner while the SMART-80 contains two tuners orientated horizontally and vertically ([3] provides information and history on the Z-fold design).

Preliminary tests for the small chamber indicated poor shielding effectiveness and a lack in confidence in creating exponentially distributed (magnitude-squared) fields with numerous ind-

pendent samples available (these results will be in next chapter). Modifications were made on the chamber to improve the performance. New RF shielding gasket material was placed where the door and panels made contact to the chamber to block any leakage at the seams. Additionally, the Z-fold tuner was noticed to wobble with each discrete step. Tightly coupling the tuner shaft to the stepper motor fixed this and created discrete uniform steps. Aluminum foil was also added to the small chamber's tuner to increase its size and add more surface to scatter the electric fields, creating more randomness in the small chamber.

The modifications gave a significant increase in the shielding effectiveness of the small chamber and created the expected statistical field behavior when the chamber was operated in isolation.

3.2: EQUIPMENT SETTINGS

3.2.1: VNA Settings

A vector network analyzer (VNA) was used as the source of RF energy for all testing. The frequency test range was $1.9 - 9.1$ GHz, matching [10]. As will be shown, approximately 100 independent samples of the chamber field were available by rotating the mechanical tuner through discrete steps. Additional measurements were performed over 100 MHz bands centered at 2 and 9 GHz, adding two more center frequencies compared to [10] while still using their same bandwidth.

The VNA output power, P_{VNA}, was set at $-20dBm$. Preliminary nested testing shows that the received signal levels were below the VNA noise floor when no coupling aperture was placed between the small chamber and the SMART-80. A microwave amplifier was therefore placed between the VNA and transmitting antenna to boost the received signal above the noise floor. The aforementioned power setting was chosen so that the VNA receive power would not exceed the VNA upper limit of $1W$ $(30dBm)$. The amplifier gain was subtracted from the received signal

levels during power processing. The amplifier was only used during nested cavity testing when the receiving antenna was located inside the small chamber.

A 30 second sweep time was chosen so both chambers have enough time to settle to steady state at each frequency before the measurement is taken. The maximum number of frequency points available in the VNA sweep, 1601, was chosen to provide the finest sampling possible over the wide frequency range with uniform frequency steps of 4.4972 MHz.

3.2.2: Antenna Characteristics

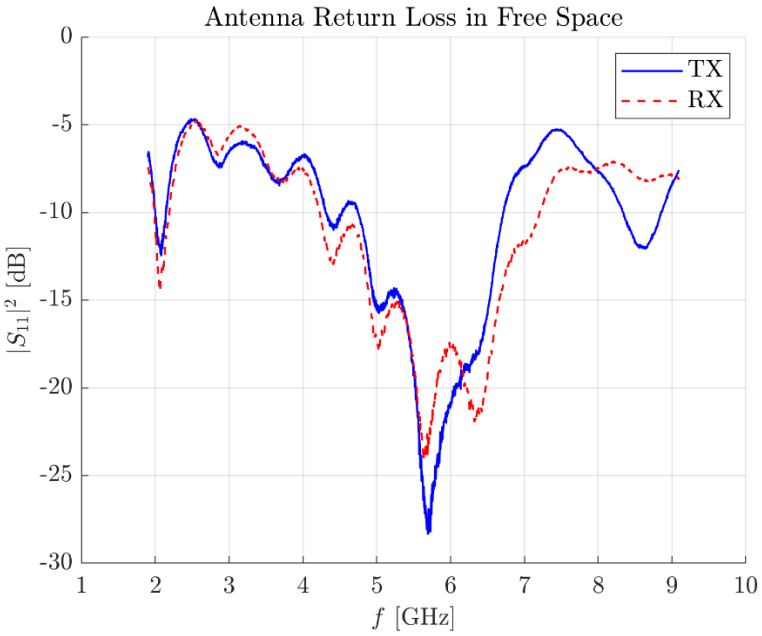

Figure 3.1: Antenna Return Loss

Two double ridge guide horn antennas were used as the transmitter (TX) and receiving (RX) antenna. The free-space return loss of the horn antennas is shown in Figure 3.1. It was calculated using

$$RL = 10\log_{10}(|S_{11}|^2), \tag{3.1}$$

where S_{11} is the reflection coefficient at the antenna input port as measured by the VNA when the antenna was placed in an anechoic chamber [40].

3.2.3: Remaining Test Equipment

A summary of all the test equipment used can be found in Table 3.2.

VNA	Agilent: 8722ES 50MHz – 40GHz S-PARAMATER NETWORK ANALYZER
Horn Antennas	Double Ridge Guide Horn Antennas (× 2) Model: SAS-571
Cables	Three (3) MICRO-COAX ®: 2m Two (2) MICRO-COAX ®: 8m
Calibration Kit	Agilent: 85054D TYPE N ECONOMY CALIBRATION KIT

Table 3.2: Test Equipment

3.3: VALIDATION OF CHAMBER OPERATION

3.3.1: Distribution Validation of Un-Nested Chambers

The measured magnitude-squared electric fields in a properly operating RC should follow the exponential distribution. As discussed previously, the AD GOF test will be applied to the measured sample sets because of its rigor when testing data whose distribution parameter has been estimated from the data itself. This test will be performed at both the 95% and 99% confidence levels. The hypothesis testing assumptions are

- H_o: Data follows an exponential distribution
- H_1: Data does not follow an exponential distribution

where H_o represents the null hypothesis and H_1 represents the alternative. A 95% confidence level indicates the test will reject the null hypothesis with 5% of all data sets collected from an ideal exponential distribution. Similarly, 99% confidence means the test rejects the null hypothesis with

1% of all exponentially distributed sets. For an ideally operating RC, the null hypothesis will be rejected with 5% (or 1%) of the data sets collected.

3.3.2: Correlation Check

As noted in A.3 in [4], a statistical analysis of field strengths measured in a RC is valid only if the samples are independent. After the chambers have been validated to yield exponentially distributed samples when operating in, a correlation check will be performed to verify that independent samples are being collected.

CHAPTER IV

CHAMBER VALIDATION

4.1: INTRODUCTION

As indicated in Chapter 1 and in [4], for a nested cavity experiment such as this, both chambers must yield independent, exponentially distributed mean-squared field samples at a defined confidence level. The SMART-80 was shown to meet all performance requirements at all test frequencies in [41-43]. The performance was reconfirmed for completeness in this project and the results will be shown. However, as mentioned Chapter 3, the small chamber, had been in disuse for a number of years and had to be brought back into operation. If the small chamber was not brought back up into proper working operation, the collected measurements would be interpreted incorrectly. This chapter will shows the modal content and shielding effectiveness (SE) of the small chamber and confirms the exponentially distributed, independent field samples for both chambers operating in isolation.

4.2: MODAL CONTENT

The theoretical number of modes supported in a rectangular-dimension reverberation chamber at and below a given frequency is estimated from the smooth approximation used in [6, 7] and derived in [44]:

$$N_s(f) = \frac{8\pi}{3} LWH \frac{f^3}{c^3} - (L + W + H)\frac{f}{c} + \frac{1}{2}, \tag{4.1}$$

where f is the operating frequency and c is the speed of light; $L, W,$ and H is the length, width, and height of a rectangular chamber, respectively. The modal density is approximated as

$$D_s(f) = \frac{dN_s(f)}{df} = 8\pi LWH\frac{f^2}{c^3} - \frac{L+W+H}{c}, \tag{4.2}$$

The number of modes within a frequency bandwidth, B_f, is approximately $B_f D_s(f_c)$ where f_c is the center frequency in the bandwidth.

Equations (4.1) and (4.2) were used to determine the number of modes at or below each center frequency and the total number of modes captured within a 100 MHz bandwidth centered at each frequency for both the SMART-80 and Small Chamber. Table 4.1 provides the modal counts and density for the individual chambers at the test band center frequencies.

Small Chamber			SMART-80		
Freq. [GHz]	$N_s(f)$	$B_f D_s(f)$	Freq. [GHz]	$N_s(f)$	$B_f D_s(f)$
1	603	183	1	124603	37396
2	4904	738	2	997306	149612
3	16603	1663	3	3366212	336637
4	39398	2957	4	7979422	598472
5	76987	4621	5	15585036	935118
6	133070	6656	6	26931156	1346574
7	211344	9060	7	42765884	1832839
8	315510	11834	8	63837319	2393915
9	449265	14978	9	90893564	3029801

Table 4.1: Modal Structure for Chambers. $B_f = 100$ MHz

Though it appears that 1 GHz might indicate an overmoded chamber, initial testing proved otherwise and will be discussed later in this chapter.

4.3: SHIELDING EFFECTIVENSS

A preliminary shielding effectiveness (SE) measurement when there is no coupling aperture on the small chamber shows how isolated the small chamber is when nested inside the SMART-80. Preliminary testing at a frequency range of 0.9 – 8.5 GHz showed poor SE as seen in

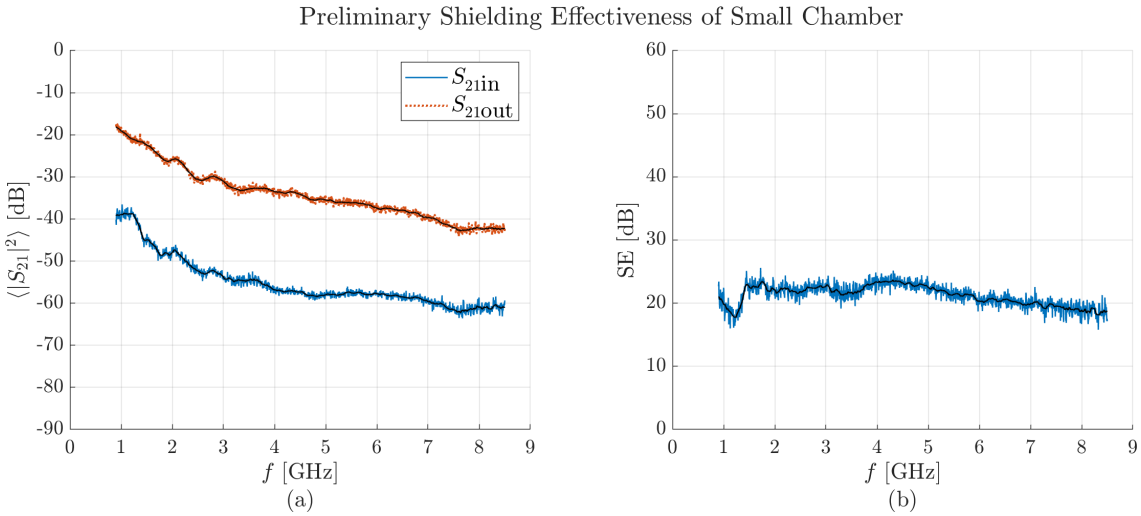

Figure 4.1: Preliminary SE of the Small Chamber

Figure 4.1. The SE was calculated using the formula found in [9, 45],

$$SE = -10\log_{10}\left(\frac{\langle |S_{21in}|^2 \rangle}{\langle |S_{21out}|^2 \rangle}\right), \tag{4.3}$$

where $\langle \sim \rangle$ indicates the ensemble average over the tuner positions and S_{21} represents the received signal from the transmitter as measured by the VNA, also known as the transmission coefficient. Pozar in [40] defines the transmission coefficient from the VNA's port 1 to the VNA's port 2 where the signal is transmitted from port 1 and received on port 2. The "in" and "out" subscript indicate when the RX antenna was *inside* the small chamber or *outside* on the floor of the SMART-80. Figures 4.2 and 4.3 provide the SE testing configuration with "in" and "out" visually clarified. Appendix A.1.3. show the experimental setup for S_{21in} and S_{21out} measurements.

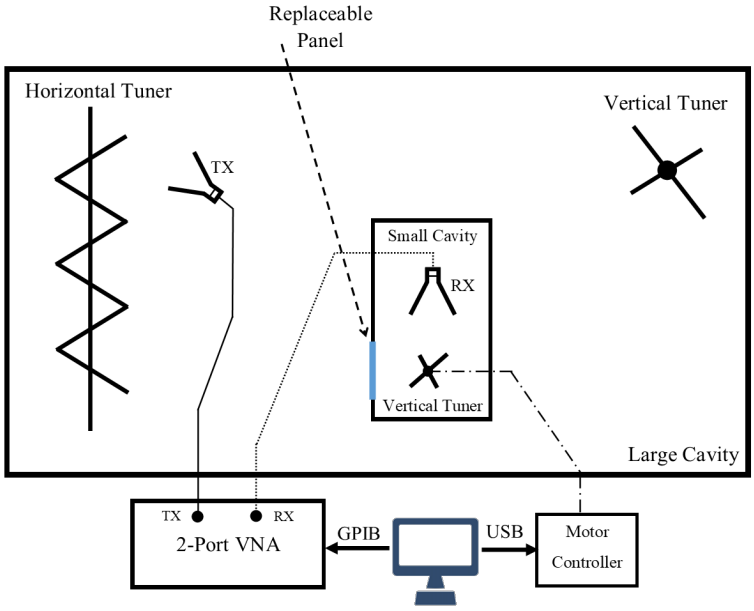

(a)

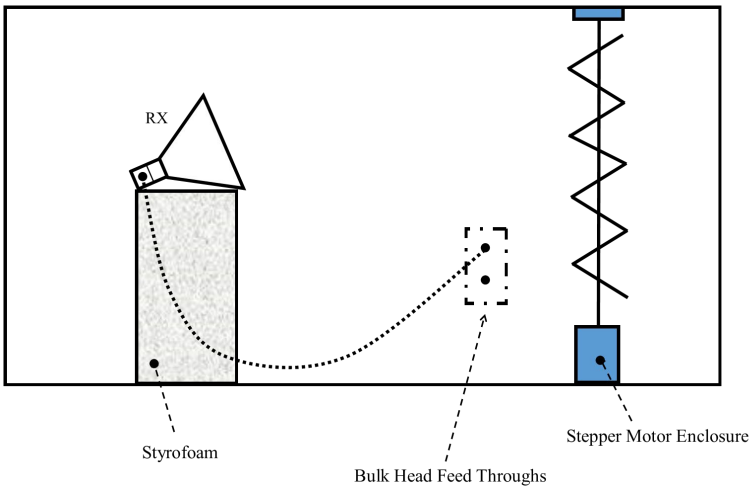

(b)

Figure 4.2: (a) $S_{21(in)}$ Setup; (b) RX Setup for inside Small Chamber

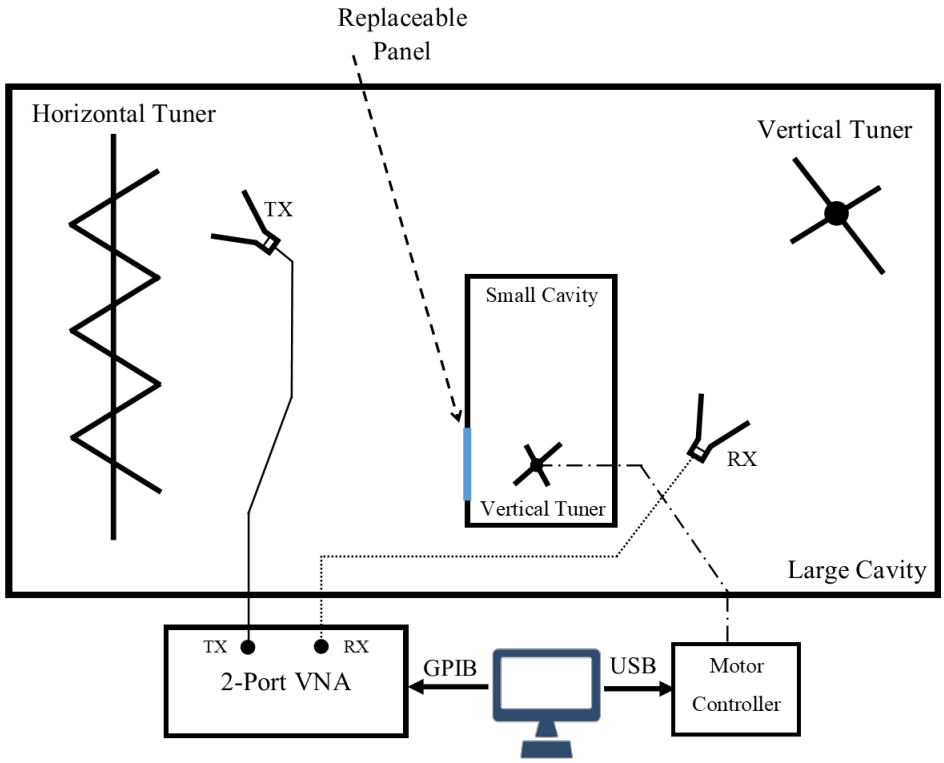

Figure 4.3: $S_{21(out)}$ Setup

As mentioned in the previous chapter, and shown in Figure 4.1, the preliminary SE was poor for a chamber such as this compared to other experiments with different apertures weakly coupling two chambers together [9, 45]. Careful repairs to the chamber included replacing the gasket material used to seal the door on the small chamber when it was shut, and using aluminum plates with gasket material attached as well to prevent any leakage from the windows on the small chamber. See appendix sections A.1.1. and A.1.2. for photos before and after repairs were made to the small chamber.

Figure 4.4 shows the SE measurement after the repairs. The SE has improved significantly, but there is a nearly constant mean S_{21in} of about -67 dB above 3 GHz, indicating that the receive signal levels were below the noise floor of the measurement VNA.

Two options to lower the noise floor of the system were considered, lowering the intermediate frequency (IF) bandwidth of the VNA or incorporating a microwave amplifier to boost the signal received and accounting for the amplifier gain in post processing. The latter option was used because lowering the IF bandwidth would considerably increase the measurement time beyond the current two hours for N = 100 tuner steps. The measured gain of the amplifier is shown in Figure 4.5.

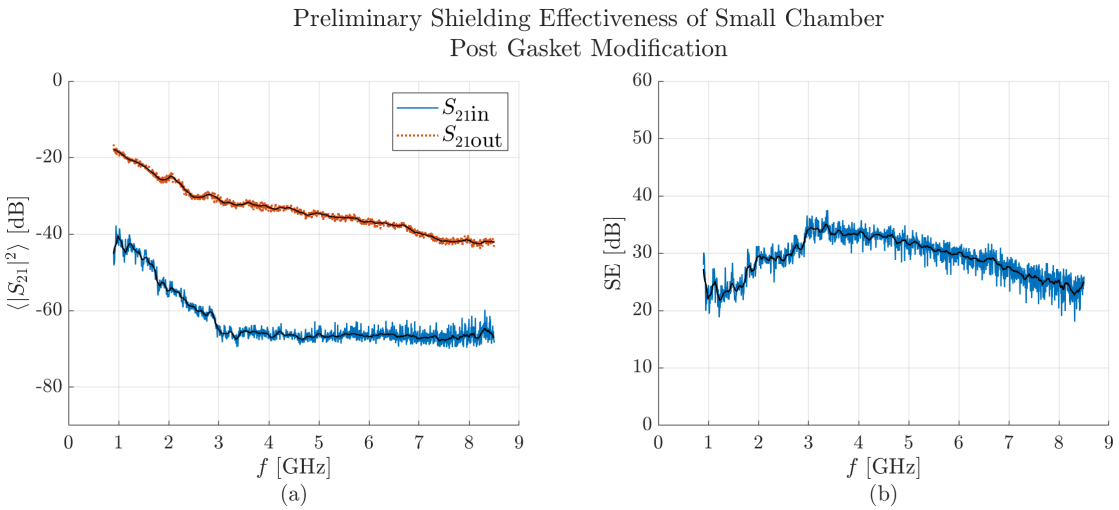

Figure 4.4: SE Post Gasket Repair

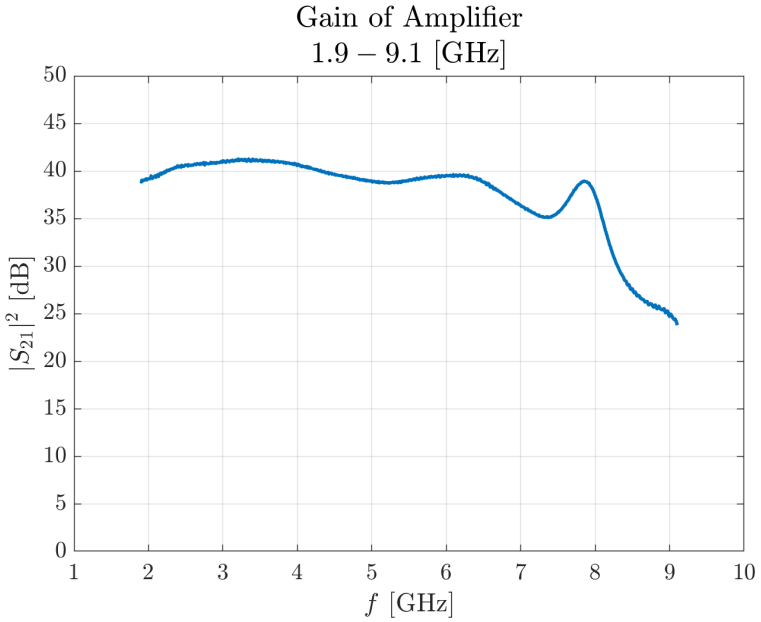

Figure 4.5: Gain of Microwave Amplifier

The mean received signal level with the amplifier in place is shown in Figure 4.6a, before and after the amplifier gain was removed. The resulting SE is shown in Figure 4.6b. From Figure 4.5, the operational band of the amplifier is 1.9 GHz to approximately 8.2 GHz. There is some concern with the decay of gain above 8.2 GHz. [4] provides a cautionary note that to receive accurate signal information, the noise floor should be at least 20 dB below the maximum signal power. With approximately a 20 dB difference between the signal with the amplifier in place and the noise level observed in Figure 4.4 before the amplifier was added, the field statistics within the 9 GHz band must be interpreted with caution. The 100 MHz bands that will be highlighted for the nested cavity statistics are centered 2, 5, and 8 GHz because they are well within the operational band of the amplifier and give a beginning, middle, and end performance of the full frequency band statistics.

The SE of the small chamber is very similar to the results Hill, in [9], measured in his series of measurements to see the SE of various types of composite material when attached to his nested chamber. The signal received has coupled into the cavity through the gasket material, which would represent real leakage in practical applications. When the aperture is in place, the seams around the gasket material will act as the coupling source when aperture excitation is not greater than the seams' excitation.

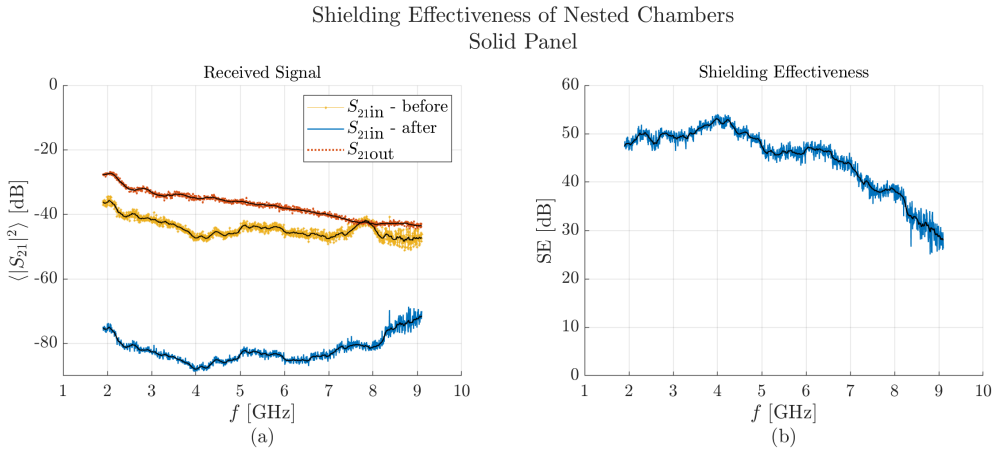

Figure 4.6: SE with Amplifier Accounted

4.4: FIELD SAMPLE STATISTICS

4.4.1: Ideal Anderson-Darling Simulations

With the small chamber showing reasonable SE, it must be confirmed that both chambers exhibit exponentially distributed data at 95% and 99% confidence. The implementation of the Anderson-Darling (AD) test to test ideal data against an exponential distribution at 95% and 99% confidence was first verified. 1601 numerically generated, ideally exponentially distributed data sets of 100 samples each were used to test against an exponential distribution using exponential distribution using the AD test. These two numbers were chosen because the VNA collects 100 field samples corresponding to the 100 different tuner positions at 1601 discrete frequencies. Figure 4.7 shows the p-values (α) returned by the AD test when the numerically generated exponential data sets are tested against an exponential distribution.

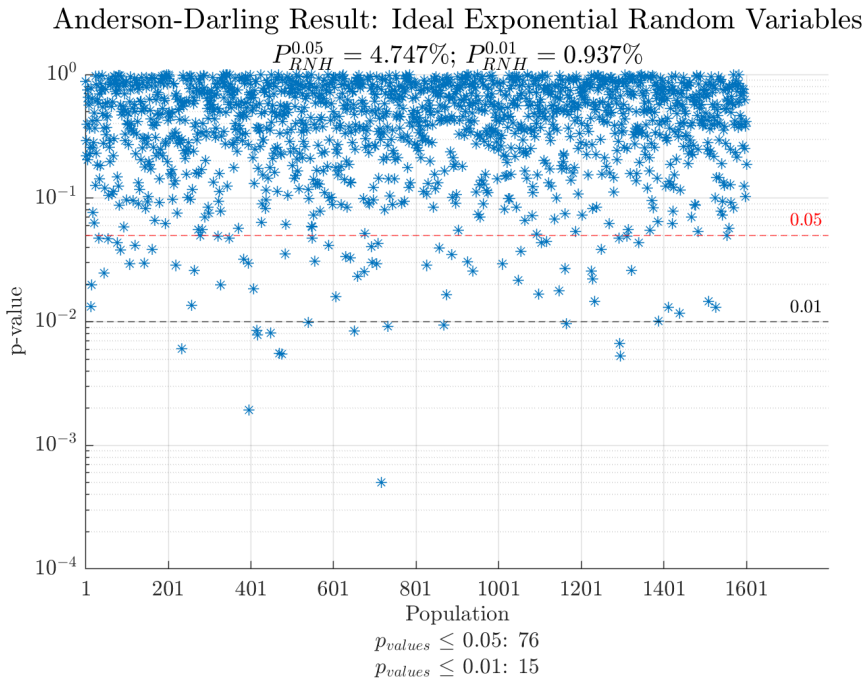

Figure 4.7: AD rejection rates with ideal exponential data when (a) $\alpha = 0.05$; (b) $\alpha = 0.01$. The sample sets are tested against an exponential distribution.

The null hypothesis is rejected when α is below 0.05 or 0.01 for the confidence levels 95% and 99%, respectively. The use of P_{RNH}^{α} represents the total percentage of samples sets that rejected the null hypothesis (RNH) at the specified α level ($\alpha = 0.05$ or 0.01). The rejection rates shown in Figure 4.7 of 4.747% and 0.937% are very close to the expected theoretical rates of 5% and 1%, indicating the AD test is working properly with the ideal data, and that the sample data follows an exponential distribution.

The same ideal exponential data sets are tested against a log-normal distribution to demonstrate the behavior of the AD test when sample sets are tested against a distribution they should not follow. Figure 4.8 shows the test results, and most of the data has been rejected as seen by the dense population at p-value $= 0.0005$. The null hypothesis of log-normal distributed samples is rejected 89.132% at 95% confidence and 74.828% at 99% confidence. Note that the null hypothesis rejection rate is under 100% at both confidence levels, showing the finite power of the AD test with 100 samples. Power, and the associated rejection rate, would increase with additional independent samples.

It can be concluded, however, that these sample sets do not follow a log-normal distribution because they were all drawn from the same distribution and the rejection rates are much greater than 5% and 1%, respectively.

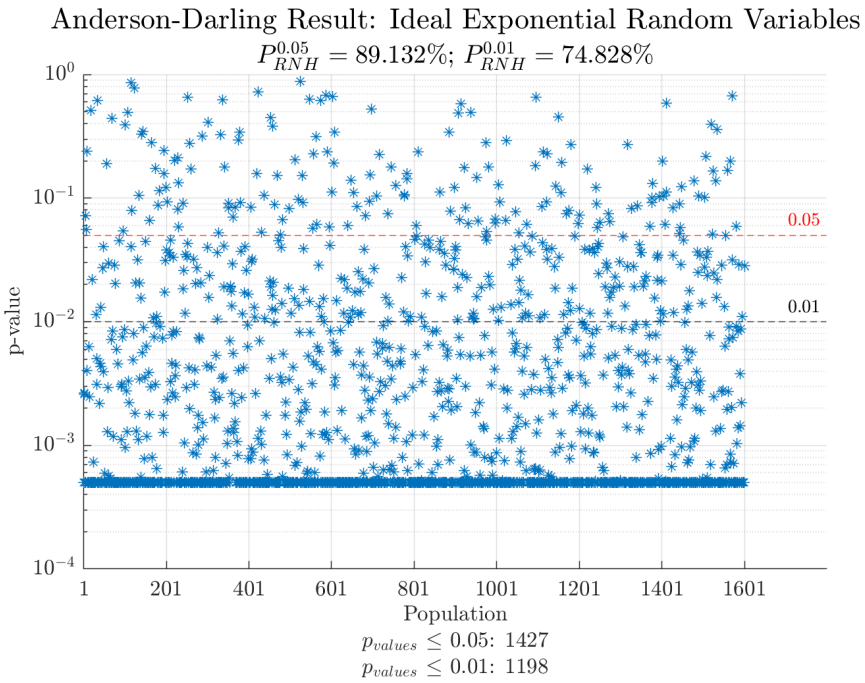

Figure 4.8: AD rejection rates with ideal exponential data when (a) $\alpha = 0.05$; (b) $\alpha = 0.01$. The sample sets are tested against a log-normal distribution.

4.4.2: Anderson-Darling Experimental Layout

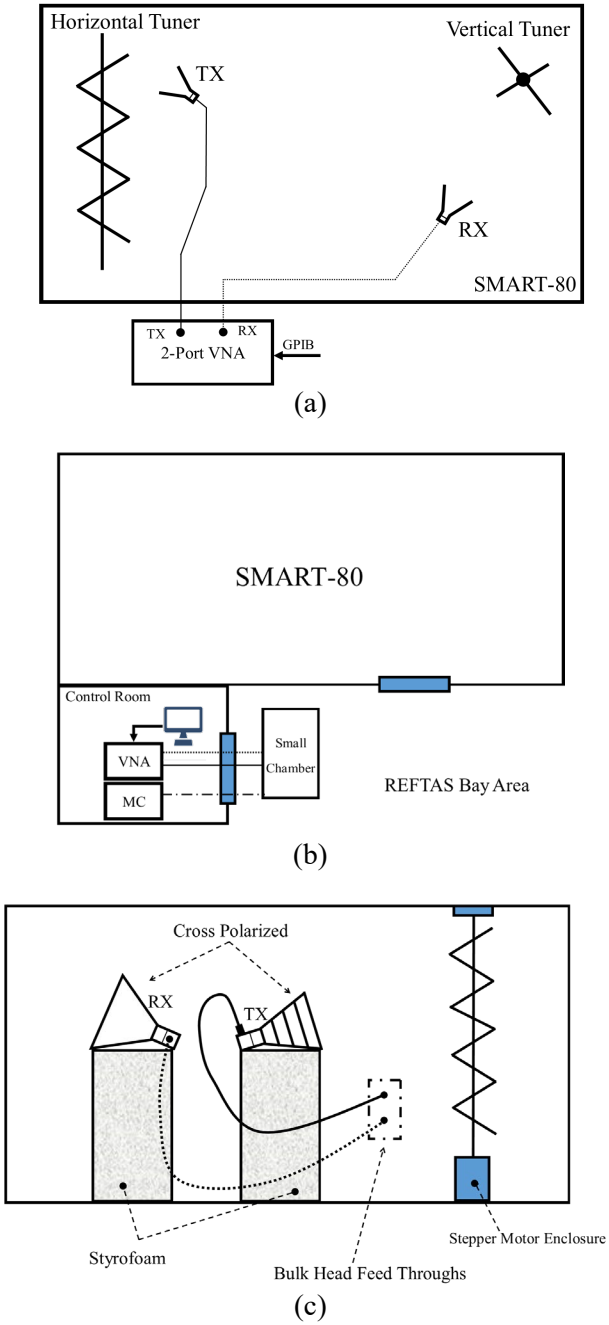

Figure 4.9: (a) SMART-80 Validation Test Setup, (b) Location of Small Chamber for Validation, (c) Internal Antenna Placement for Small Chamber Validation Test Setup

Figure 4.9a shows the schematic for how the antennas were placed in the SMART-80 to collect the hypothesized exponential samples. Figure 4.9b and 4.9c show the location of the small

chamber and how the antennas were placed inside the small chamber to collect the hypothesized exponential samples. Appendix A.1.4 provide the pictures for what Figure 4.9a looked like, and how the antennas were placed and oriented for Figure 4.9c.

4.4.3: Experimental Field Statistics – Small Chamber

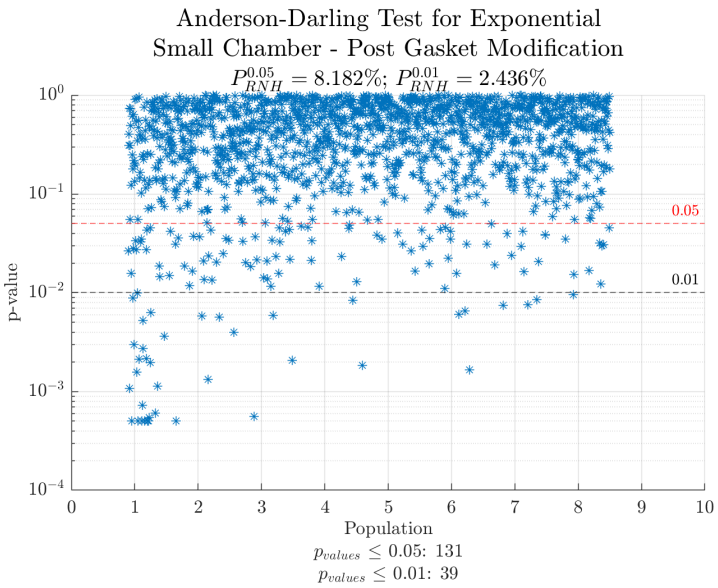

Figure 4.10: Preliminary AD results after gasket modification

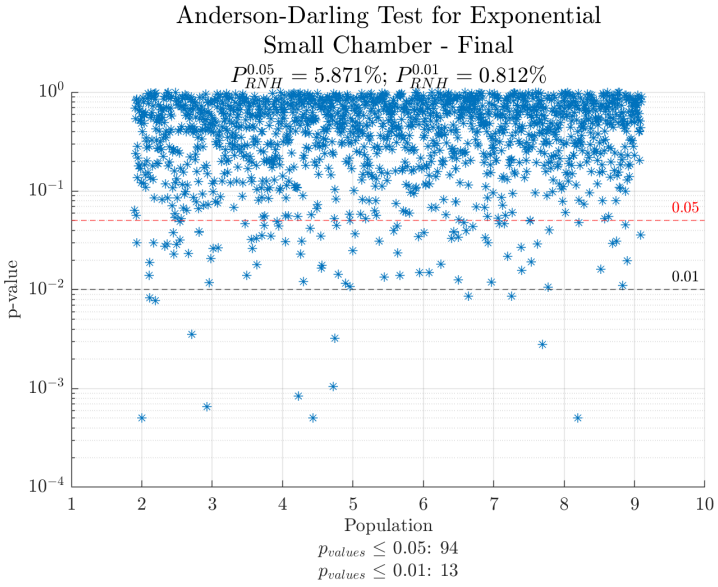

Figure 4.11: Small Chamber AD results, Final

Figure 4.10 shows the AD test when applied to the samples collected from a frequency range of $0.9 - 8.5$ GHz. The rejection rate is too high (8.182% and 2.436% for 95% and 99% confidence, respectively), especially at the lower frequencies indicating insufficient stirring. Adding aluminum foil (see appendix Figure A.9.) was used to enlarge the tuner and the tuner itself was also tightened to the stepper motor shaft. With there being higher rejection rates at the lower frequencies, the frequency test band was also shifted to $1.9 - 9.1$ GHz. Figure 4.11 shows the AD test after these modifications.

The rejection rates at both at the 95% and 99% confidence levels are 5.8713% and 0.8119%, respectively. With the rejection rates near that of an ideal chamber, the small chamber is now able to create the exponential data sets.

4.4.4: Experimental Field Statistics – SMART-80

As indicated, for completeness, an AD test was performed on the SMART-80's collected samples. The setup for the experiment was a frequency range of $1.9 - 9.1$ GHz with 1601 frequency samples, $N = 100$ tuner steps.

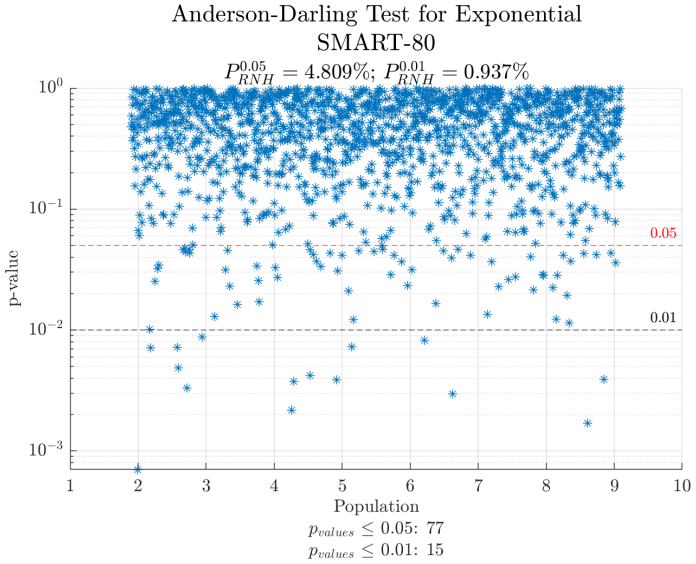

Figure 4.12: SMART-80 AD Results

Figure 4.12 shows that the SMART-80 is acting as an almost ideal environment to create fields that follow an exponential distribution. With rejection rates of 4.8095% and 0.93691% for the 95% and 99% confidence levels, the SMART-80 is performing as expected.

4.4.5: Quality Factor

The quality factor (in the frequency domain) of an RC can be calculated from the measured field samples using

$$Q = \frac{16\pi^2 V}{\lambda^3} \times \frac{\langle P_r \rangle}{P_t}, \tag{4.4}$$

where V is the chamber volume, λ is the wavelength, and $\langle P_r \rangle / P_t = \langle |S_{21}|^2 \rangle$ [6, 7, 9, 41, 46]. For the construction of a RC, metals with higher conductivity used to construct the walls creates a higher quality factor because the wall's ohmic losses will be minimized resulting in a high Q [4, 6]. [4] defines the quality (Q) factor as a measurement of the ability of a chamber or cavity to store

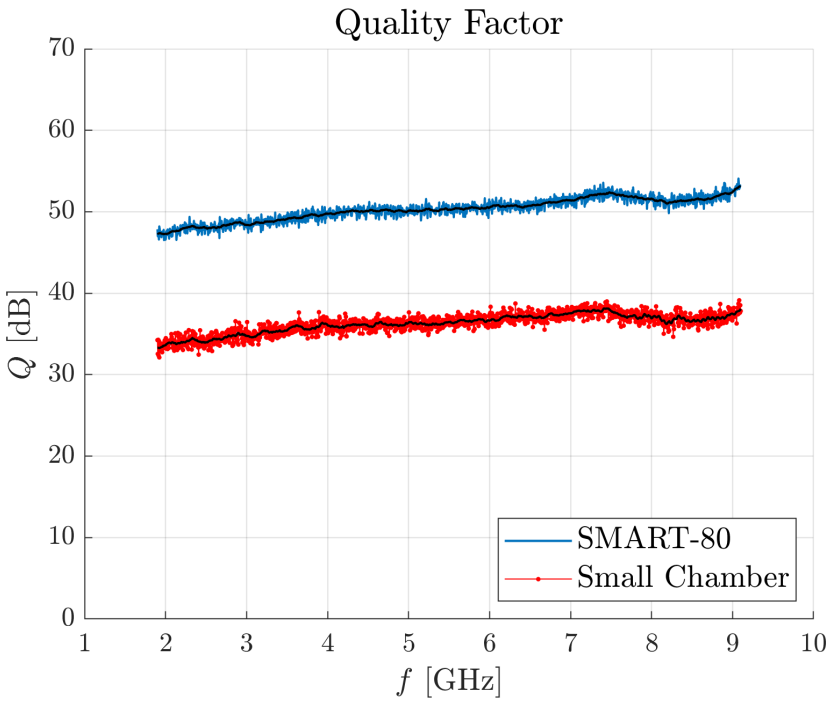

Figure 4.13: Q factor of both chambers

energy relative to its rate of dissipation. It states that the dominate loss mechanisms of an empty chamber are from absorption in the walls, loading by the antennas, leakage from unintended apertures, or from intentional loading. The Q of both chambers was measured and is shown in Figure 4.13 for documentation completeness.

It is not surprising that the small chamber has a lower quality factor because, as Equation (4.4) indicates, it is proportional to the chamber internal volume. Additionally, the steel type 5 walls of the small chamber are less conductive than the galvanized steel walls of the SMART-80.

4.5: AUTOCORRELATION CHECK

The final unnested test to be conducted is to verify that both chambers are creating independent field samples under tuner rotation. The correlation coefficient of the samples collected at a single frequency as the tuner is rotated is estimated using [4]

$$r_m = \frac{\frac{1}{n-1}\sum_{i=0}^{n-1}\{(x_i-\mu)(x_{i+m}-\mu)\}}{\sqrt{\left(\frac{\sum_{i=0}^{n-1}(x_i-\mu)^2}{n-1}\right)}\sqrt{\left(\frac{\sum_{i=0}^{n-1}(x_{i+m}-\mu)^2}{n-1}\right)}}, \tag{4.5}$$

where, r_m is the correlation coefficient, n is the total number of tuner steps, x_i is the i^{th} magnitude-squared field sample associated with the i^{th} tuner step, x_{i+m} is the sample lagged by m tuner steps, and μ is the estimated sample mean. The two values in the denominator of Equation (4.5) are the same with cyclic samples provided by rotating the tuner, so (4.5) becomes

$$r_m = \frac{\sum_{i=0}^{n-1}\{(x_i-\mu)(x_{i+m}-\mu)\}}{\sum_{i=0}^{n-1}(x_i-\mu)^2}. \tag{4.6}$$

According to [4], a correlation below $\frac{1}{e}$ (≈ 0.37) indicates that the samples can be considered independent and was used. Setting the threshold to 0.5 was also used to see the total number of instances where the correlation was much greater than 0.37.

Section 4.5.1: Autocorrelation Experimentation Results

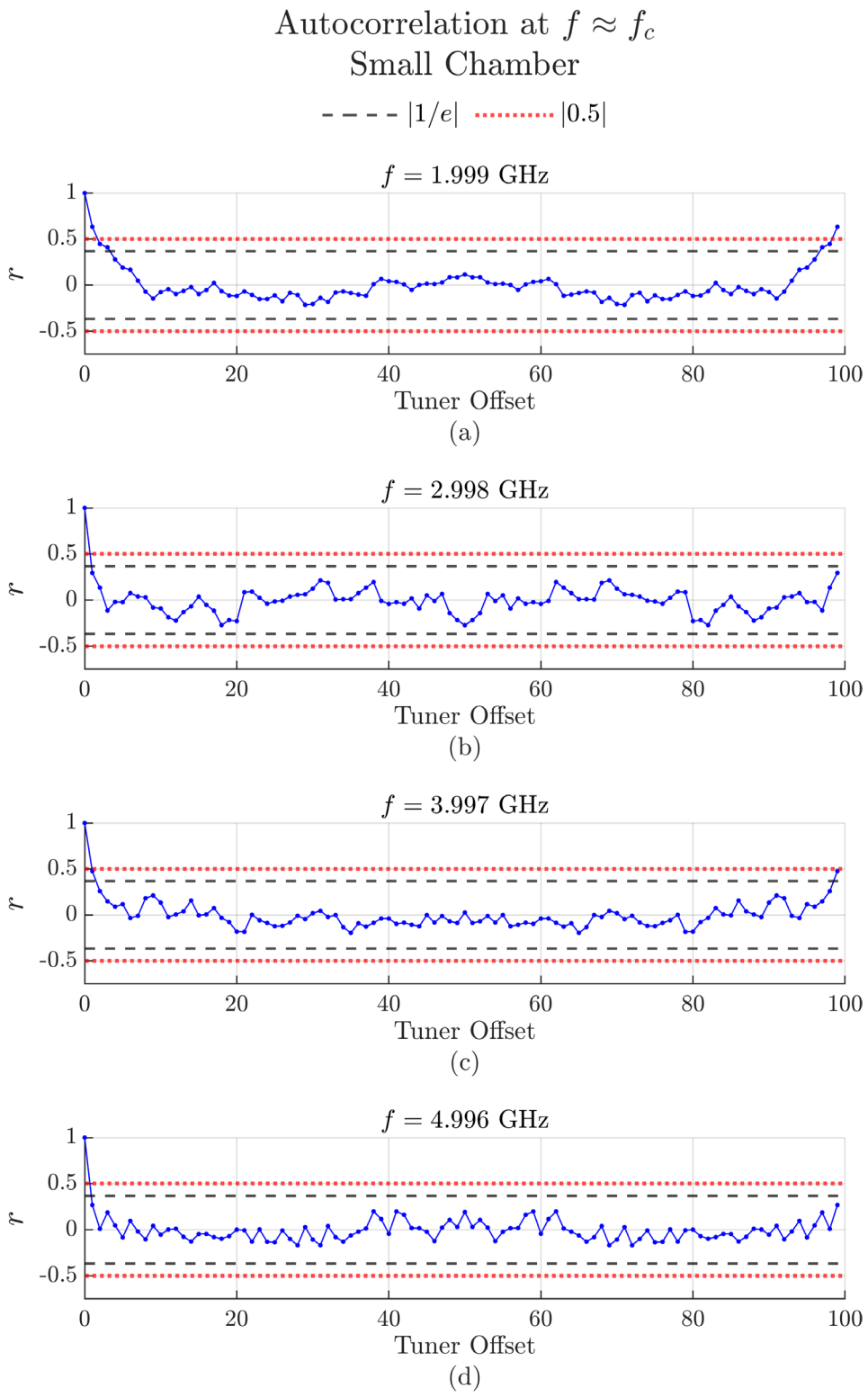

Figure 4.14: Autocorrelation of small chamber tuner at $f_c \approx 2, 3, 4, 5$ GHz

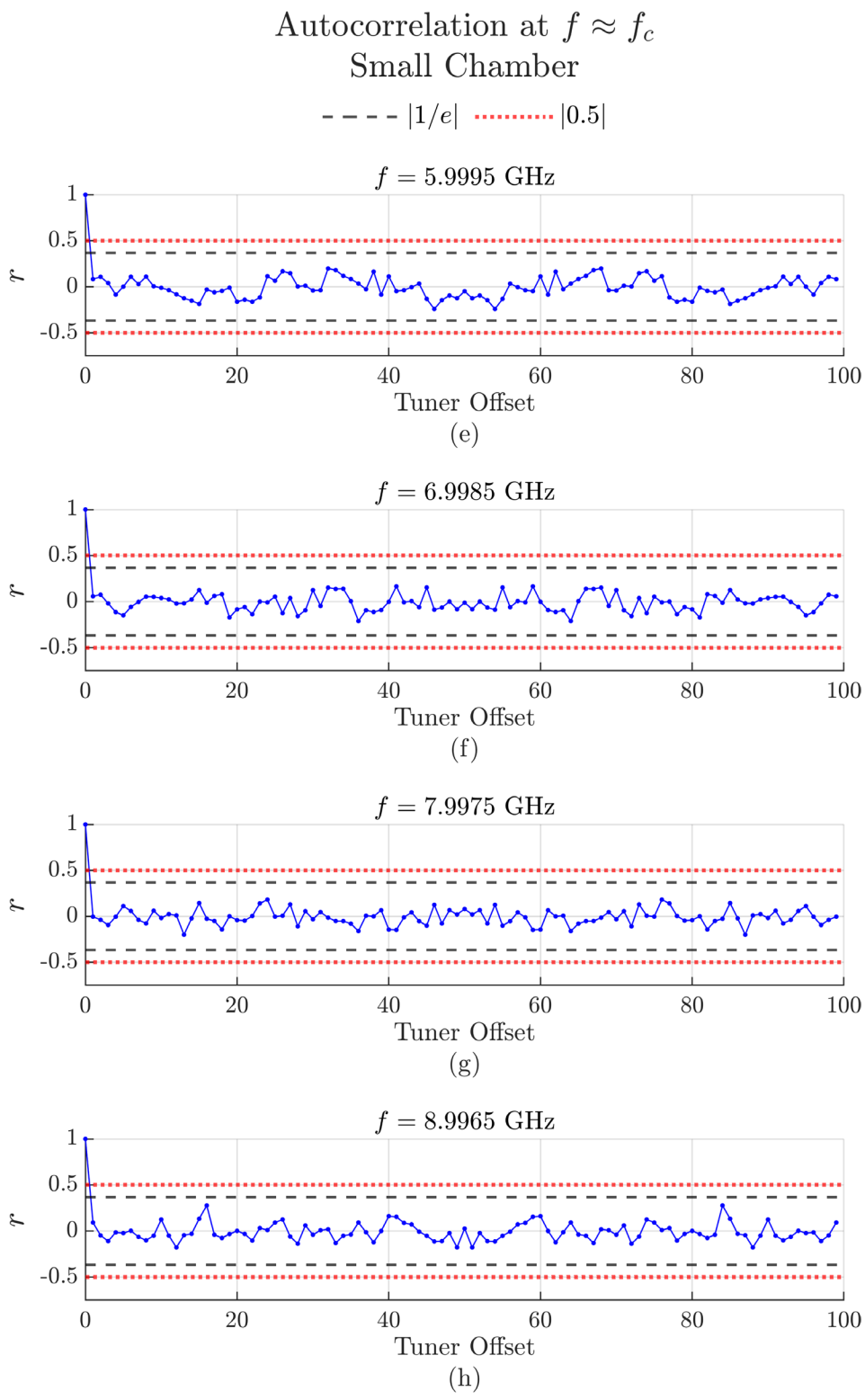

Figure 4.14 cont.: Autocorrelation for the small chamber tuner at $f_c \approx 6, 7, 8, 9$ GHz

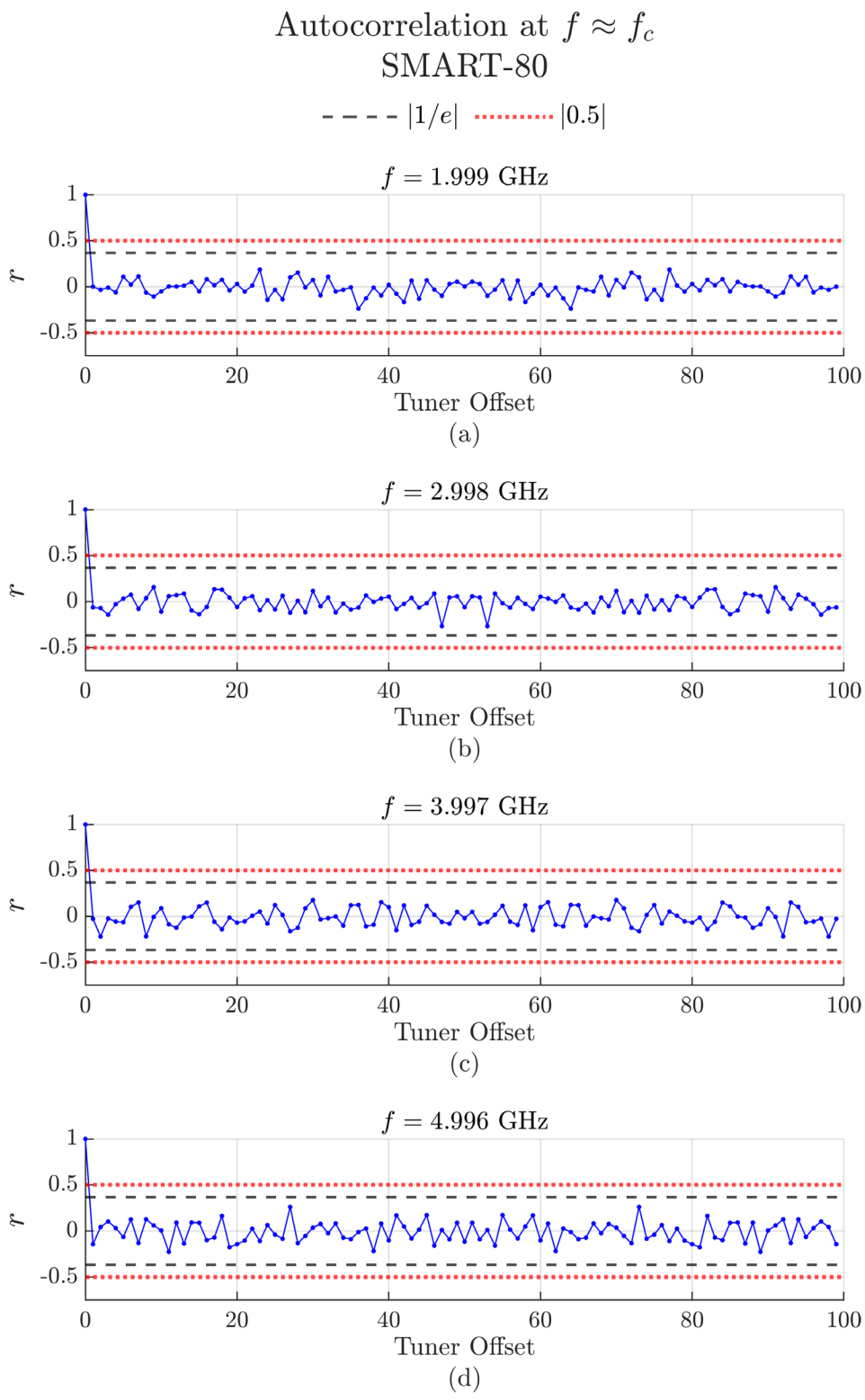

Figure 4.15: Autocorrelation of SMART-80 tuners. $f_c \approx 2, 3, 4, 5$ GHz

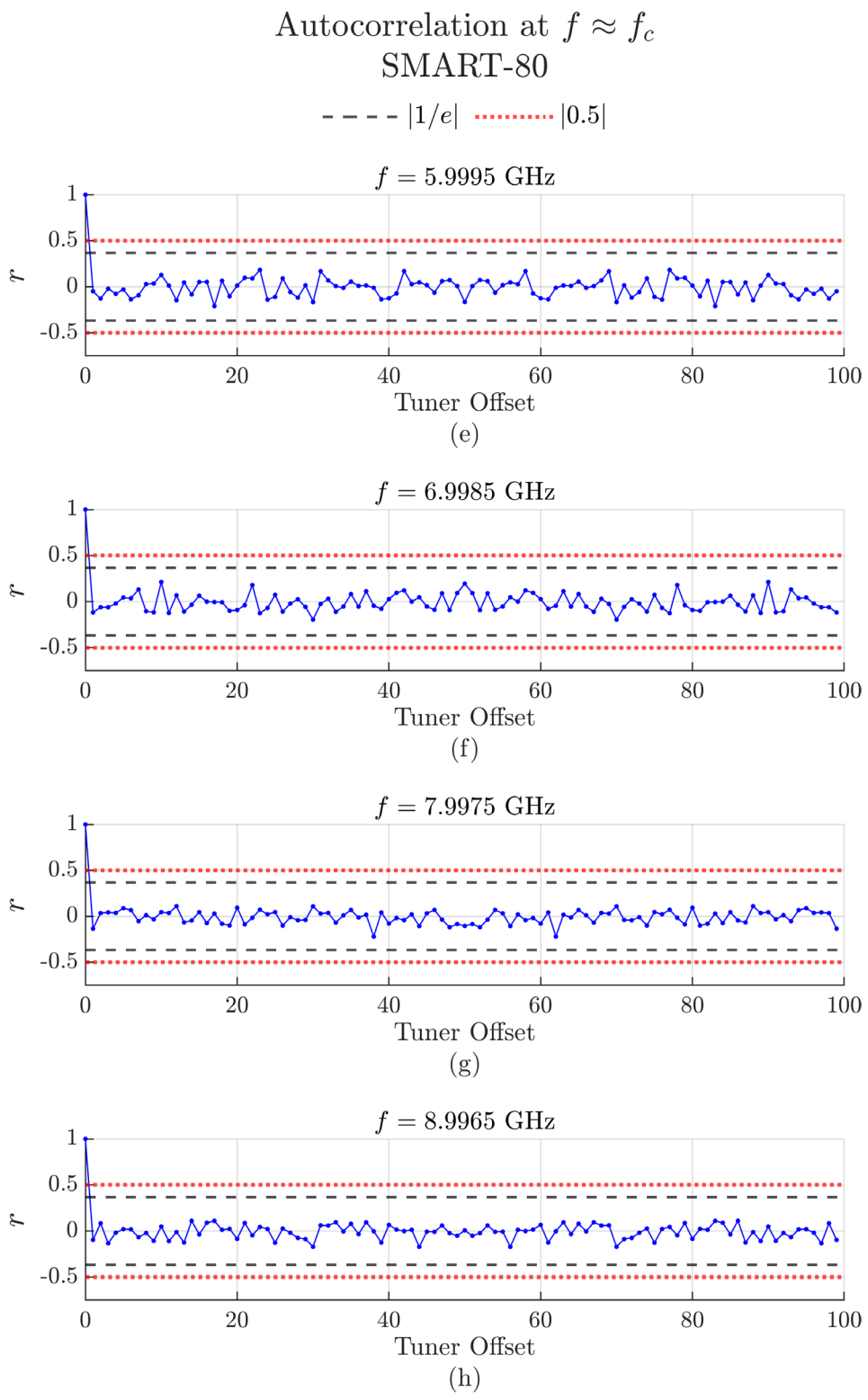

Figure 4.15 cont: Autocorrelation for SMART-80 tuners. $f_c \approx 6, 7, 8, 9$ GHz

Total number of instances where the first three lags cross the $|1/e|$ and $|0.5|$ thresholds.
The total number of samples in each bandwidth is shown.

		Small Chamber						SMART-80					
Frequency	Total Frequency Samples	$\|1/e\|$			$\|0.5\|$			$\|1/e\|$			$\|0.5\|$		
Bandwidth [GHz]	Samples in each Bandwidth	r_1	r_2	r_3	r_1	r_2	r_3	r_1	r_2	r_3	r_1	r_2	r_3
$f < 2$	23	16	1	1	6	0	0	0	0	0	0	0	0
$2 \leq f < 3$	222	77	1	2	13	0	0	0	0	0	0	0	0
$3 \leq f < 4$	222	17	0	1	0	0	0	0	0	0	0	0	0
$4 \leq f < 5$	222	4	0	0	0	0	0	0	0	0	0	0	0
$5 \leq f < 6$	223	3	0	0	0	0	0	0	0	0	0	0	0
$6 \leq f < 7$	222	0	0	0	0	0	0	0	0	0	0	0	0
$7 \leq f < 8$	222	2	0	0	0	0	0	0	0	0	0	0	0
$8 \leq f < 9$	222	2	0	0	0	0	0	0	0	0	0	0	0
$9 \leq f$	23	0	0	0	0	0	0	0	0	0	0	0	0

Table 4.2: Number of breaches in each frequency bandwidth indicated by the autocorrelation function

The autocorrelation found from 100 field samples measured in the small chamber at the frequencies closest to the test-band center frequencies are shown in Figure 4.14. It can be easily seen at Figure 4.14a and Figure 4.14c, there is some indication of correlation at lag 1 for the small chamber at these lower frequencies.

Figures 4.14d-h show a decrease in correlation as the approximate center frequencies increase for the small chamber. Figure 4.15, representing the correlation behavior for the SMART-80, shows no indication of correlation at any lag for the approximated center frequencies.

Table 4.2 shows the total number of samples contained in each bandwidth and the total number of instances where the first three lags break the indicated threshold. Like figure 4.15a, there is indication of some correlation with lag-1 at lower frequency bands for the small chamber. When the frequency is less than 2 GHz, 16 of the 23 (70%) lag-1 correlation coefficients exceed the 0.37 threshold while 6 of 23 (27%) exceed 0.5. At the next frequency band, 77 of the 222 ($\approx 35\%$) correlation coefficients exceed 0.37 and 13 of 222 (6%) exceed 0.5. At higher frequencies, a limited number of lag-1 correlation coefficients exceed the 0.37 threshold but none exceed 0.5. There is little indication of correlation at lags of 2 or greater. The small correlation at lag-1 in the 1.9 – 3

GHz frequency band indicates that there is somewhere between 50 and 100 independent samples. The total number of correlation coefficients that broke the 0.37 threshold at lag-2 and lag-3 (Table 4.2) is small enough to be considered statistical anomalies for the small chamber. However, with the AD showing near 5% and 1% rejection rates for the small chamber, the correlation is sufficiently small and does not significantly affect the statistical analysis and can be neglected.

The SMART-80 shows no indication of correlation within any frequency band, showing that all 100 samples are independent at all test frequencies.

4.6: SUMMARY

The statistical tests show that both chambers have provided a sufficient number of independent, magnitude-square field samples to do the nested cavity study. Additionally, the SE of the small chamber has been shown to adequately isolation the outer and inner chamber environments for weakly-coupled chamber measurements. The AD test was performed on the magnitude-squared samples from both chambers and the results for each were consistent with exponentially distributed samples at 95% and 99% confidence. Though the autocorrelation check indicated correlation at the lower frequencies for the small chamber, with the AD showing the exponential behavior of the small chamber at almost ideal rejection rates, the correlation has no significant impact on the statistics.

CHAPTER V

NESTED CAVITY MEASUREMENTS

5.1: CHAPTER LAYOUT

The following chapter contains two sections. The first presents the SE when the two chambers are nested with various coupling apertures. The second shows the statistical fits of the double-Rayleigh (DR) and exponential distributions to the field samples measured within the smaller chamber of the nested cavity operation for two coupling configurations.

5.2: SHIELDING EFFECTIVENESS

This section will show the SE of when the solid panel (SP) and several aperture plates were used to coupled the nested chamber. The case in which the SP was used to determine the small chamber's SE when in isolation was presented in the previous chapter. The results will be show again here for convenience and completeness.

5.2.1: Aperture Layout

The apertures selected for this study are based on similar sizes used in [10, 35, 47]. Figure 5.1 provides a layout of the panel with all the apertures in place while Table 5.1 provides the dimensions of each aperture. (A single dimension indicates the diameter of a circular aperture.) When each aperture was tested separately, conductive tape with conductive adhesive generously covered the apertures that were not being tested. The conductive properties shielded the aperture to

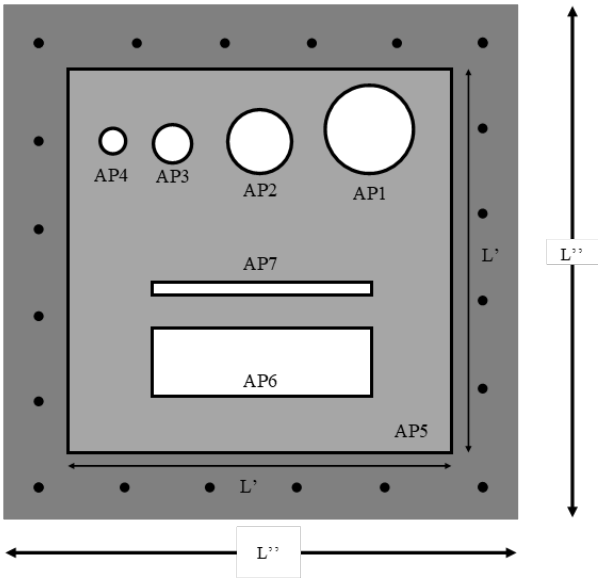

Aperture	Dimension(s) (cm)
AP1	3.5
AP2	2.54
AP3	1.59
AP4	0.95
AP5	30 by 30
AP6	15 by 6
AP7	15 by 1
Dimension	**Measurement (cm)**
L'	30
L''	40.64

Table 5.1: Aperture and Plate Dimensions

Figure 5.1: Aperture Layout

prevent any unwanted leakage. AP5 represents the dimensions of the aperture when the panel was completely removed from the small chamber, exposing a 30 × 30 cm window.

5.2.2: Shielding Effectiveness Results

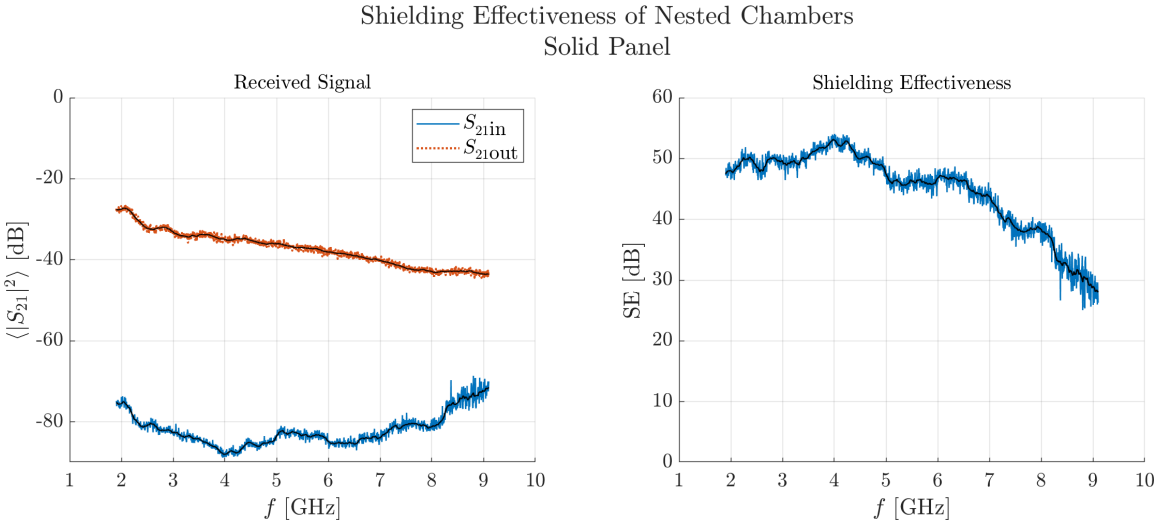

Figure 5.2: Shielding Effectiveness – Solid Panel (repeated from chapter 4)

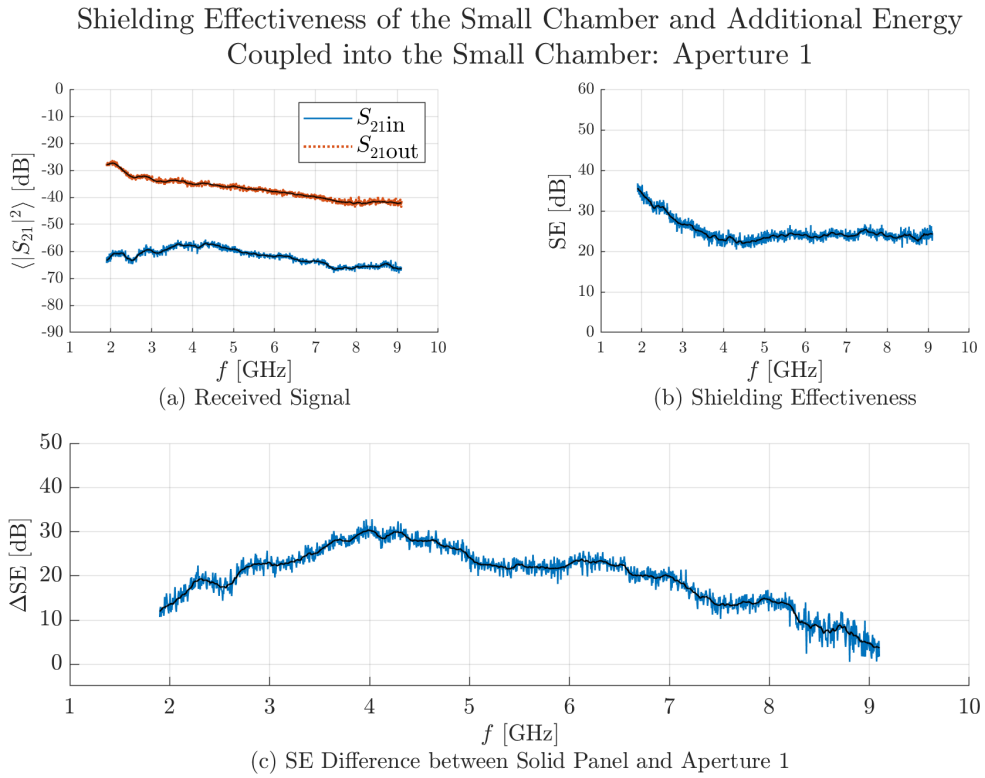

Figure 5.3: Shielding Effectiveness - AP1

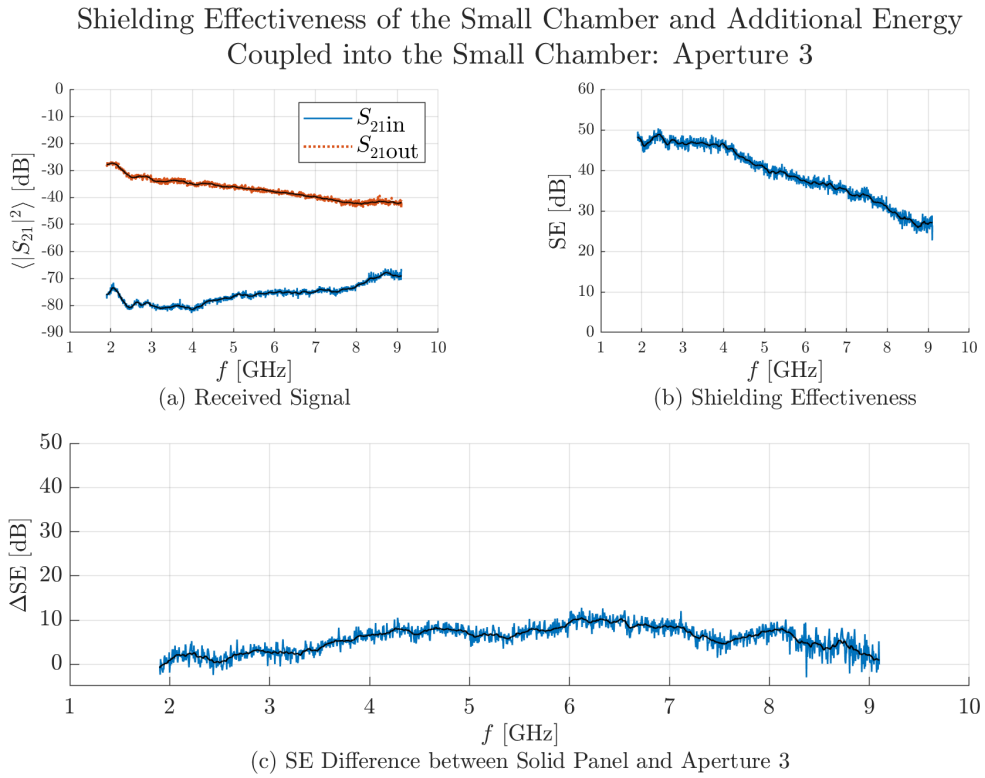

Figure 5.4: Shielding Effectiveness - AP3

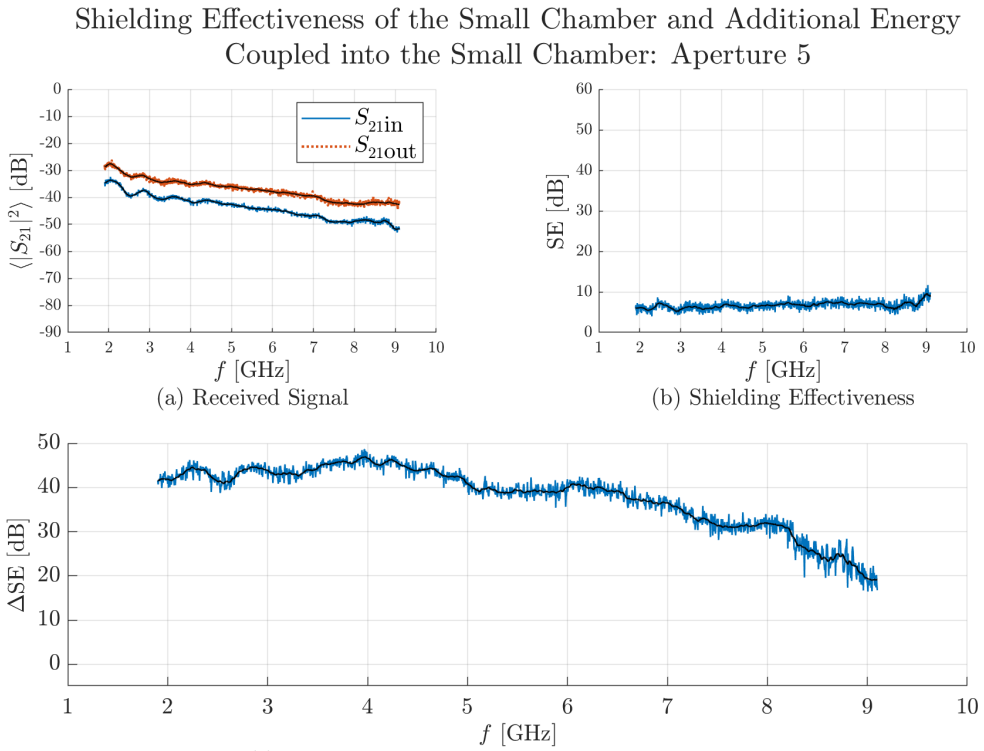

(a) Received Signal

(b) Shielding Effectiveness

(c) SE Difference between Solid Panel and Aperture 5

Figure 5.5: Shielding Effectiveness – AP5

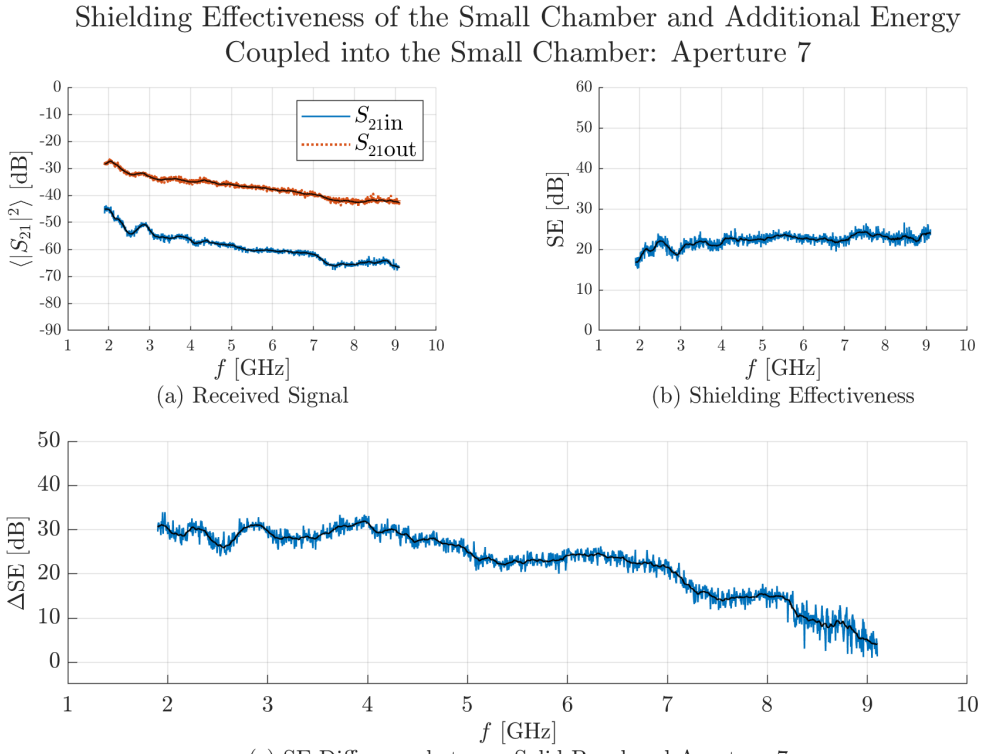

(a) Received Signal

(b) Shielding Effectiveness

(c) SE Difference between Solid Panel and Aperture 7

Figure 5.6: Shielding Effectiveness - AP7

5.2.3: SE Discussion

Figures 5.3 – 5.6 show the collected signal (a), SE (b), and the additional energy coupled (AEC) into the chamber referenced to when the small chamber has the SP in place (c). The AEC into the small chamber was calculated as such,

$$AEC = SE_{SP}\ (\text{dB}) - SE_{APX}\ (\text{dB}), \tag{5.1}$$

where SE_{SP} is the shielding effectiveness of the small chamber with the solid panel in place, SE_{APX} is the shielding effectiveness of the small chamber when a certain aperture defined by "X" was in place. This was useful to have an idea of how much energy physically couples into the chamber establishing the random fields within the cavity for the various apertures. [9] discusses the relation between SE and size of the aperture relative to wavelength.

The SE with aperture AP3 in place, shown in Figure 5.4, is the highest of the four apertures considered. AP3 is a circular aperture of 1.59 cm diameter, the smallest maximum dimension of the four apertures. Wavelengths at frequencies below 18.855 GHz are therefore greater than the aperture diameter. The lowest frequency tested (1.9 GHz) has a wavelength of 15.77 cm, which is much larger than the AP3 diameter in terms of the lowest usable frequency (LUF). The aperture therefore gives weak coupling between the chambers. As the frequency increases and the wavelength gets smaller, the SE decreases because the aperture size is electrically larger and coupling increases. The SE of AP3 and SP (Figure 5.4c) are similar since the coupling through the aperture is only slight greater than the leakage when the solid plate is in place. The SE of AP3 is similar to the grid hole case in [45].

The largest circular aperture, AP1, Figure 5.3, gives a lower SE than AP3. This should not be surprising because the physical diameter of the aperture has increased to 3.5 cm. The energy

coupling is correspondingly higher, with a mean peak of 30 dB occurring at around 4 GHz. The SE behavior of AP1 is similar to the SE of circular apertures measured in [9].

AP5 is the case in which the entire panel was removed from the small chamber, giving a 30×30 cm coupling window. There is poor SE with a mean of approximately 6 dB across the entire frequency band. This suggests that the two chamber cavities are acting as a single resonant environment because the dimensions of the window are much greater than the LUF.

The SE when AP7, a 15×1 cm "slit" aperture, was in place is shown in Figure 5.6. The SE has significantly increased compared to AP5 but is still not quite has strong as when the two circular apertures were in place (AP1 and AP3). With the largest dimension of the aperture being 15 cm, which is only slightly smaller than the LUF wavelength, it is not unexpected that the SE is not as strong as AP1 and AP3.

5.2.4: Statistical Predictions Based on SE

The SE measurements show that the coupling between the two chambers is weakest when, of all configurations considered, the SP is place. The only energy coupling into the small cavity is what is leaked into it through the gaskets seams on the door and window. This weakest coupling provides the most likely conditions for the inner cavity fields to follow the DR distribution.

AP1 and AP3 give relatively high SE, higher than was measured in [10], which also indicates that the field statistics inside the cavity might converge to that of DR. However, as the frequency increases, the electrical size of the aperture increases, decreasing the SE and increasing the cavity coupling. The field statistics are therefore predicted to transition from DR to exponential as the frequency increases.

AP5 is predicted to give exponential field statistics because the two chambers are expected to be acting as one as previously discussed.

The slit case, AP7, shows greater SE than [10]'s "long center" case, which may show favorable conditions for DR fields at the lower frequency bands. As the frequency increases, however, the statistics are expected to transition to exponential because largest dimension is increasing in size (electrically).

5.3: STATISTICAL ANALYSIS

The following section will show the statistical behavior of the measured fields in the small (inner) chamber of the nested-cavity test when two techniques are employed to obtain independent field samples. The VNA swept across the 1.9 – 9.1 GHz frequency range (1601 frequencies in the range) to allow for frequency stirring, while the external and internal mechanical tuners were moved in sync through 100 steps to give mechanical mode tuning. This allowed for 1601 individual electric fields, excited by their frequencies, to be sampled 100 times, so the statistical behavior at each frequency can be observed. The theoretical CDFs and ECDF at three discrete frequencies within each frequency band are presented: the lowest frequency within the band (extreme low), the frequency closest to the center frequency, and the highest frequency within the band (extreme high). Each distribution plot will also show the respective p-values from the GOF tests performed on the hypothesized distribution against the empirical distribution.

After the mechanically tuned distributions have been shown, the Kolmogorov-Smirnov (KS) two sample test will be used to determine if a combination of frequency + mechanically stirring the data is appropriate. The KS two sample test is useful because it does not require any prior information about the underlying distribution of the samples. The test simply indicates whether two independent distributions do not follow the same underlying distribution with a certain confidence. The null hypothesis is rejected when they likely do not follow the same distribution [48]. The KS two sample test will show how likely the samples collected at two different frequencies in the 100 MHz bandwidth follow different underlying distributions at a 95% confidence. If the null hypothesis is rejected with too many frequency pairs (for example much

higher than 5% at 95% confidence), then frequency + mechanically stirring the data should not be used, or at the very least, the bandwidth of the frequency stirring should be adjusted.

Two cases will be presented in this section: the solid panel case and AP1. The solid panel case creates the most isolated environments for the multiplicative effect of the independent variables to occur from the leakage through the gaskets. AP1 was selected because it maintained high SE. As discussed in Chapter 4, three frequency bands will also be highlighted for the two cases: 100 MHz bands centered at $2, 5,$ and 8 GHz.

The section also presents the global total rejection rates at 95% confidence from the AD and chi-square GOF test for all the apertures and frequency bands in a table.

5.3.1: Goodness of Fit Testing

As discussed previously, the Anderson-Darling (AD) test will be used to provide a sense of confidence in how well the empirical data follows the exponential distribution. The respective AD p-value will be provided below each CDF plot with the notation "$EX - A^D$."

Pearson's chi-square test will be used to determine if the empirical data is well described by the DR distribution. As mentioned previously, the chi-square is less powerful than the AD. To show the difference in power, the chi-squared test is also used to test the fit of the exponential distribution to the empirical data. The notation "$DR - \chi^2$" and "$EX - \chi^2$ " represents when the double-Rayleigh (DR) and exponential (EX) CDFs were tested against the ECDF using the chi-squared test. The chi-squared test is dependent on the number bins selected for the observation counts. [49, 50] indicate a common way to find the bin count is to use $b = floor(\sqrt{N})$, where N is the number of field samples available. Using this so-called square root choice, 10 bins were used for 100 samples. When the frequency + mechanically stirred data was used to create the CDF plots,

the 100 MHz bandwidth give 2,200 samples, therefore 46 bins were used. Using MATLAB's 'histcount()' function, the CDF data was divided into equal-probability bin widths.

The symbols ⊕ and ⊗ are used to indicate when the GOF test has failed to reject the null hypothesis or has rejected the null hypothesis, respectively, on all the CDF plots. This is to provide a quick visual of how the distribution performed under the test. The tests are performed at a confidence level of 95%.

5.3.2: Solid Panel

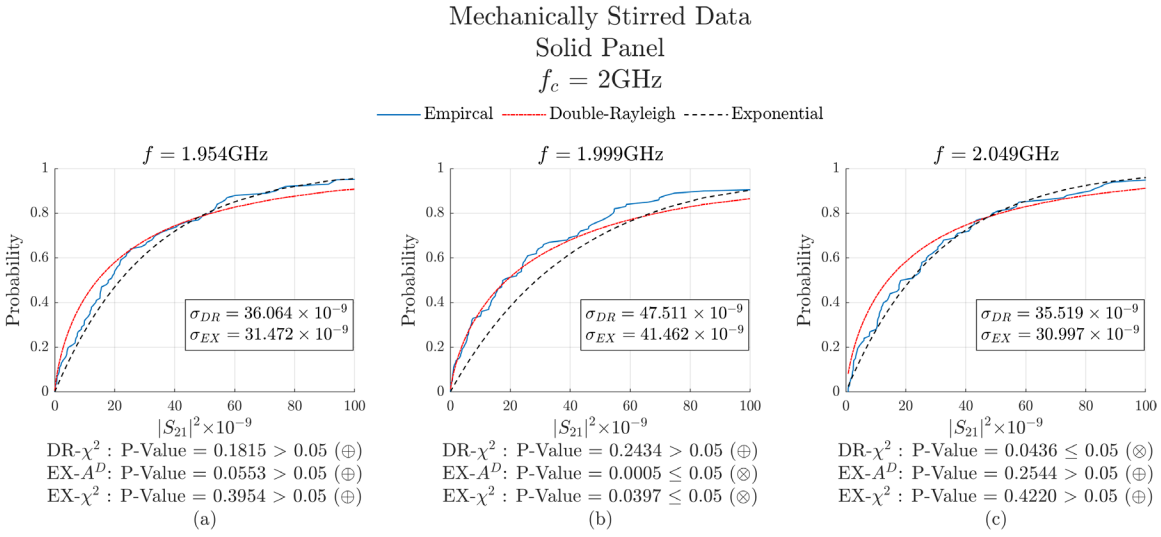

Figure 5.7: Mechanically Stirred Statistics - Solid Panel - $f_c = 2$ GHz. σ_{DR} is the maximum likelihood (ML) estimated parameter for the DR distribution. σ_{EX} is the ML estimated parameter for the exponential distribution.

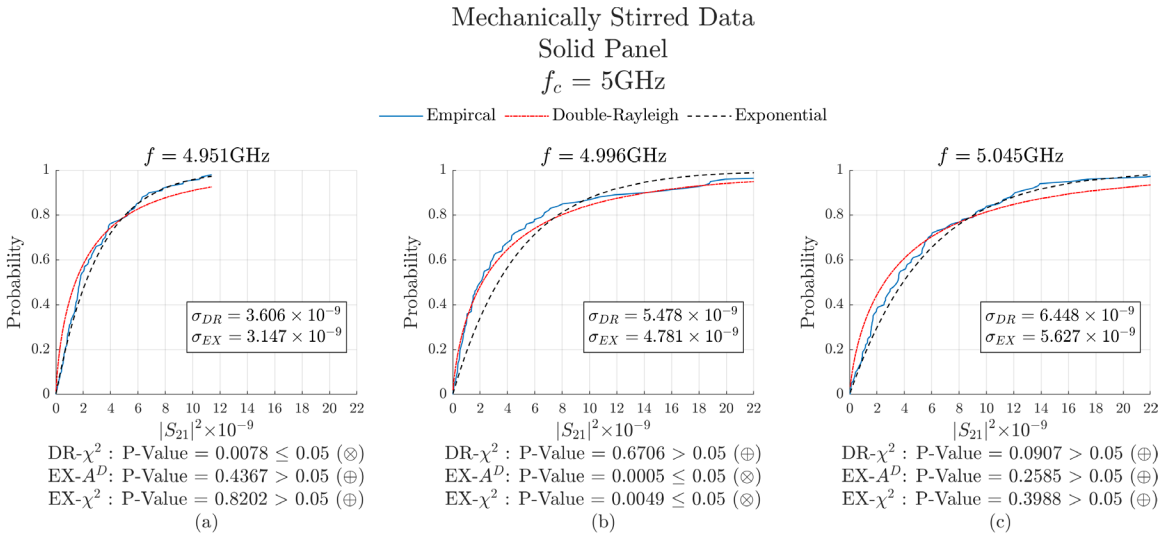

Figure 5.8: Mechanically Stirred Statistics - Solid Panel - $f_c = 5$ GHz. σ_{DR} is the maximum likelihood (ML) estimated parameter for the DR distribution. σ_{EX} is the ML estimated parameter for the exponential distribution.

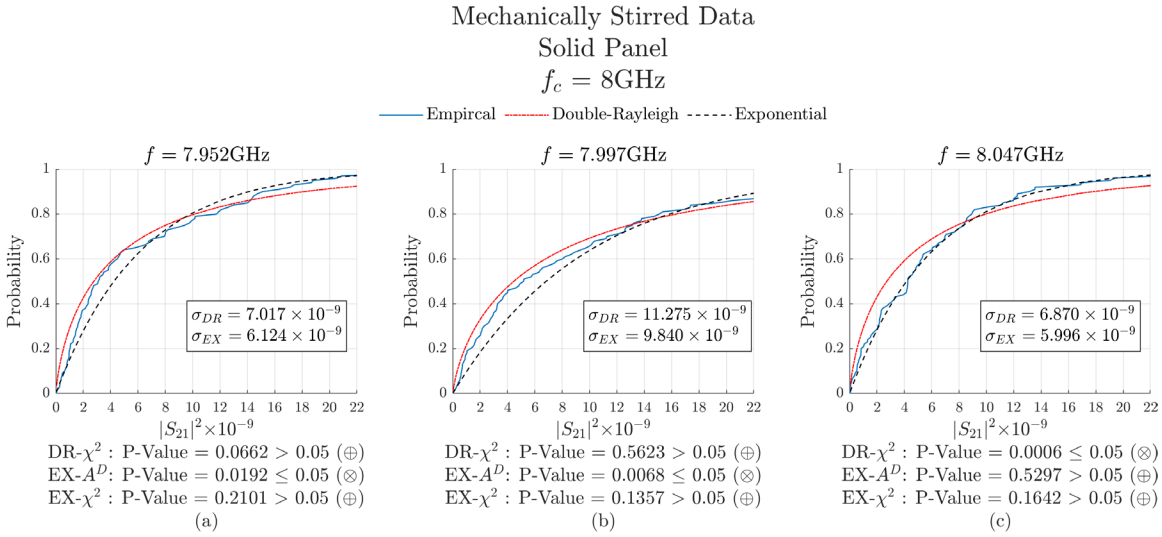

Figure 5.9: Mechanically Stirred Statistics - Solid Panel - $f_c = 8$ GHz. σ_{DR} is the maximum likelihood (ML) estimated parameter for the DR distribution. σ_{EX} is the ML estimated parameter for the exponential distribution.

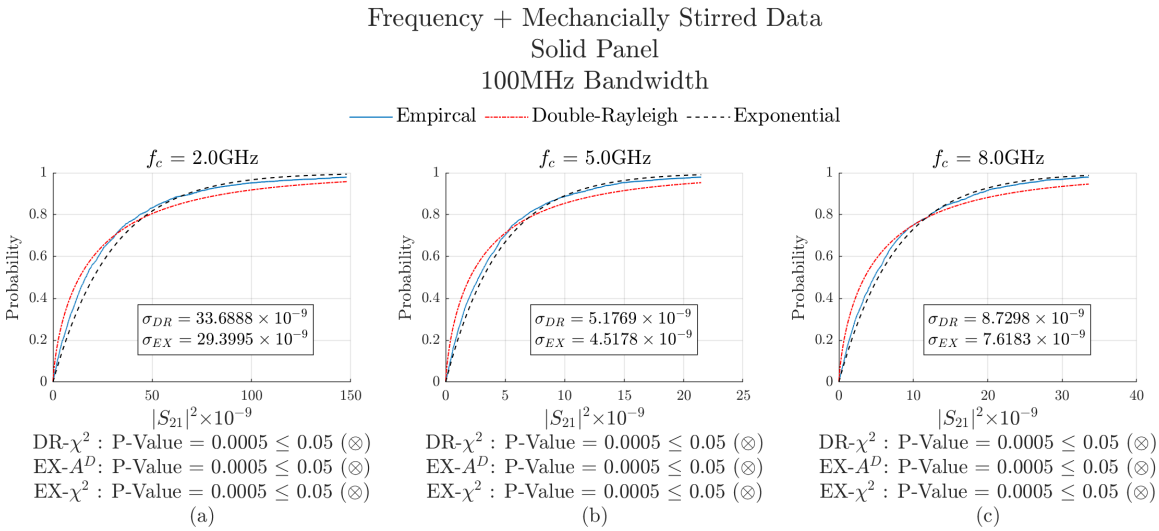

Figure 5.10: Frequency + Mechanically Stirred Statistics for $f_c = 2, 5$, and 8 GHz – Solid Panel. σ_{DR} is the maximum likelihood (ML) estimated parameter for the DR distribution. σ_{EX} is the ML estimated parameter for the exponential distribution.

Total Number of Rejections* in each 100MHz Bandwidth - Solid Panel

Distribution	2 [GHz]	5 [GHz]	8 [GHz]
DR - χ^2	17	12	16
EX - A^D	10	5	7
EX - χ^2	6	3	1

*22 statistical tests in each bandwidth

Table 5.2: Total number of statistical test rejections in each $f_c = 2, 5$, and 8GHz's 100 MHz bandwidth based on their respected GOF tests – Solid Panel.

Figures 5.7 through 5.9 show the ECDFs of the measured mean-squared fields at the extreme low, center, and extreme high of the frequencies of each test band when the sold plate was in place. Also shown in each plot are the theoretical CDFs of the MLE fit of the exponential and DR distributions to the measurements. There is no visual consistency in how well either distribution fits the data as it moves over the three extremes in the bandwidths. At $f_c = 2$ GHz (Figure 5.7), both GOF tests fail to reject the null hypothesis that the data follows a DR or exponential distribution at the low frequency. For the middle frequency, the test rejects the exponential distribution and the last frequency rejects the DR. Notice also how the estimated parameters for

each distribution vary significantly from low, middle, and high frequency, suggesting that they do not follow the same underlying distribution. Figures 5.8 and 5.9 at 5 GHz and 8 GHz center frequency, respectively, tell a similar story of lacking visual, GOF, and estimated parameter consistency.

Performing the KS two sample test on each of the frequency pairs within the frequency band provided information on how well the underlying distribution remained throughout the entire bandwidth. The test was performed by taking the sample set at the first frequency and testing it against itself and the samples at the remaining 21 frequencies, then testing the second-frequency sample set and testing it against itself and the sets at the remaining 20 frequencies, and so forth. The total number of test cases can be calculated as a triangle number, which has a formula of $n(n+1)/2$ [51], and the resulting number of cases is 253. However, the tests are not independent since the same sample sets are reused multiple times. At 2 GHz, there were 27 instances of the null hypothesis that the samples follow the same CDF being rejected at a 95% confidence level. With approximately 10.7% of the test pairs rejecting the null hypothesis, the distributions appear to be following a consistent underlying distribution and the addition of frequency stirring is appropriate The total number of rejections at 5 GHz is 45 and 50 at 8 GHz, corresponding to 17.8% and 19.8% rejection rates, respectively.

Table 5.2 shows the total number of rejections when all 22 sample sets at discrete frequencies within the test bandwidth were tested against the DR and exponential distributions. The grey boxes indicate more than two rejections within the bandwidth. The DR distribution is rejected frequently in all cases. The exponential is rejected less often as the frequency increases but is still rejected at a higher than the expected 5% rate.

Figure 5.10 shows the frequency + mechanical stirred sample sets. The GOF tests rejects each hypothesized distribution for all three cases.

5.3.3: Aperture 1

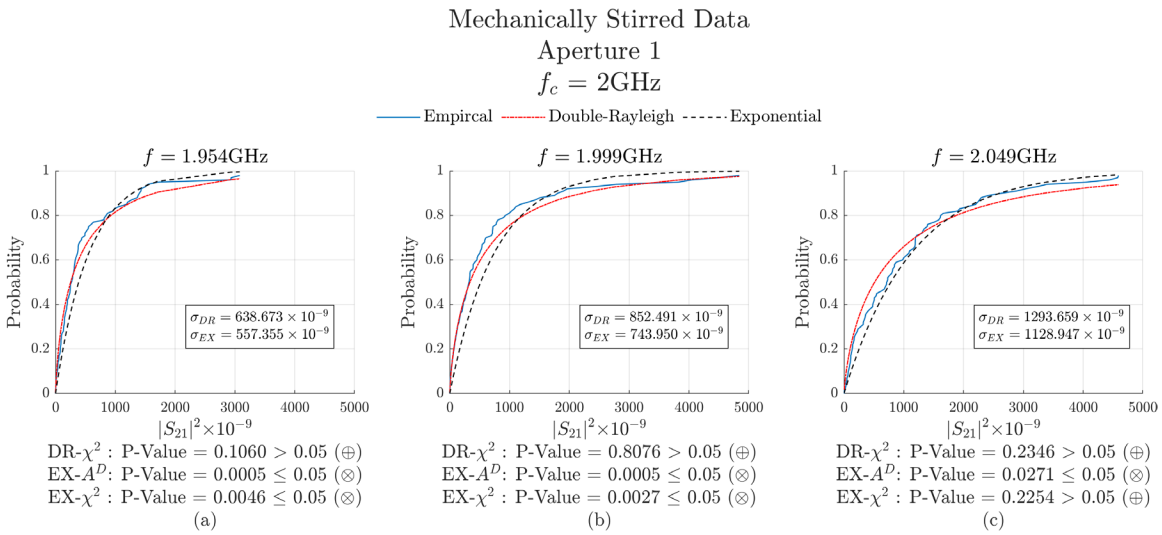

Figure 5.11: Mechanically Stirred Statistics – Aperture 1 - $f_c = 2$ GHz. σ_{DR} is the maximum likelihood (ML) estimated parameter for the DR distribution. σ_{EX} is the ML estimated parameter for the exponential distribution.

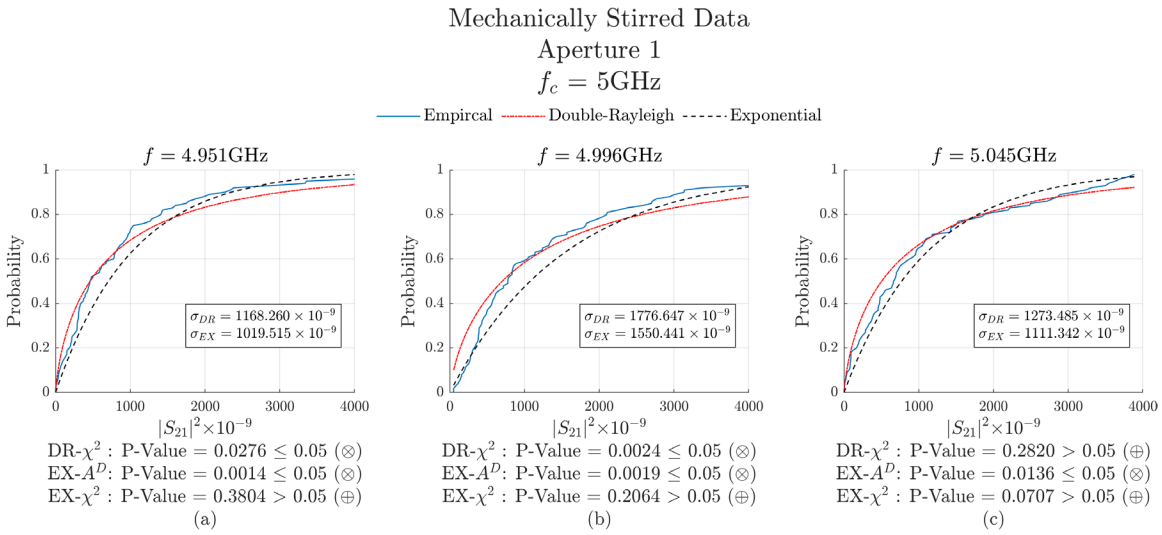

Figure 5.12: Mechanically Stirred Statistics – Aperture 1 - $f_c = 5$ GHz. σ_{DR} is the maximum likelihood (ML) estimated parameter for the DR distribution. σ_{EX} is the ML estimated parameter for the exponential distribution.

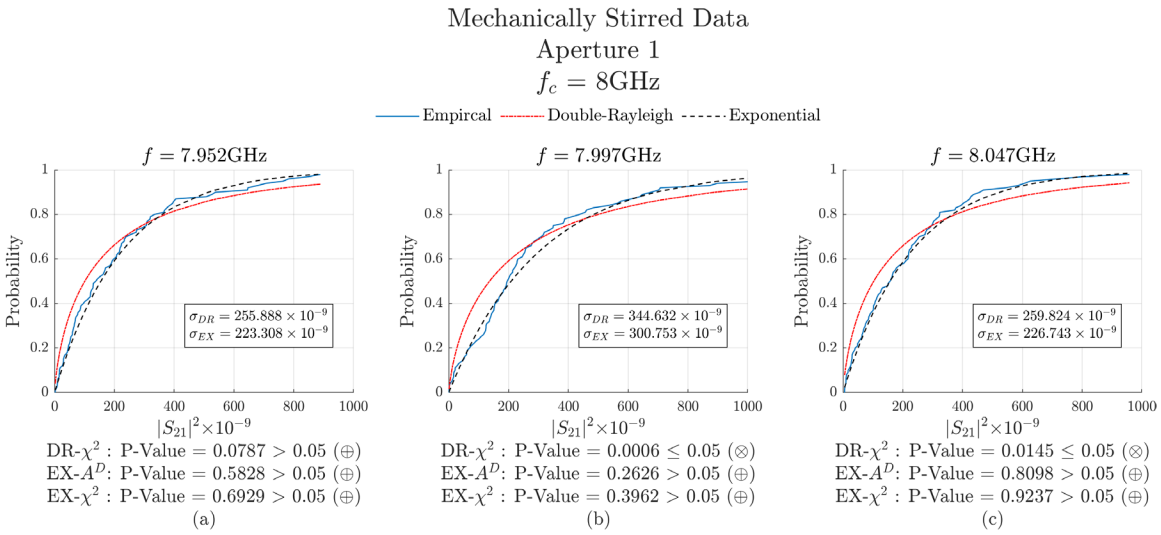

DR-χ^2 : P-Value = 0.0787 > 0.05 ($\oplus$)
EX-A^D: P-Value = 0.5828 > 0.05 ($\oplus$)
EX-χ^2 : P-Value = 0.6929 > 0.05 ($\oplus$)
(a)

DR-χ^2 : P-Value = 0.0006 ≤ 0.05 ($\otimes$)
EX-A^D: P-Value = 0.2626 > 0.05 ($\oplus$)
EX-χ^2 : P-Value = 0.3962 > 0.05 ($\oplus$)
(b)

DR-χ^2 : P-Value = 0.0145 ≤ 0.05 ($\otimes$)
EX-A^D: P-Value = 0.8098 > 0.05 ($\oplus$)
EX-χ^2 : P-Value = 0.9237 > 0.05 ($\oplus$)
(c)

Figure 5.13: Mechanically Stirred Statistics – Aperture 1 - $f_c = 8$ GHz. σ_{DR} is the maximum likelihood (ML) estimated parameter for the DR distribution. σ_{EX} is the ML estimated parameter for the exponential distribution.

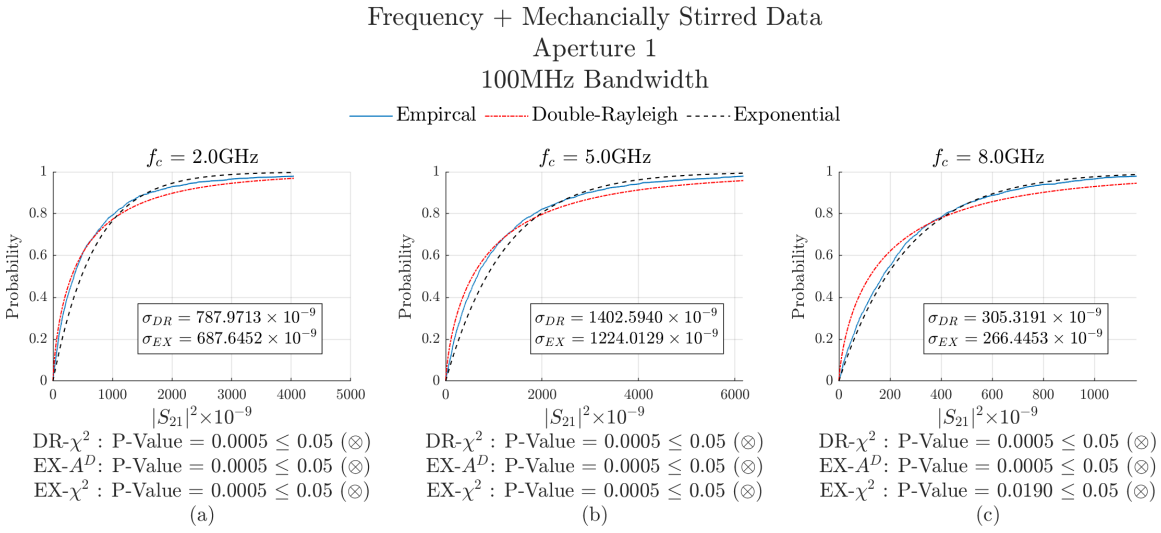

DR-χ^2 : P-Value = 0.0005 ≤ 0.05 ($\otimes$)
EX-A^D: P-Value = 0.0005 ≤ 0.05 ($\otimes$)
EX-χ^2 : P-Value = 0.0005 ≤ 0.05 ($\otimes$)
(a)

DR-χ^2 : P-Value = 0.0005 ≤ 0.05 ($\otimes$)
EX-A^D: P-Value = 0.0005 ≤ 0.05 ($\otimes$)
EX-χ^2 : P-Value = 0.0005 ≤ 0.05 ($\otimes$)
(b)

DR-χ^2 : P-Value = 0.0005 ≤ 0.05 ($\otimes$)
EX-A^D: P-Value = 0.0005 ≤ 0.05 ($\otimes$)
EX-χ^2 : P-Value = 0.0190 ≤ 0.05 ($\otimes$)
(c)

Figure 5.14: Frequency + Mechanically Stirred Statistics for $f_c = 2, 5$, and 8 GHz – Aperture 1. σ_{DR} is the maximum likelihood (ML) estimated parameter for the DR distribution. σ_{EX} is the ML estimated parameter for the exponential distribution.

Total Number of Rejections* in each 100MHz Bandwidth - Aperture 1

Distribution	2 [GHz]	5 [GHz]	8 [GHz]
DR- χ^2	4	8	15
EX-A^D	16	19	5
EX-χ^2	11	5	2

*22 statistical tests in each bandwidth

Table 5.3: Total number of statistical test rejections in each $f_c = 2, 5$, and 8GHz's 100 MHz bandwidth based on their respected GOF tests – Aperture 1.

Figure 5.11 shows the statistical test results when the field samples were collected with AP1 in place. The DR CDF seems to 'fit better' compared to the behavior when the solid panel was in place at the same three frequencies. The visual analysis, though, still shows a lack of consistency in a goodness-of-fit for the DR. Relying strictly on the chi-squared test, the DR fails to reject the null hypothesis for all three frequencies, but it being a low-power test these results should be interpreted with caution. Table 5.3 shows that for 2 GHz, the DR is rejected less with AP1 in place when compared to when the solid panel was in place (see Table 5.2 for solid panel). However, with four DR distributions rejected in this band, the total amount rejected is still higher than expected. The AD test rejects the exponential at all three frequencies while chi-squared rejects the exponential at the low and middle frequency.

Figures 5.12 and 5.13 show similar results, and as the frequency increases, the DR is rejected at a higher rate. This can be further justified by the abrupt changes in the estimated DR parameter shown on each plot. It should not be expected for the parameter to be exactly the same time at each frequency, but it changed considerably despite the operating frequency changing 50 MHz.

The KS two sample test was performed against AP1 sample sets. The rejections in each bandwidth are as follows:

- f_c = 2 GHz: 58 rejected values (22.9%)
- f_c = 5 GHz: 30 rejected values (11.85%)
- f_c = 8 GHz: 47 rejected values (18.6%)

the rejected rates are approximately the same here as was in the solid panel case, but are different when compared to the respective frequency.

Referring back to Table 5.3, it shows an interesting result that as the frequency climbs higher, the DR is rejected more often, and the exponential distribution is rejected less often. However, even though the exponential distribution is rejected less frequently (AD test), the total number of distributions rejected is still high

The GOF tests rejected the null hypothesis for all frequency + mechanically stirred sample sets with AP1 in place.

5.3.4: Global Analysis

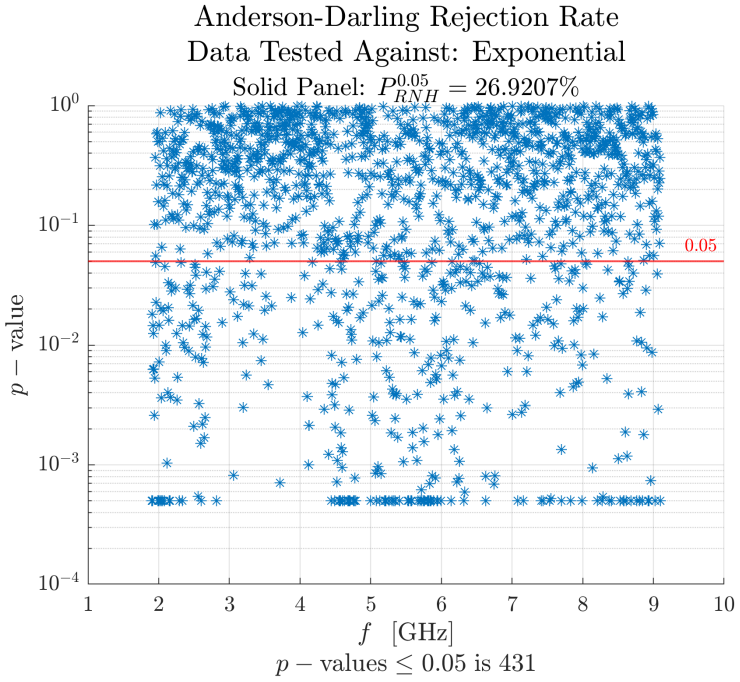

Figure 5.15: Solid panel global rejection rate under the AD GOF test. Data is testing against an exponential distribution.

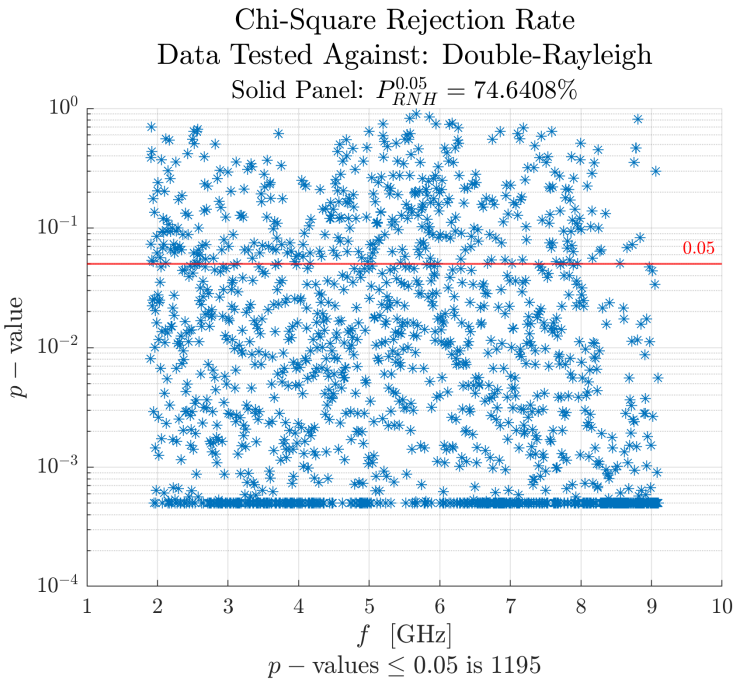

Figure 5.16: Solid panel global rejection rate under the chi-squared GOF test. Data is testing against the theoretical DR distribution.

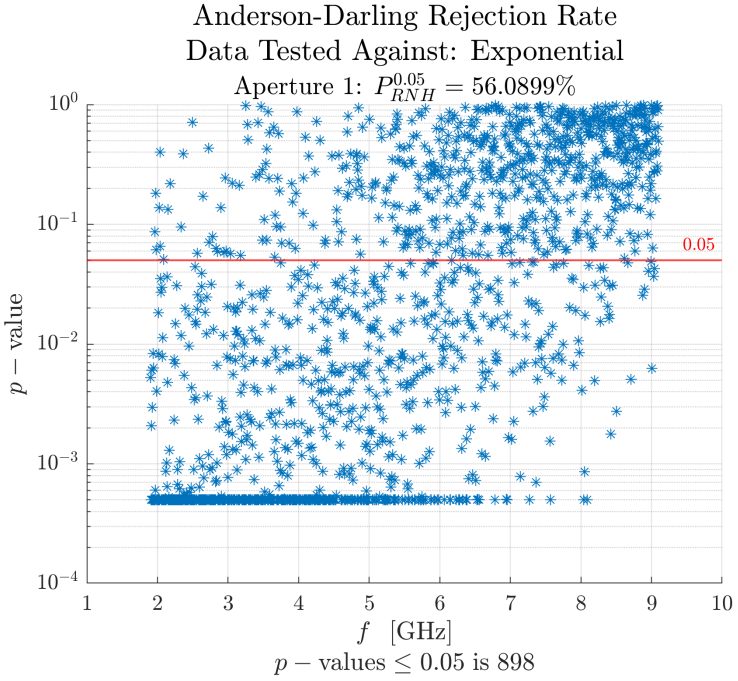

Figure 5.17: Aperture 1 global rejection rate under the AD GOF test. Data is testing against an exponential distribution.

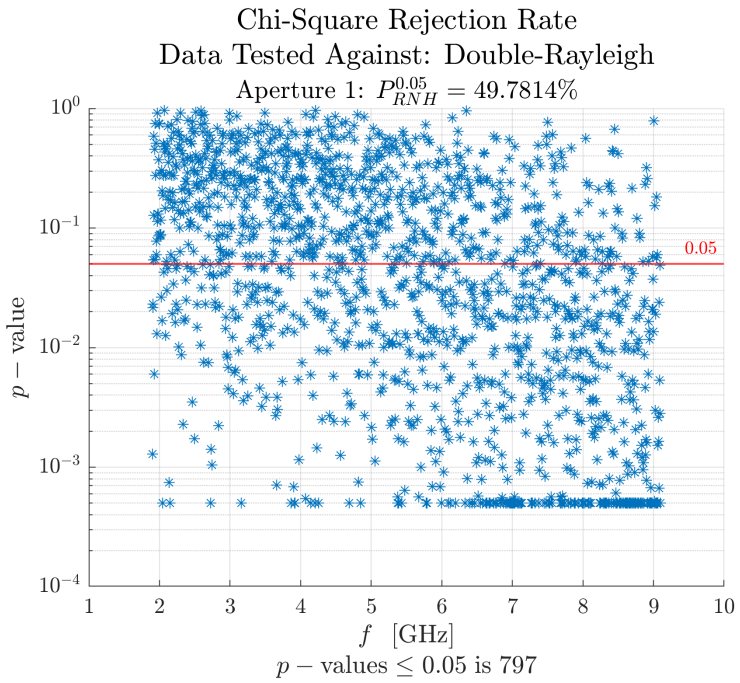

Figure 5.18: Aperture 1 global rejection rate under the chi-squared GOF test. Data is tested against the theoretical DR distribution.

Total Number of Rejections in each 100MHz Bandwidth*
and the Global Rejection Rate** (95% Confidence)

Aperture	Distribution	Center Frequencies f [GHz] 2	3	4	5	6	7	8	9	Global Range [GHz] 1.9-9.1
SP	DR - χ^2	17	17	18	12	12	18	16	22	1195
	EX - A^D	10	1	1	5	10	3	7	3	431
	EX - χ^2	6	1	1	3	3	2	1	2	197
AP1	DR - χ^2	4	7	4	8	12	15	15	17	797
	EX - A^D	16	19	19	19	12	7	5	5	898
	EX - χ^2	11	13	12	5	1	4	2	1	457
AP2	DR - χ^2	12	7	4	9	4	6	11	18	751
	EX - A^D	8	20	19	16	22	13	9	1	957
	EX - χ^2	3	10	13	10	14	4	1	0	451
AP3	DR - χ^2	13	18	15	15	11	13	16	19	1102
	EX - A^D	10	0	9	13	13	11	3	1	509
	EX - χ^2	2	1	2	4	8	5	1	1	207
AP4	DR - χ^2	10	16	18	13	15	20	18	21	1299
	EX - A^D	12	1	0	8	6	2	1	2	275
	EX - χ^2	3	0	0	5	2	2	1	2	130
AP5	DR - χ^2	20	19	19	22	21	18	20	21	1441
	EX - A^D	1	0	3	0	1	1	2	0	79
	EX - χ^2	0	0	1	1	2	0	1	0	67
AP6	DR - χ^2	15	15	17	17	20	17	18	20	1365
	EX - A^D	7	5	1	2	2	1	0	1	148
	EX - χ^2	3	3	3	1	2	1	0	0	103
AP7	DR - χ^2	6	7	13	16	16	19	20	18	1100
	EX - A^D	21	18	5	6	3	3	3	1	488
	EX - χ^2	14	4	3	6	1	0	1	1	251

*Local bandwidths have 22 statistical tests
**Global frequency range has 1601 statistical tests

Table 5.4: Local and global total rejection rate. Tested at 95% confidence.

Table 5.4 shows the total number of rejected sample sets for each local frequency band centered at $f_c = 2, 3, \ldots 9$ GHz, and the total number of rejected sample sets for the global frequency range. The sample sets were tested at a 95% confidence. The gray boxes represent a frequency band whose total number of rejections was greater than 2. There is no indication in any of the eight local frequency bands for any test case where the DR distribution had a total amount of rejections less than or equal to two at the 95% confidence for each sample set. For the global frequency range under perfect conditions, approximately 80 total values would be rejected (5%). As seen in Table 5.4, the lowest total number of rejections is 751 for AP2 at the same confidence level (no where near the ideal 80 values), even though the chi-squared test is less powerful than the AD test. The lower power of the chi-squared test is evident by its lower overall rejection rate (globally) than the AD when tested against an exponential distribution at a 95% confidence.

Another observation about the data can be seen in the Figures 5.15-5.18. Like the relationship between SE and aperture size compared to wavelength (SE decreases as frequency increases) a similar behavior can be seen in these figures. As frequency increases, the trend in rejected DR distributions increases, while the trend in rejected exponential distributions decreases, which is seen in Figures 5.17 and 5.18. This is not surprising because the two chambers will couple greater together as the electrical size of the aperture increases.

As noted earlier, a hypothesis under test in this work was that the field within the inner cavity of a weakly coupled, nested-cavity configuration with both environments mode stirred should follow the DR distribution. However, DR-distributed measured samples was rejected at much greater than 5% of the time at 95% confidence even using the fairly low power chi-squared GOF test. The DR distribution appears to be of limited, if any, value in describing the field statistics in the configurations tested. The use of the Weibull distribution to describe the fields statistics is considered in the next chapter.

CHAPTER VI

TWO-PARAMATER WEIBULL DISTRIBUTION

6.1: INTRODUCTION

The Weibull distribution was selected as a candidate to describe the measured nested-cavity field statistics because there have been some successes with this distribution under non-ideal reverberation chamber scenarios [52-54]. The two parameter Weibull distribution allows adaptation to a more general distributions than the single parameter DR or exponential distributions. Also, both the Rayleigh and exponential distributions are special cases of the Weibull distribution. Finally, an advantage to the Weibull distribution is that the AD test can test against it when the parameters are estimated. Historically, the Weibull distribution is a distribution with no physical basis, it is purely an empirical distribution with no physical meaning [55] when applied to reverberation chamber fields. (The author found a single case where the Weibull distribution was derived from a physical process unrelated to RC operation [56].)

6.2: REVIEW OF THE WEIBULL DISTIRBUTION

The PDF of the two-parameter Weibull distribution is

$$f(x) = \frac{\beta}{\sigma}\left(\frac{x}{\sigma}\right)^{\beta-1} \exp\left(-\left(\frac{x}{\sigma}\right)^{\beta}\right), \tag{6.1}$$

where β is the shape parameter and σ is the scale parameter. The two-parameter Weibull distribution reduces to the Rayleigh distribution when $\beta = 2$ and the exponential distribution when

$\beta = 1$. The shape and scale parameter were estimated from a particular sample set using the maximum-likelihood estimation (MLE).

6.3: STATISTICAL ANALYSIS – WEIBULL

The following section will show the testing of the samples measured with the solid panel and AP1 against the Weibull distribution. As in chapter 5,three frequencies will be highlighted for both the solid panel and AP1, centered at 2, 5, and 8 GHz. The AD and chi-squared goodness of fit tests will test the data against the Weibull distribution. The rejection rate in the local bands will be discussed first followed by a global comparison of the Weibull distribution rejection rates against those of the exponential and DR distributions. "$WB - AD$" and '$WB - \chi^2$" represent when the sample set was tested against a Weibull (WB) distribution using the AD or chi-square (χ^2) tests, respectively.

Section 6.3.1: Solid Panel – Weibull

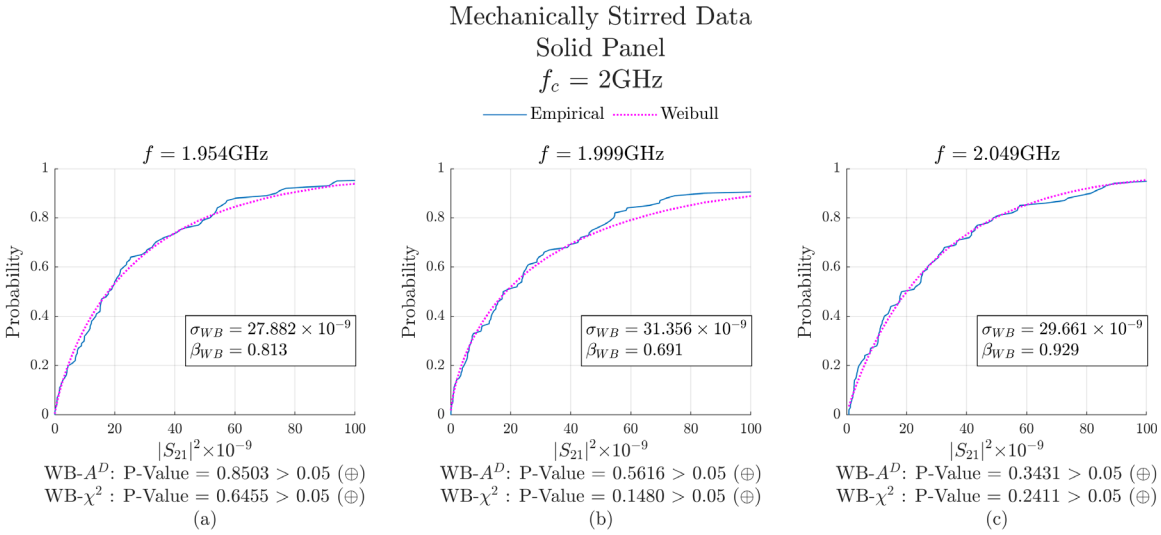

Figure 6.1: Mechanically Stirred Statistics - Solid Panel - $f_c = 2$ GHz. σ_{WB} and β_{WB} is the maximum likelihood (ML) estimated scale and shape parameter for the Weibull distribution.

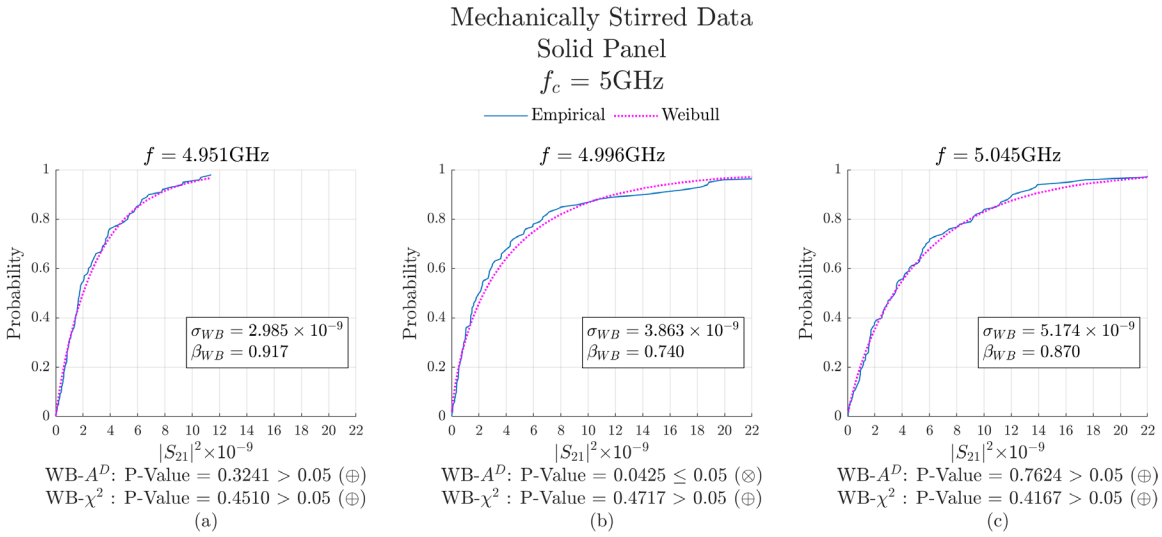

Figure 6.2: Mechanically Stirred Statistics - Solid Panel - f_c = 5 GHz. σ_{WB} and β_{WB} is the maximum likelihood (ML) estimated scale and shape parameter for the Weibull distribution.

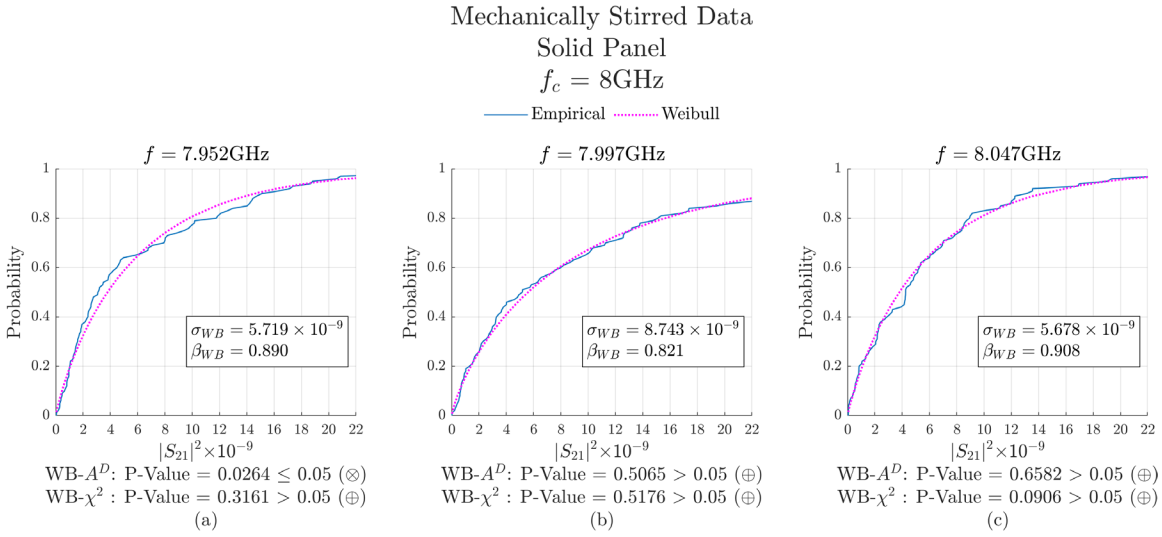

Figure 6.3: Mechanically Stirred Statistics - Solid Panel - f_c = 8 GHz. σ_{WB} and β_{WB} is the maximum likelihood (ML) estimated scale and shape parameter for the Weibull distribution.

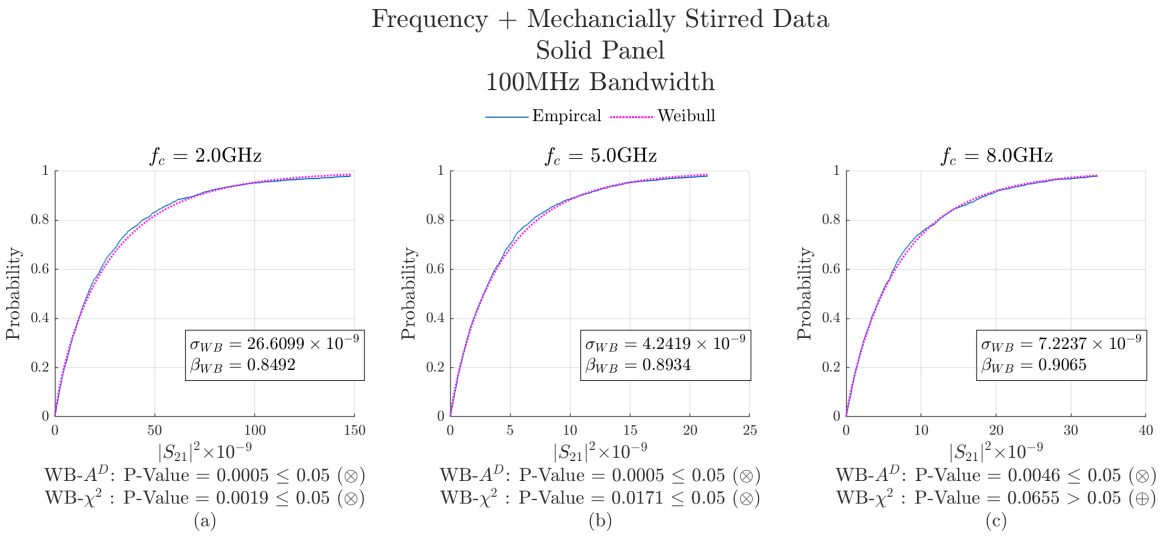

Figure 6.4: Frequency + Mechanically Stirred Statistics for $f_c = 2, 5$, and 8 GHz – Solid Panel. σ_{WB} and β_{WB} is the maximum likelihood (ML) estimated scale and shape parameter for the Weibull distribution.

Total Number of Rejections* in each 100MHz Bandwidth - Solid Panel

Distribution	2 [GHz]	5 [GHz]	8 [GHz]
WB - A^D	4	3	1
WB - χ^2	3	2	1

*22 statistical tests in each bandwidth

Table 6.1: Total number of rejections in each $f_c = 2, 5$, and 8GHz's 100 MHz bandwidth based on their respected GOF tests for the Weibull distribution – Solid Panel.

Figures 6.2 through 6.4 show the theoretical CDFS of the MLE fit of the Weibull distribution on the ECDFs of the measured mean-squared fields at extreme low, center, and high frequencies of each test band width the solid plate in place. Visually, the estimated Weibull distribution overall gives a more consistent fit to the empirical data than the exponential or DR distribution in the previous chapter. Also, the fit parameters are more consistent within the 100 MHz frequency bands than was previously seen.

The Weibull distribution fits when frequency + mechanical stirring was applied are shown in Figure 6.4. Visually, the fits appear excellent. However, the GOF tests reject the Weibull distribution for every case except when the chi-squared test was applied to the at 8-GHz band samples. Note that 2200 samples are included in the frequency + mechanically stirred sets, giving the tests great power in rejecting the Weibull distribution with only small data deviations.

Table 6.1 shows the total rejections of the Weibull distribution out of 22 trials in each bandwidth using both the AD and chi-squared tests. The AD test rejects the Weibull distribution significantly less frequently than the less powerful chi-squared rejects the DR distribution with the same data samples. As the frequency increases, the Weibull rejection rate reduces.

Section 6.3.2: Aperture 1 – Weibull

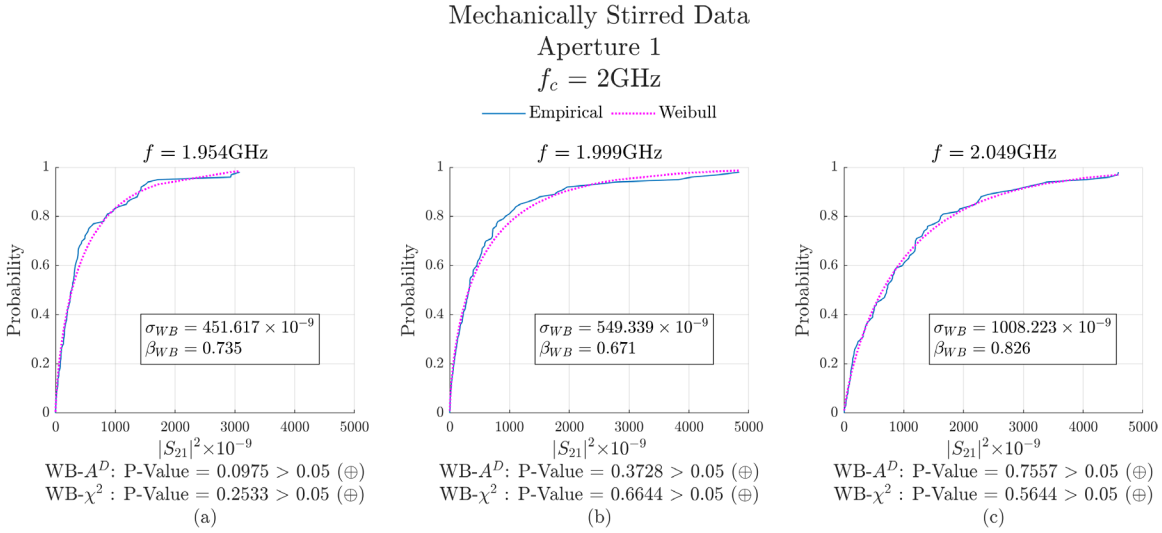

Figure 6.5: Mechanically Stirred Statistics – Aperture 1 - $f_c = 2$ GHz. σ_{WB} and β_{WB} is the maximum likelihood (ML) estimated scale and shape parameter for the Weibull distribution.

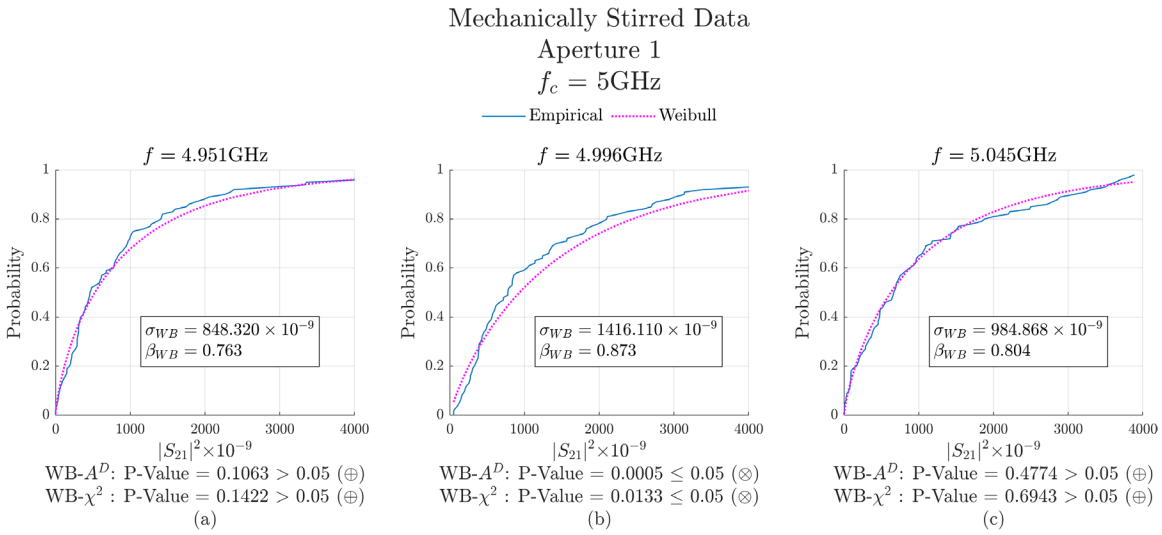

Figure 6.6: Mechanically Stirred Statistics – Aperture 1 - f_c = 5 GHz. σ_{WB} and β_{WB} is the maximum likelihood (ML) estimated scale and shape parameter for the Weibull distribution.

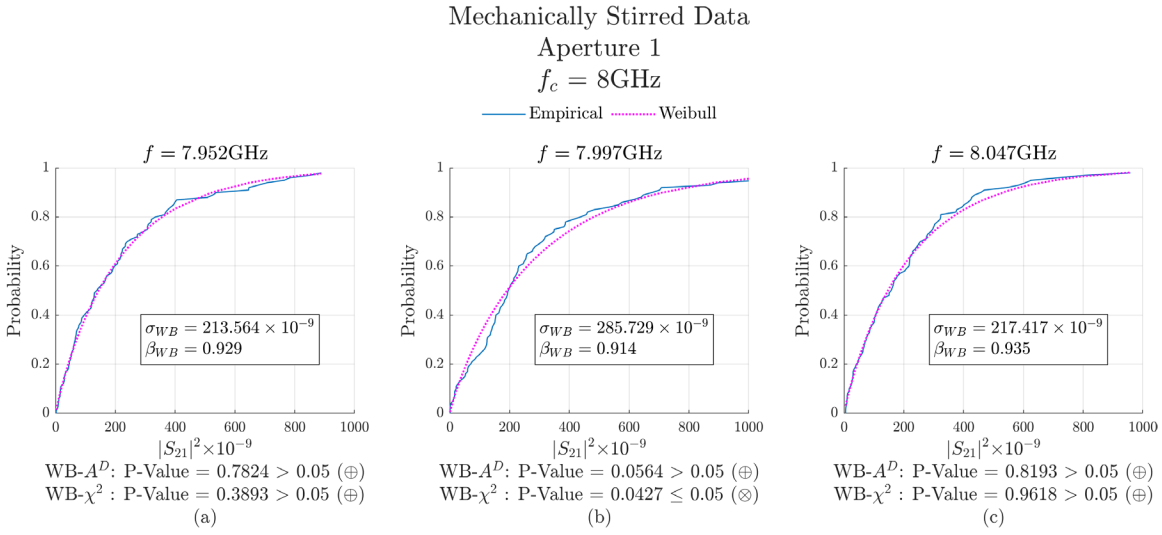

Figure 6.7: Mechanically Stirred Statistics – Aperture 1 - f_c = 8 GHz. σ_{WB} and β_{WB} is the maximum likelihood (ML) estimated scale and shape parameter for the Weibull distribution.

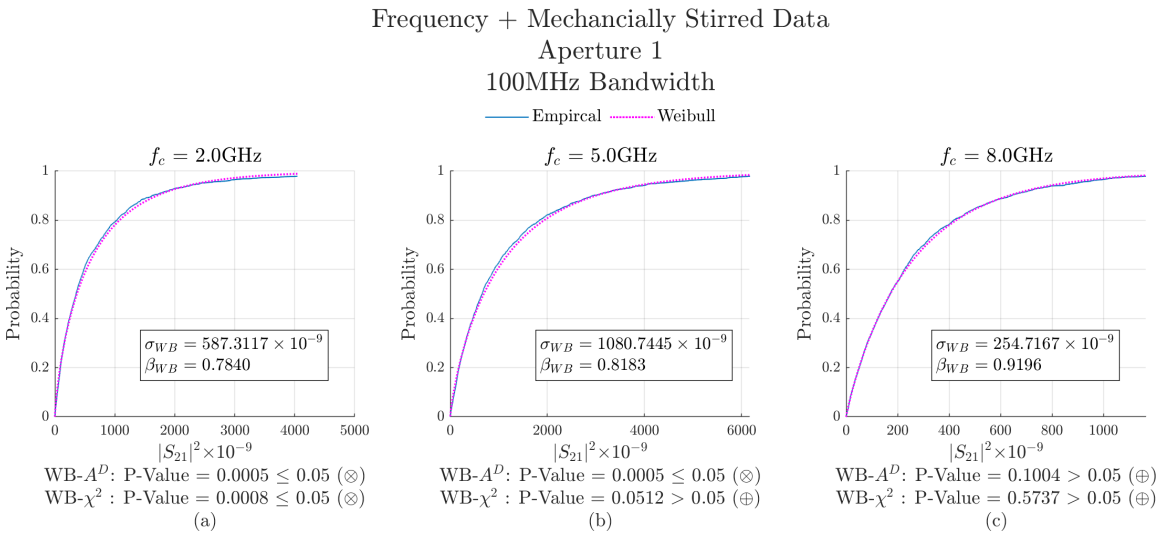

Figure 6.8: Frequency + Mechanically Stirred Statistics for $f_c = 2, 5$, and 8 GHz. σ_{WB} and β_{WB} is the maximum likelihood (ML) estimated scale and shape parameter for the Weibull distribution.

Total Number of Rejections* in each 100MHz Bandwidth - Aperture 1

Distribution	2 [GHz]	5 [GHz]	8 [GHz]
WB - A^D	4	5	2
WB - χ^2	0	1	2

*22 statistical tests in each bandwidth

Table 6.2: Total number of rejections in each $f_c = 2, 5$, and 8GHz's 100 MHz bandwidth based on their respected GOF tests for the Weibull distribution – Aperture 1.

The Weibull distribution again shows a consistently better visual fit to the ECDFs than the DR distribution, as seen in Figure 6.5 – 6.7. The GOF tests also show the same consistency. The only case where the Weibull distribution was rejected by both GOF tests was in Figure 6.6b.

Looking now at the frequency + mechanically stirred data in Figure 6.8, again the estimated Weibull distribution gives a good visual fit to the ECDFs. However, the only place where the AD

and chi-squared tests do not reject the null hypothesis of Weibull distributed data is at the 8 GHz band.

Table 6.2 shows that the Weibull distribution has low rejection rates in the three bands, but the total number of rejected distributions is still high in the lower frequencies for the more powerful AD test. The gray boxes indicate the total number of rejected distributions in the frequency band was greater than 2.

Section 6.3.3: Global Analysis – Weibull

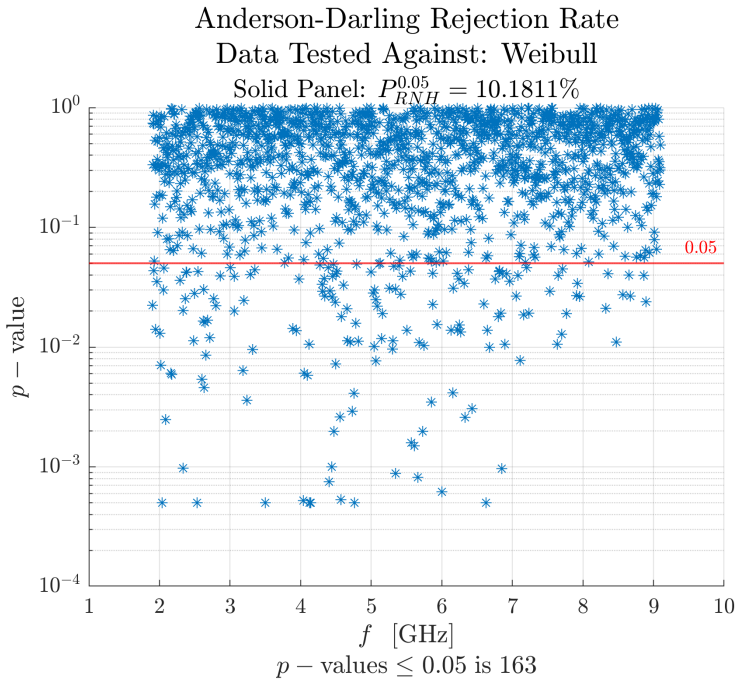

Figure 6.9: Solid panel global rejection rate under the AD GOF test. Data is testing against a Weibull distribution.

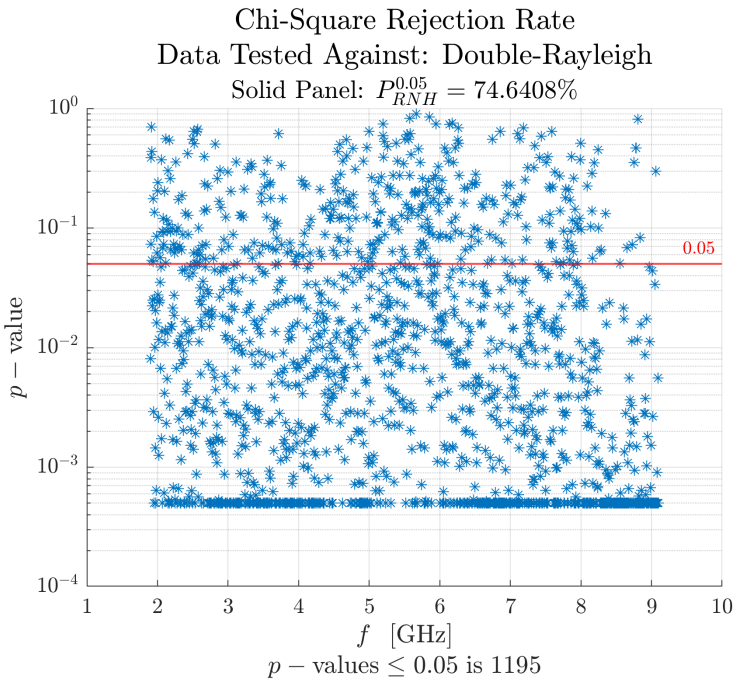

Figure 6.10: Solid panel global rejection rate under the chi-squared GOF test. Data is testing against the theoretical DR distribution. (Repeat of Figure 5.16)

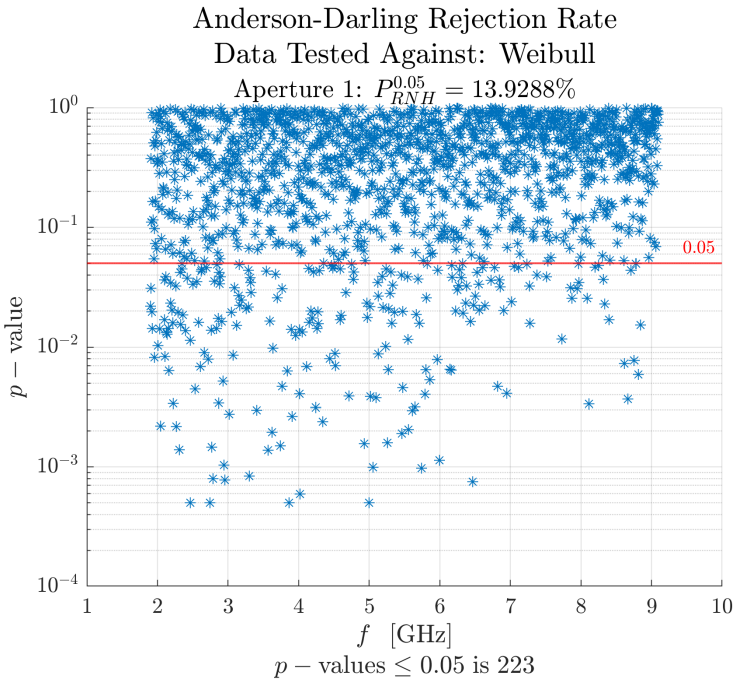

Figure 6.11: Aperture 1 global rejection rate under the AD GOF test. Data is testing against a Weibull distribution.

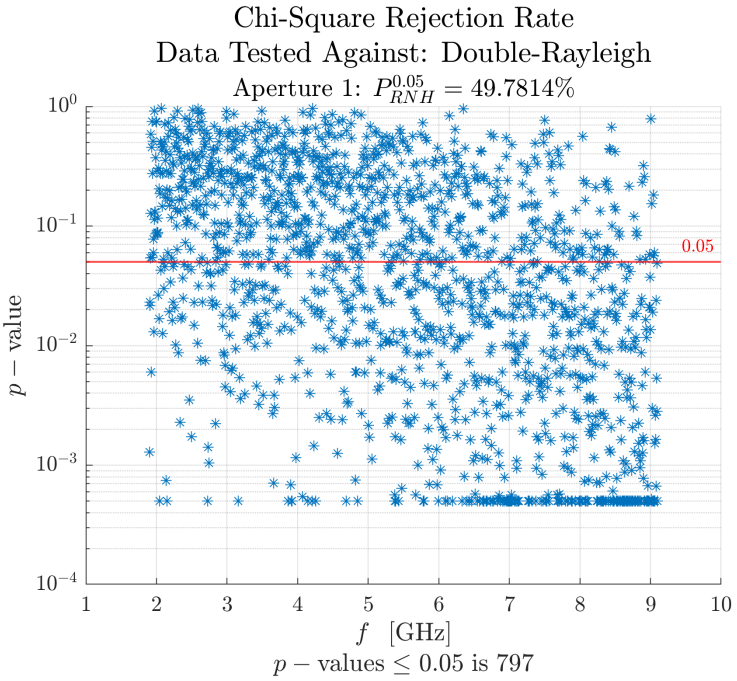

Figure 6.12: Aperture 1 global rejection rate under the chi-squared GOF test. Data is testing against the theoretical DR distribution. (Repeat of Figure 5.18)

Total Number of Rejections in each 100MHz Bandwidth*
and the Global Rejection Rate** (95% Confidence)

Aperture	Distribution	Center Frequencies f [GHz] 2	3	4	5	6	7	8	9	Global Range [GHz] 1.9-9.1
SP	DR - χ^2	17	17	18	12	12	18	16	22	1195
	EX - A^D	10	1	1	5	10	3	7	3	431
	EX - χ^2	6	1	1	3	3	2	1	2	197
	WB - A^D	4	1	2	3	1	1	1	0	163
	WB - χ^2	3	0	1	2	1	1	1	1	98
AP1	DR - χ^2	4	7	4	8	12	15	15	17	797
	EX - A^D	16	19	19	19	12	7	5	5	898
	EX - χ^2	11	13	12	5	1	4	2	1	457
	WB - A^D	4	3	4	5	3	1	2	0	223
	WB - χ^2	0	5	4	2	1	0	2	2	99
AP2	DR - χ^2	12	7	4	9	4	6	11	18	751
	EX - A^D	8	20	19	16	22	13	9	1	957
	EX - χ^2	3	10	13	10	14	4	1	0	451
	WB - A^D	0	5	2	4	4	2	2	1	203
	WB - χ^2	0	4	0	2	1	1	2	3	77
AP3	DR - χ^2	13	18	15	15	11	13	16	19	1102
	EX - A^D	10	0	9	13	13	11	3	1	509
	EX - χ^2	2	1	2	4	8	5	1	1	207
	WB - A^D	3	0	1	6	4	3	1	1	173
	WB - χ^2	0	2	2	3	5	2	1	2	92
AP4	DR - χ^2	10	16	18	13	15	20	18	21	1299
	EX - A^D	12	1	0	8	6	2	1	2	275
	EX - χ^2	3	0	0	5	2	2	1	2	130
	WB - A^D	3	3	1	1	1	0	1	1	125
	WB - χ^2	1	0	1	1	2	2	1	3	90
AP5	DR - χ^2	20	19	19	22	21	18	20	21	1441
	EX - A^D	1	0	3	0	1	1	2	0	79
	EX - χ^2	0	0	1	1	2	0	1	0	67
	WB - A^D	1	1	2	1	1	2	1	2	77
	WB - χ^2	0	0	1	1	4	1	0	3	74
AP6	DR - χ^2	15	15	17	17	20	17	18	20	1365
	EX - A^D	7	5	1	2	2	1	0	1	148
	EX - χ^2	3	3	3	1	2	1	0	0	103
	WB - A^D	3	2	2	2	3	1	1	1	105
	WB - χ^2	3	1	1	1	5	0	1	1	88
AP7	DR - χ^2	6	7	13	16	16	19	20	18	1100
	EX - A^D	21	18	5	6	3	3	3	1	488
	EX - χ^2	14	4	3	6	1	0	1	1	251
	WB - A^D	4	2	2	2	2	2	3	2	142
	WB - χ^2	5	2	1	2	2	1	2	2	93

*Local bandwidths have 22 statistical tests

**Global frequency range has 1601 statistical tests

Table 6.3: Local and global total rejection rates. Tested at 95% confidence. (Extension of Table 5.4)

Table 6.3 is an extension of Table 5.4, but with the added local and global performance of the Weibull distribution when the samples were tested using the AD and chi-square test. This table as a whole shows that the Weibull distribution is consistently a better fit to the measured data than the exponential or DR distribution even under conditions where the latter two are theoretically supported. The Weibull distribution shows significantly lower rejection rate in the local bands than the exponential distribution using the AD test and the DR distribution using the chi-square. This characteristic is also seen in every single test case for the global frequency range.

Figures 6.9 – 6.12 show, again, that as the frequency increases, the rejection rate decreases for the Weibull distribution while the DR distribution rejection rate increases.

6.4: SUMMARY

The two paramater Weibull distribution has shown to be a better distribution describing the nested field statistics that the exponential and DR. The Weibull showed low rejection rates, but did have not have a consistent rejection rate at a 95% confidence in either the local frequency bands or the global frequency range. When a nested cavity is weakly coupled to a larger cavity, the Weibull performs as a good generic distribution to describe the nested statistics. The chambers were weakly coupled for the solid panel and apertures 1-4 cases, and at the lower frequencies for aperture 7.

CHAPTER VII

SUMMARY AND CONCLUSION

7.1: SUMMARY OF WORK DONE

For this nested cavity study, the use of simultaneous mechanical tuning in the small chamber and SMART-80 was used to change the boundary conditions of both internal and external cavity environments. The small chamber had to be brought back up into operation with the replacement of shielding gasket material attached to the edges of door and on new aluminum plates used to block the chamber's windows. The tuner also had to be modified with additional aluminum foil to extend the tuner's boundary conditions creating more surface to scatter the electric fields. The small chamber was then validated for operation to be used for this study. An operational bandwidth was found but had slightly less than ideal operation at the lower frequencies. The Anderson-Darling goodness-of-fit rejected the collected sample sets (when tested against an exponential distribution at a 95% confidence) at a slightly higher than theoretical level and the tuner produced slightly less than 100 independent samples the lower frequencies. However, these results were not enough to invalidate the study. The SMART-80 had no repairs because it has been in frequent use and has shown proper performance for a reverberation chamber.

The shielding effectiveness of the small chamber when nested inside the SMART-80 was measured over a large frequency band (1.9 – 9.1 GHz) with different coupling apertures.

After the small chamber demonstrated its ability to weakly couple to the SMART-80, the statistical behavior of the square-magnitude of a single component of the received field was studied. The use of appropriate goodness-of-fit tests were used to evaluate if the collected sample sets did not come from the hypothesized distributions when the parameters were estimated using the maximum-likelihood estimation. The goodness-of-fit tests used to evaluate the nested chamber's fields were the Anderson-Darling and Pearson's chi-square tests. The Anderson-Darling was used to test the sample sets against the exponential and Weibull distributions at a 95% confidence, and the chi-square was used to test the collected sample sets against the same two distributions and the hypothesized double-Rayleigh distribution at the same confidence level.

Plotting the theoretical cumulative distributions on top of the empirical distribution was also useful to see how well the hypothesized distributions fit the empirical, though this did not have a confidence level and was strictly used as a visual indicator.

7.2: CONCLUSIONS

The statistics of the Weibull distribution converge to an exponential distribution where there is strong coupling and the two environments act a single resonant space, which is consistent with [10]. When the two cavities are weakly coupled, the double-Rayleigh distribution had higher than expected rejection rates. The Weibull distribution had significantly less rejection rates than either the exponential and double-Rayleigh when the two chambers were weakly coupled, and confirmed to an exponential distribution at the higher frequencies. The Weibull being a two parameter distribution it is able to better adapt to more general cases than single-parameter distribution families. Taking into account that the Weibull still had high rejection rates when the two cavities were weakly coupled, but much lower than the other two distributions, it has application as a general distribution for low precision work.

REFERENCES

[1] H. A. Mendes, "A New Approach to Electromagnetic Field-Strength Measurements in Shielded Enclosures," presented at the Wescon, Los Angeles, CA, 1968.

[2] P. F. Wilson, "Acoustic and electromagnetic reverberation chambers: Similarities and differences," in *2016 Asia-Pacific International Symposium on Electromagnetic Compatibility (APEMC)*, 17-21 May 2016 2016, vol. 01, pp. 880-882, doi: 10.1109/APEMC.2016.7522898.

[3] R. Serra *et al.*, "Reverberation chambers a la carte: An overview of the different mode-stirring techniques," *IEEE Electromagnetic Compatibility Magazine,* vol. 6, no. 1, pp. 63-78, 2017, doi: 10.1109/memc.2017.7931986.

[4] *Electromagnetic compatibility (EMC) – Part 4-21: Testing and measurement techniques – Reverberation chamber test methods*, 2.0 ed. (IEC 610004-21). International Electrotechnical Commission (IEC), 2011.

[5] "EMC Society." IEEE. https://www.emcs.org/About-Us.html (accessed 7/13/2022, 2022).

[6] M. L. Crawford and G. H. Koepke, *Design, evaluation, and use of a reverberation chamber for performing electromagnetic susceptibility/vulnerability measurements* (NBS technical note ; 1092). Gaithersburg, MD: U.S. Dept. of Commerce, National Bureau of Standards, 1986.

[7] D. A. Hill, *Electromagnetic Theory of Reverberation Chambers* (NIST Technical Note ; 1506). Gaithersburg, MD: U.S. Dept. of Commerce, National Institute of Standards and Technology, 1998.

[8] J. Ladbury, G. Koepke, and D. Camell, *Evaluation of the NASA Langley Research Center Mode-Stirred Chamber Facility* (NIST Technical Note ; 1508). U.S. Dept. of Commerce, National Institute of Standards and Technology, 1999.

[9] D. A. Hill, *Electromagnetic Fields in Cavities* (Electromagnetic Wave Theory). Hoboken, New Jersey: John Wiley & Sons, Inc., 2009, p. 280.

[10] Y. He and A. C. Marvin, "Aspects of field statistics inside nested frequency-stirred reverberation chambers," in *IEEE International Symposium on Electromagnetic Compatibility (EMC)*, 2009: IEEE, pp. 171-176, doi: 10.1109/ISEMC.2009.5284658.

[11] P. Corona, G. Latmiral, and E. Paolini, "Performance and Analysis of a Reverberating Enclosure with Variable Geometry," *IEEE Transactions on Electromagnetic Compatibility,* vol. EMC-22, no. 1, pp. 2-5, 1980, doi: 10.1109/temc.1980.303814.

[12] M. L. Crawford and G. H. Koepke, "Electromagnetic Radiation Test Facilities Evaluation of Reverberation Chambers Location at NSWC, Dahlgren, Virginia," *NBSIR,* 1986.

[13] T. A. Loughry, "Frequency Stirring: An Alternate Approach to Mechanical Mode-Stirring for the Conduct of Electromagnetic Susceptibility Testing," PHILLIPS LAB KIRTLAND AFB NM, 1991.
[14] M. Ganji, H. Bevrani, N. Hami Golzar, and S. Zabihi, "The Weibull–Rayleigh Distribution, Some Properties, and Applications," *Journal of Mathematical Sciences,* vol. 218, no. 3, pp. 269-277, 2016, doi: 10.1007/s10958-016-3028-2.
[15] V. Erceg, S. J. Fortune, J. Ling, A. J. Rustako, and R. A. Valenzuela, "Comparisons of a Computer-Based Propagation Prediction Tool with Experimental Data Collected in Urban Microcellular Environments," *IEEE Journal on Selected Areas in Communications,* vol. 15, no. 4, pp. 677-684, 1997, doi: 10.1109/49.585778.
[16] H. W. Lilliefors, "On the Kolmogorov-Smirnov Test for the Exponential Distribution with Mean Unknown," *Journal of the American Statistical Association,* vol. 64, no. 325, pp. 387-389, 1969, doi: 10.1080/01621459.1969.10500983.
[17] D. J. Steinskog, D. B. Tjøstheim, and N. G. Kvamstø, "A Cautionary Note on the Use of the Kolmogorov–Smirnov Test for Normality," *Monthly Weather Review,* vol. 135, no. 3, pp. 1151-1157, 2007, doi: 10.1175/mwr3326.1.
[18] J. L. Romeu, "Anderson-Darling: A Goodness of Fit Test for Small Samples Assumptions," *START: Selected Topics in Assurance Related Technologies,* vol. 10, 5, 2003.
[19] M. L. McHugh, "The chi-square test of independence," *Biochemia medica,* vol. 23, no. 2, pp. 143-149, 2013, doi: 10.11613/BM.2013.018.
[20] S. J. Haberman, "A Warning on the Use of Chi-Squared Statistics with Frequency Tables with Small Expected Cell Counts," *Journal of the American Statistical Association,* vol. 83, no. 402, pp. 555-560, 1988, doi: 10.1080/01621459.1988.10478632.
[21] A. O. Lima, G. B. Lyra, M. C. Abreu, J. F. Oliveira-Júnior, M. Zeri, and G. Cunha-Zeri, "Extreme Rainfall Events Over Rio de Janeiro State, Brazil: Characterization Using Probability Distribution Functions and Clustering Analysis," *Atmospheric Research,* vol. 247, 2021, doi: 10.1016/j.atmosres.2020.105221.
[22] A. Papoulis, *Probability, Random Variables, and Stochastic Processes*, 3rd ed. McGraw-Hill, 1991.
[23] R. E. Ziemer, *Elements of Engineering Probability and Statistics*. Upper Saddle River, NJ 07458: Prentice-Hall, 1997.
[24] C. A. Balanis, *Advanced Engineering Electromagnetics*, 2 ed. Hoboken, NJ: John Wiley & Sons, 2012.
[25] R. F. Harrington, *Time-Harmonic Electromagnetic Fields* (Electromagnetic Wave Theory). New York, NY: John Wiley & Sons, 2001.
[26] R. Serra, "Introduction of Randomness in Deterministic, Physically-Consistent Descriptions of Reverberation Chambers and Experimental Verification," PhD, Politechnico di Torino, Turin, Italy, 2009.
[27] A. Goldsmith, *Wireless Communications*. New York: Cambridge University Press, 2005.
[28] J. G. Kostas and B. Boverie, "Statistical model for a mode-stirred chamber," *IEEE Transactions on Electromagnetic Compatibility,* vol. 33, no. 4, pp. 366-370, 1991, doi: 10.1109/15.99120.

[29] N. J. Redding, "Estimating the Parameters of the K Distribution in the Intensity Domain," Defence Science and Technology Organization, Australia, DSTO-TR-0839, 1999.
[30] A. Pandey and S. Yadav, "Physical Layer Security in Cooperative AF Relaying Networks With Direct Links Over Mixed Rayleigh and Double-Rayleigh Fading Channels," *IEEE Transactions on Vehicular Technology,* vol. 67, no. 11, pp. 10615-10630, 2018, doi: 10.1109/tvt.2018.2866590.
[31] K. Pearson, *On the criterion that a given system of deviations from the probable in the case of a correlated system of variables is such that it can be reasonably supposed to have arisen from random sampling. By Karl Pearson*. England, 1900.
[32] W. Rolke and C. G. Gongora, "A Chi-Square Goodness-of-Fit Test for Continuous Distributions against a known Alternative," *Computational Statistics,* vol. 36, no. 3, pp. 1885-1900, 2020, doi: 10.1007/s00180-020-00997-x.
[33] M. Saculinggan and E. A. Balase, "Empirical Power Comparison Of Goodness of Fit Tests for Normality In The Presence of Outliers," *Journal of Physics: Conference Series,* vol. 435, 2013, doi: 10.1088/1742-6596/435/1/012041.
[34] M. A. Stephens, "EDF Statistics for Goodness of Fit and Some Comparisons," *Journal of the American Statistical Association,* vol. 69, no. 347, pp. 730-737, 1974, doi: 10.1080/01621459.1974.10480196.
[35] N. Nourshamsi, J. C. West, C. E. Hager, and C. F. Bunting, "Generalized Extreme Value Distributions of Fields in Nested Electromagnetic Cavities," *IEEE Transactions on Electromagnetic Compatibility,* vol. 61, no. 4, pp. 1337-1344, 2019, doi: 10.1109/temc.2019.2911927.
[36] S. B. Vardeman, *Statistics for Engineering Problem Solving* (PWS foundations in engineering series). Boston: PWS Pub. Co., 1994.
[37] A. Leon-Garcia, *Probablity, Statistics, and Random Processes for Electrical Engineering*. Upper Saddle River, NJ: Pearson Education, 2008.
[38] S. Mohanty, "Estimation of Parameters of Some Continuous Distribution Functions," Master of Science, Mathematics, National Institute of Technology - Rourkela, 2012.
[39] S. M. Homan, "ROBUST ESTIMATION OF THE PARAMETERS OF THE EXPONENTIAL AND WEIBULL DISTRIBUTIONS," ProQuest Dissertations Publishing, 1983.
[40] D. M. Pozar, *Microwave engineering*, 4th ed. Hoboken, NJ: Wiley, 2012.
[41] V. Rajamani, C. F. Bunting, and J. C. West, "Differences in Quality Factor Estimation in Frequency and Time Domain," in *Asia-Pascific Symposium on Electromagnetic Compatibility (APECM)*, Singapore, 2012: IEEE, doi: 10.1109/APEMC.2012.6237893.
[42] V. Rajamani, C. F. Bunting, and J. C. West, "Effects of Loading on Independent Samples and Uniformity of a Reverberation Chamber," in *IEEE International Symposium on Electromagnetic Compatibility*, Denver, CO, USA, 2013: IEEE, doi: 10.1109/ISEMC.2013.6670412.

[43] R. Bakore, J. C. West, and C. F. Bunting, "Experimental Validation of a Discrete Spectral Representation of the Electromagnetic Field within an Ideal Reverberation Chamber," in *IEEE International Symposium on Electromagnetic Compatibility & Signal/Power Integrity (EMCSI)*, Washington, DC, USA, 2017: IEEE, doi: 10.1109/ISEMC.2017.8077961.

[44] B.-H. Liu, D. C. Chang, and M. T. Ma, *Eigenmodes and Composite Quality Factor of a Reverberating Chamber* (NBSIR). U.S Department of Commerce, National Bureau of Standards, 1983.

[45] C. L. Holloway *et al.*, "Use of Reverberation Chambers to Determine the Shielding Effectiveness of Physically Small, Electrically Large Enclosures and Cavities," *IEEE Transactions on Electromagnetic Compatibility,* vol. 50, no. 4, pp. 770-782, 2008, doi: 10.1109/temc.2008.2004580.

[46] J. C. West, J. N. Dixon, N. Nourshamsi, D. K. Das, and C. F. Bunting, "Best Practices in Measuring the Quality Factor of a Reverberation Chamber," *IEEE Transactions on Electromagnetic Compatibility,* vol. 60, no. 3, pp. 564-571, 2018, doi: 10.1109/TEMC.2017.2753724.

[47] N. Nourshamsi, "Statistical Anlaysis of Electromagnetic Complex Cavities," ProQuest Dissertations Publishing, 2018.

[48] A. Rai, Z. Ahmad, M. J. Hasan, and J.-M. Kim, "A Novel Pipeline Leak Detection Technique Based on Acoustic Emission Features and Two-Sample Kolmogorov-Smirnov Test," *Sensors (Basel, Switzerland),* vol. 21, no. 24, p. 8247, 2021, doi: 10.3390/s21248247.

[49] A. K. Ng, A. Kai Keng, and C. Guan, "Automatic selection of neuronal spike detection threshold via smoothed Teager energy histogram," 2013: IEEE, pp. 1437-1440, doi: 10.1109/NER.2013.6696214.

[50] R. L. Nuzzo, "Histograms: A Useful Data Analysis Visualization," *PM&R,* https://doi.org/10.1002/pmrj.12145 vol. 11, no. 3, pp. 309-312, 2019/03/01 2019, doi: https://doi.org/10.1002/pmrj.12145.

[51] H. E. Ross and B. I. Knott, "Dicuil (9th century) on triangular and square numbers," *British journal for the history of mathematics,* vol. 34, no. 2, pp. 79-94, 2019, doi: 10.1080/26375451.2019.1598687.

[52] C. Lemoine, P. Besnier, and M. h. Drissi, "Investigation of Reverberation Chamber Measurements Through High-Power Goodness-of-Fit Tests," *IEEE Transactions on Electromagnetic Compatibility,* vol. 49, no. 4, pp. 745-755, 2007, doi: 10.1109/temc.2007.908290.

[53] G. Orjubin, E. Richalot, S. Mengue, and O. Picon, "Statistical Model of an Undermoded Reverberation Chamber," *IEEE Transactions on Electromagnetic Compatibility,* vol. 48, no. 1, pp. 248-251, 2006, doi: 10.1109/temc.2006.870705.

[54] M. Qu, G. Lu, J. Lin, Y. Wang, and Y. Guan, "An investigation of statistical distribution properties in reverberation chamber," in *2008 International Conference on Microwave and Millimeter Wave Technology*, 21-24 April 2008 2008, vol. 3, pp. 1435-1437, doi: 10.1109/ICMMT.2008.4540714.

[55] W. Weibull, "A Statistical Distribution Function of Wide Applicability," *Journal of Applied Mechanics,* 1951.

[56] W. K. Brown and K. H. Wohletz, "Derivation of the Weibull distribution based on physical principles and its connection to the Rosin–Rammler and lognormal distributions," *Journal of applied physics,* vol. 78, no. 4, pp. 2758-2763, 1995, doi: 10.1063/1.360073.

APPENDICES

PHOTOS OF SMALL CHAMBER AND TEST SETUPS

A.1: OVERVIEW

This chapter will showcase the small chamber before and after the repairs and modifications were made on it, as well as the test setups. The repairs and modifications include the new gasket material used on the outline of the door and windows to prevent leakage, as well as additional aluminum foil on the small chamber's tuner to help create more randomness in the chamber. The test setups are the S_{21in}, S_{21out}, and for the measurements used to collect hypothesized exponential data for the AD tests.

A.1.1.: Photos before Repairs and Modifications

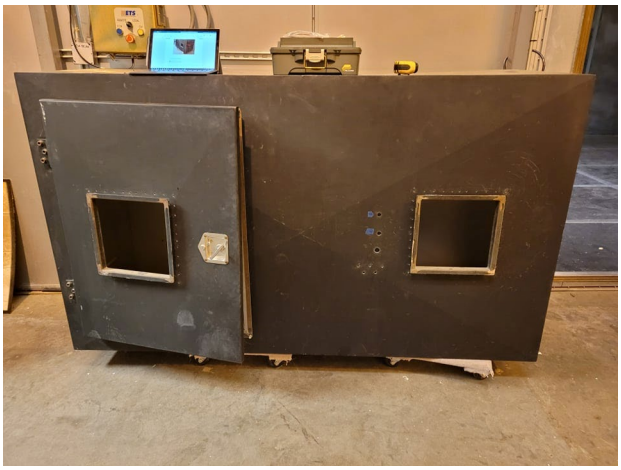

Figure A.1: Small chamber without windows sealed (pre-repairs)

(a)

(b)

Figure A.2.: (a) Right and (b) left window aperture sealing setup (pre-repair). Plexi glass is sandwiching copper mesh to the small chamber to prevent leakage from the window. This was found to be inefficient.

(a)

(b)

Figure A.3.: Previous gasket material on the small chamber. The red circles indicate concerns of torn gasket material or a large gap which can potentially create spaces for energy to leak. (pre-repairs)

Figure A.4.: Small Chamber Tuner with no aluminum added on to it. (pre-repairs)

A.1.2.: Photos after Repairs and Modifications

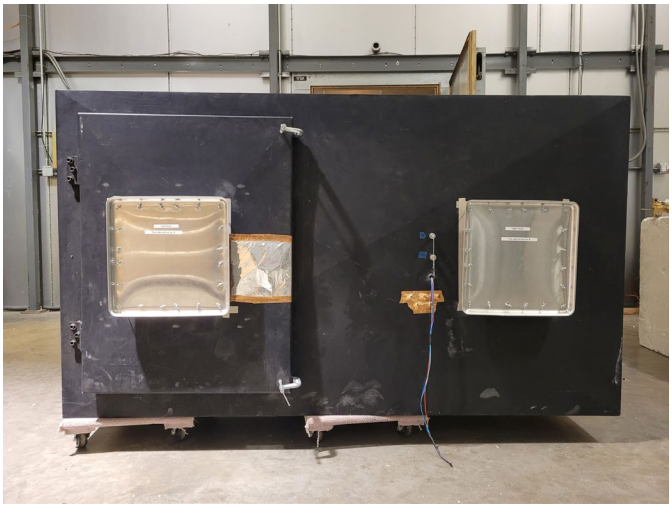

Figure A.5.: Small chamber post repairs with aluminum panels covering both windows. The door handle was covered because it was leaking energy at its seams. The use of two clamps were used to keep the door tightly shut. (post repairs)

Figure A.6.: New gaskets on the perimeter of the enclosure's door frame and door. Aluminum foil has been added over the back side of the window to prevent anymore leakage out of the left window.

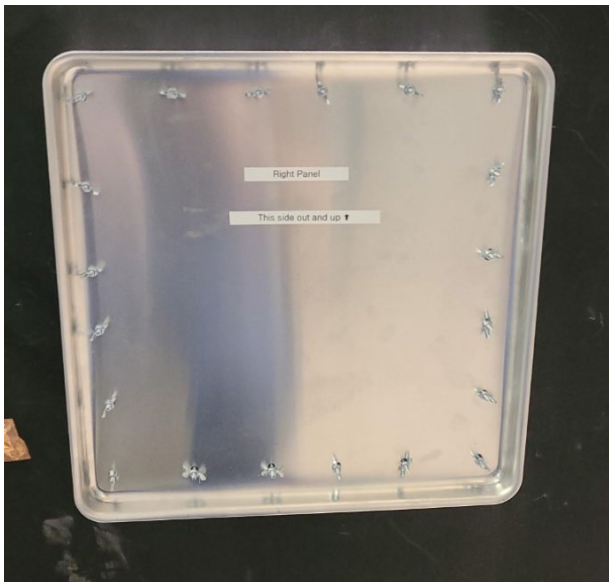

(a) (b)

Figure A.7.: Closer inspection of the outside panels. Shown in (a) and (b) is the front and side of the right panel. Both left and right panels are the same.

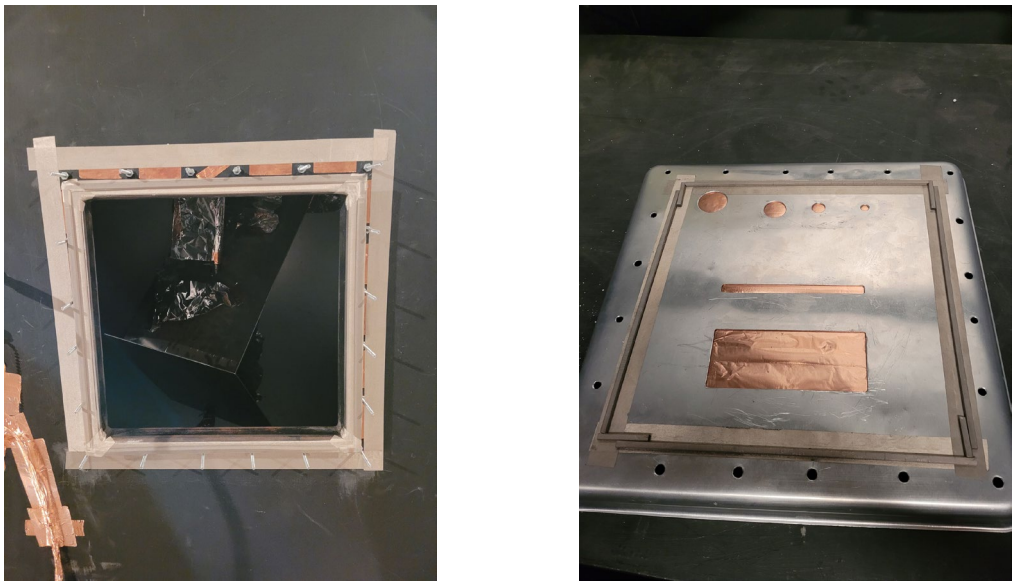

(a) (b)

Figure A.8.: (a) shows the gasket material on the perimeter of the window aperture. (b) shows the solid panel with apertures cut on it (but covered in conductive tape), with a perimeter of gasket material. This was so there would be a double wall preventing leakage out of the seam when the plate was put on the chamber. The solid panel (not pictured here) has a similar perimeter.

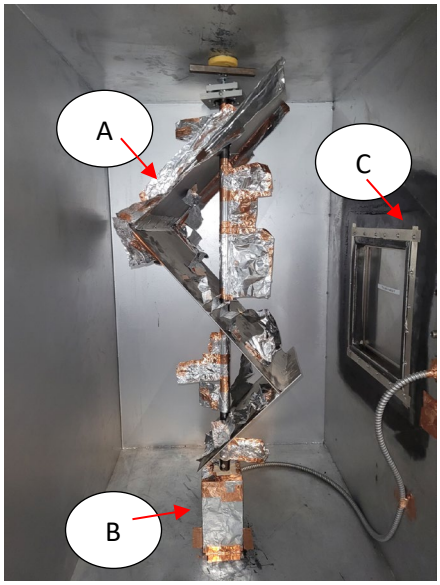

Figure A.9.: Tuner with aluminum foil on it. (A) Tuner with additional aluminum foil and motor control box also covered in aluminum foil and conductive tape (B). Screws that pass through the chamber from inside to outside touch conductive tape (C). These screws are used to attach the aluminum plates to the small chamber.

A.1.3.: S_{21in} and S_{21out} test setup

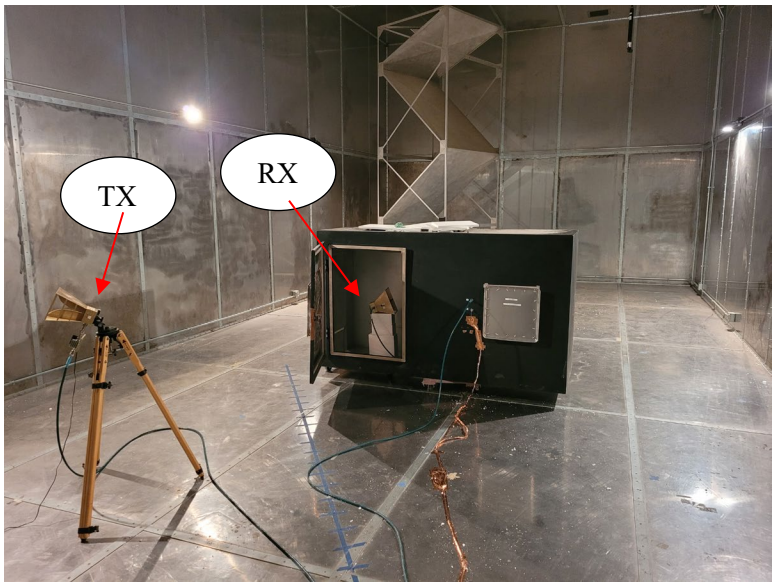

Figure A.10.: S_{21in} experimental setup. Transmitter (TX) and receiver (RX) are identified. Transmitter has microwave amplifier attached to it. Door is opened to see how the RX was placed inside the small chamber. For all testing the door was shut.

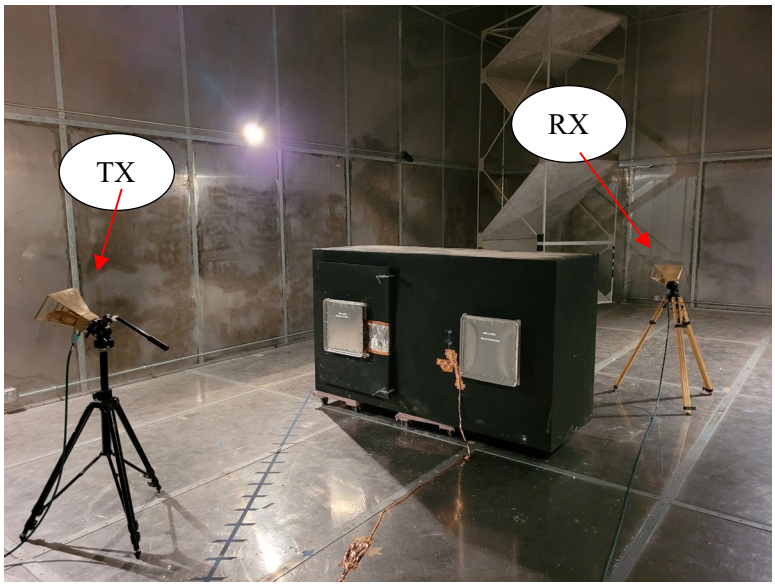

Figure A.11.: S_{21out} experimental setup. Transmitter (TX) and receiver (RX) are identified. Microwave amplifier is not needed for this setup so it was removed from the transmitter.

A.1.4.: Antenna Placement for Anderson-Darling test

Figure A.12.: Antenna placement and orientation for the small chamber's AD test.

Figure A.13.: Antenna placement and orientation for the SMART-80's AD test.

VITA

Marshall Daniel Sowell

Candidate for the Degree of

Master of Science

Thesis: THE STATISTICAL BEHAVIOR OF ELECTROMAGNETIC FIELDS WITHIN APERTURE-COUPLED NESTED REVERBERANT CAVITIES

Major Field: Electrical Engineering

Biographical:

Education:

Completed the requirements for the Master of Science in Electrical Engineering at Oklahoma State University, Stillwater, Oklahoma in July, 2022.

Completed the requirements for the Bachelor of Science in Electrical Engineering at Florida State University, Panama City, Florida in 2020.

Experience:

SMART Scholarship Summer Internship at the Naval Surface Warfare Center Dahlgren, 2021.

Oklahoma State University REFTAS group research member, 2020 – 2022.

NREIP Summer Internship at the Naval Surface Warfare Center Panama City, 2019.